5102-115
Thermal Power Systems
Advanced Solar Thermal Technology Project

DOE/JPL-1060-17
Distribution Category UC-62

The Effects of Regional Insolation Differences Upon Advanced Solar Thermal Electric Power Plant Performance and Energy Costs

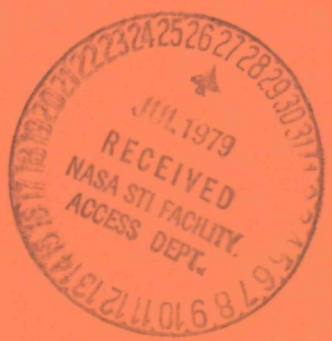

March 15, 1979

Prepared for
U.S. Department of Energy
Through an agreement with
National Aeronautics and Space Administration
by
Jet Propulsion Laboratory
California Institute of Technology
Pasadena, California

(JPL PUBLICATION 79-39)

N79-27660

JET PROPULSION LABORATORY *California Institute of Technology • 4800 Oak Grove Drive, Pasadena, California 91103*

September 15, 1979

Recipients of Jet Propulsion Laboratory
Publication 79-39

SUBJECT: Errata

Please note the following corrections to advance copies to JPL Publication 79-39, DOE/JPL-1060-17. The Effects of Regional Insolation Differences Upon Advanced Solar Thermal Electric Power Plant Performance and Energy Costs. A. F. Latta, J. M. Bowyer, T. Fujita, P. H. Richter. This errata supercedes errata dated August 7, 1979.

Pg 9 Table 3, first bullet at top of table, should read 10 MWe Power Plants. Last line second column should read 1.0.

Pg A-21 Line 36 should read extrapolation instead of estimation.

Pg A-22 Calculations for Fourier should read:

$$\tilde{z}\,(K_x, K_y) = \int_{-\infty}^{\infty}\int \left[\sum_{i=1}^{N} Z_i\,\delta(x-x_i)\,\delta(y-y_i)\right] e^{-i(K_x x + K_y y)}dxdy$$

$$= \sum_{i=1}^{N} z_i e^{i\,(K_x x_i + K_y y_i)}$$

K_x = spatial frequency in x-direction,

K_y = spatial frequency in y-direction.

Telephone (213) 354-4321 *Twx 910-588-3269* *Twx 910-588-3294*

Errata (Continued)

Pg A-22 Should $K_{xm} = \frac{\pi}{\Delta x}$, $K_{ym} = \frac{\pi}{\Delta y}$

Pg A-23 Line should read weighted δ-functions. Calculations should read

$$\frac{1}{4\pi^2} \iint_{-\infty}^{\infty} \tilde{F}\,(K_x, K_y)\, d K_x\, d K_y = 1$$

Pg A-24 4th paragraph Watt should read Aerospace.

Pg A-35 Paragraph 4 line 5 should read A-18.

Pg A-41 Ref. A-6 should read Aerospace Report ATR-78(7592)-1, Dec. 1, 1977.

Pg B-16 and B-17 Figures are reversed. Figure B-5 belongs with Caption B-6, vice versa.

Pg B-21 Legend in top right-hand corner, the last line should read:

○ Parabolic Trough (PT)

Pg B-23 Legend in top right-hand corner, the first line should read:

□ Paraboloidal Dish

The last line should read:

○ Parabolic Trough (PT).

Leo R. Levine, for

Irl E. Newlan, Manager
Technical Information and Documentation
Division

5102-115
Thermal Power Systems
Advanced Solar Thermal Technology Project

DOE/JPL-1060-17
Distribution Category UC-62

The Effects of Regional Insolation Differences Upon Advanced Solar Thermal Electric Power Plant Performance and Energy Costs

A. F. Latta
J. M. Bowyer
T. Fujita
P. H. Richter

March 15, 1979

Prepared for
U.S. Department of Energy
Through an agreement with
National Aeronautics and Space Administration
by
Jet Propulsion Laboratory
California Institute of Technology
Pasadena, California

(JPL PUBLICATION 79-39)

Prepared by the Jet Propulsion Laboratory, California Institute of Technology, for the U.S. Department of Energy through an agreement with the National Aeronautics and Space Administration.

The JPL Solar Thermal Power Systems Project is sponsored by the U.S. Department of Energy and forms a part of the Solar Thermal Program to develop low-cost solar thermal electric generating plants.

ABSTRACT

This study determines the performance and cost of four 10 MWe advanced solar thermal electric power plants sited in various regions of the continental United States. Each region has different insolation characteristics which result in varying collector field areas, plant performance, capital costs and energy costs.

In the context of advanced technology, the solar plants are conceptualized to begin commercial operation in the year 2000. It is assumed that major subsystem performance will have improved substantially as compared to that of pilot plants currently operating or under construction. The net average annual system efficiency is therefore roughly twice that of current solar thermal electric power plant designs. Similarly, capital costs reflecting goals based on high-volume mass production that are considered to be appropriate for the year 2000 have been used. These costs, which are approximately an order of magnitude below the costs of current experimental projects, are believed to be achievable as a result of the anticipated sizeable solar penetration into the energy market in the 1990-2000 timeframe.

The paraboloidal dish, central receiver, cylindrical parabolic trough, and compound parabolic concentrators comprise the advanced collector concepts studied. All concepts exhibit their best performance when sited in regional areas such as the sunbelt where the annual insolation is high. The regional variation in solar plant performance has been assessed in relation to the expected rise in the future cost of residential and commercial electricity supplied by conventional utility power systems in the same regions.

The report contains a discussion of the regional insolation data base, a description of the solar systems performance and costs, and a presentation of a range for the forecast cost of conventional electricity by region and nationally over the next several decades.

FOREWORD

The advanced thermal technology work reported herein is a part of the thermal power systems activities of the Department of Energy's Division of Solar Technology. A primary objective of this effort is to support development of advanced, low-cost, long-life, reliable solar thermal power systems which will supplement and eventually replace current fossil-fueled, electricity-generating plants.

The National Aeronautics and Space Administration's (NASA) Jet Propulsion Laboratory (JPL) and Lewis Research Center (LeRC) were selected in 1977 to assist in managing and coordinating this work. These two organizations, working with universities, government agencies, industry and the scientific community in general, are to lead in developing new concepts and establishing a broad technology base in advanced small power systems which can be used to accelerate the commercialization of these systems.

This report presents results of a study which determines the performance and cost characteristics of four selected advanced solar thermal power systems operating under widely varying insolation patterns associated with different regions of the country. The cost of electricity derived from the solar plants is compared to that from conventional (fossil and nuclear) power systems operating in the same region.

The body of this report presents a summary of the key findings and conclusions regarding the potential attractiveness of advanced solar thermal power systems on a regional basis. Supporting detailed data and analyses are presented in a series of appendices covering (A) the regional insolation data base, (B) performance and cost characterization of the four selected solar thermal systems, including presentation in more detail than is provided in the body of the report, of results obtained by computer simulations of the power plants, and (C) a limited analysis of power plant performance and cost sensitivities to variations in certain major plant components and component costs.

ACKNOWLEDGMENTS

Guidance and support during all phases of this study was provided by Vincent Truscello, Thermal Power Systems Project Manager, and John Becker, Advanced Solar Thermal Technology Project Technical Manager. The authors especially wish to acknowledge their contributions, which greatly facilitated the effort.

Direct contributors to the study effort at JPL include John Biddle, who participated in developing computer simulations for the Compound Parabolic (CPC) and the parabolic trough; Ram Manvi, who provided inputs regarding the system cost and performance data base; Alan Aghan, who supported the entire computational effort involving both system simulation development and operation of the computer code; Gerrie Hill, Jo Jean Kos, Lois Fite, and Iffat Khan, who provided computer programming support; and Cedric Daksla and Dave Berokoff, who assisted in data analysis and preparation of charts. The combined effort of all the individuals acknowledged above provided essential support which added materially to the study.

Projections for advanced/solar thermal systems were accomplished with the support of Government/DOE laboratories and industrial firms that are actively engaged in developing the solar thermal systems treated in the study. Among the many individuals contacted, the following provided particularly valuable inputs: Roger Cole and Bill Schertz of Argonne National Laboratory contributed invaluable assistance in characterizing the CPC, including provision of a basic computer simulation code; Jim Leonard and Walt Schimmel of Sandia Laboratories, Albuquerque, supplied computer codes and data for the parabolic trough system; Pat Eicher, Jim and Joan Woodard, Bill Wilson, Clay Mavis, and Louis Talerico, of Sandia Laboratories, Livermore, conveyed information pertaining to advanced central receiver systems, Loren Vant Hull of the University of Houston and Dick Holl of McDonnell-Douglas developed specific data relating to the optical performance of the central receiver; and Bob Stochl of NASA/LeRC supported efforts directed toward projecting the performance of Brayton/Rankine combined cycle systems.

Special acknowledgement is due the senior author, Mr. Allen F. Latta, for his diligent and sincere efforts in the performance of this research. His enthusiastic dedication to the development of solar energy as a partial solution to the energy problem will always be remembered by his many colleagues and friends who were deeply saddended by his accidental death just prior to publication of this report.

This study was supported by DOE, Division of Solar Energy under Interagency Agreement, EX-76-A-29-1060, with NASA. The effort was performed under the management of Mr. Martin Gutstein, Program Manager, DOE Thermal Power Systems, and the authors are particularly appreciative of his support and helpful suggestions.

CONTENTS

Tables

STATEMENT OF THE PROBLEM AND ASSESSMENT OF THE RESULTS

This study addresses the following two key questions:

- What is the effect of regional insolation (solar energy) characteristics on the techno-economics of a spectrum of advanced solar thermal power plants?
- How do the projected energy costs of solar thermal plants operating in different regions compare with energy costs of conventional systems in these regions?

Since advanced solar thermal systems in the 1990-2000 timeframe are assumed to achieve projected performance and cost goals, it is this timeframe that is considered here. The study entailed the selection and characterization of a set of advanced solar thermal power plants that are representative of the diverse spectrum of concepts. These selected power plant concepts were then configured to produce minimum energy costs at chosen sites within the continental United States. In this way, the effect of regional insolation characteristics on the design, performance, and economics of the selected set of solar thermal plants has been determined. Projections of energy costs for conventional systems are used as a basis for assessing the relative attractiveness of solar systems operating in different regions.

A. SUMMARY

A first-order screening to determine the feasibility of using solar thermal power as an energy source in different regions of the country has been accomplished, and the results of this screening are reported here. Whenever insolation was sufficient or whenever sufficient energy had been stored during prior periods of insolation to allow plant operation above some fraction of rated output, the solar plant was assumed to deliver power at partial to full rating. No plant was allowed to deliver power in excess of its rating at any time. The most significant conclusion of this study is that two-axis tracking solar thermal systems --- specifically, the central receiver and paraboloidal dish --- were relatively more efficient at all locations and thus, potentially attractive for electric power generation in all regions of the continental United States.

B. REGIONAL INSOLATION CHARACTERISTICS

The insolation data base for the continental United States, encompassing direct measurements as well as inferred data from meteorological observations, was analyzed to develop insolation contours. Solar insolation and the development of various models for this insolation are discussed in Appendix A of this report. These contours were then used as a guide in selecting eight sites representative of the wide range of regional insolation characteristics encountered within the continental United States. The

selected sites and contours of annual mean or average daily direct normal insolation are shown in Figure 1.

The chosen sites are compared in Table 1 in terms of four characteristic parameters which provide insight regarding some of the major differences among the sites. The locations and the year in which the insolation data were taken are given in descending order of annual total direct insolation. For concentrating solar collector systems, annual total direct insolation is a measure of the energy available. A large variation from a high of 2848 kWh/m^2 per year for Barstow, California, to a low of 1253 kWh/m^2 per year for Maynard, Massachusetts, is shown.

The year associated with the insolation data at each site was selected by analyzing long-term insolation data at that site. A recent year, representative of long-term trends, was chosen since recent data are considered to be more reliable from the viewpoint of instrument accuracy and measuring/data reduction techniques.

Referring to Table 1, it is seen that the annual total hours of insolation vary between 4000 h and 4500 h for all the sites except Maynard, MA, which has a value of only 2813 h. The annual average daily direct insolation is the annual total direct insolation divided by the number of days in the year. This parameter, which is proportional to total annual direct insolation, is used to identify contour curves in Figure 1. It is noted that the data in Table 1 and the contour curves of Figure 1 are in approximate agreement and that differences are indicative of uncertainties associated with developing contours based on limited data of varying quality. Microclimatic

Table 1. Insolation Characteristics of Chosen Sites

Location (year)*	Annual Total Direct Insolation $kWh/(m^2y)$	Annual Total Hours of Direct Insolation h/y	Annual Average Daily Direct Insolation $kWh/(m^2d)$	Annual Average Hourly Insolation (Based on Hours of Direct Insolation) kW/m^2
Barstow, CA (1976)	2848	4494	7.781	0.6337
Albuquerque, NM (1975)	2538	4300	6.953	0.5902
Omaha, NB (1974)	1688	4263	4.625	0.3960
Medford, OR (1973)	1602	4326	4.389	0.3704
Miami, FL (1975)	1424	4138	3.901	0.3442
Cape Hatteras, NC (1973)	1421	4094	3.893	0.3471
Madison, WI (1971)	1298	4143	3.556	0.3132
Maynard, MA	1253	2813	3.433	0.4456

*Year in which insolation data was taken.

Figure 1. Insolation Patterns and Selected Sites

effects associated with any chosen site add to the level of uncertainty and tend to require a large number of strategically located measuring stations to develop accurate contours. Nevertheless, the contour curves are valuable in providing an overall view of prevailing insolation patterns.

In addition to the amount of available insolation, the intensity is also important with regard to the design and performance of solar thermal plants. Intensity level determines the efficiency of the receiver and engine when operating temperature is specified. In general, a higher intensity results in higher efficiency: For the receiver, re-radiation losses, which are essentially constant for a fixed temperature, become a smaller fraction of the heat processed by the receiver. As a result, receiver efficiency improves. If the engine rating is selected to match peak efficiency levels, the engine tends to operate closer to its design efficiency at near-design levels of solar insolation. A measure of insolation level is provided by the annual average hourly insolation as shown in Table 1. In general, intensity level decreases as the annual total insolation or amount of insolation decreases. However, there are exceptions as exemplified by Maynard, MA, which has the lowest amount of insolation while having the third highest intensity. When insolation is available in Maynard, MA, it tends to have high intensity whereas, in areas such as Miami, Fl, atmospheric conditions dictate lower intensities over longer periods of time.

C. SELECTED ADVANCED SOLAR THERMAL POWER PLANTS

There is a spectrum of solar thermal power systems employing collectors ranging from low-temperature, fixed orientation to high-temperature, two-axis tracking concepts. (Refs 1 through 5) The four collector concepts illustrated in Figure 2 were chosen as being representative of the complete spectrum.

- Compound Parabolic Concentrator (CPC) -- a fixed-orientation (non-tracking) collector which uses shaped reflecting surfaces to concentrate solar flux on a linear receiver; reflecting surface alignment is adjusted periodically (no more than twelve times per year) for maximum performance.

- Parabolic Trough -- a one-axis tracking collector which utilizes a parabolic trough to reflect solar flux onto a linear receiver located along the trough's focal line; tracking is accomplished by rotating the surface about its focal line.

- Heliostat/Central Receiver -- a two-axis tracking design which employs a field of reflecting surfaces, controlled so that the solar flux is beamed toward a tower-mounted receiver; a near-term embodiment of this concept is the 10 MW pilot plant being constructed near Barstow, CA.

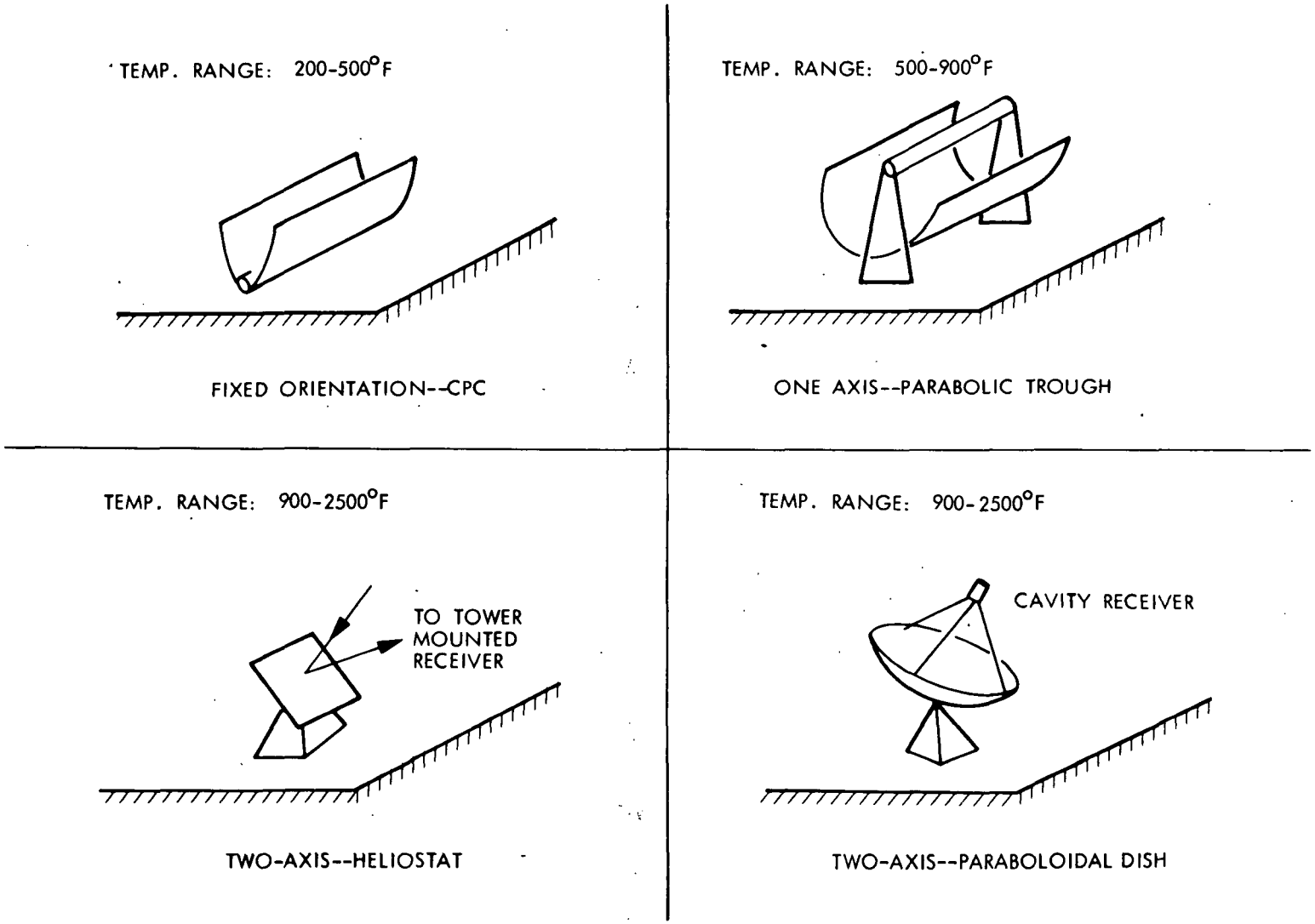

Figure 2. Selected Solar Thermal Collector Concepts

- Paraboloidal Dish -- a modular two-axis tracking approach comprising a field of paraboloidal dish concentrators, each of which focuses solar flux into the aperture of cavity receiver located at its focal point; a small heat engine-generator assembly is located behind the receiver at the focal point.

A complete solar thermal power system was configured for each of the selected generic collector concepts using advanced technology projections for subsystems/components. These projections are generally reflective of the performance and cost goals for advanced solar systems that are supported by recent studies encompassing advanced design approaches and mass production manufacturing. These design and manufacturing studies indicate that the goals are within reach.

The key factors governing the achievement of advanced solar thermal system energy cost targets (~50 mills/kWeh) are (1) the efficiency of the system in capturing and converting solar energy into electrical energy and (2) the unit cost of the collectors. These factors are interrelated. For a plant with a given output, the size or area of the collector field is inversely proportional to system efficiency. If the efficiency is low, the field becomes large and plant costs increase. To compensate, low-efficiency systems must employ low-cost collectors if they are to be competitive.

In Table 2, the design performance characteristics of the four selected systems are presented. The projected performance levels are predicated on advancements in technology and refined designs for all key subsystems consistent with our projections for the existing conditions in the 1990-2000 timeframe. For the concentrator,

Table 2. Design Performance Characteristics

• Year 2000 Startup • 10 MWe Plants

Plant Type	Dish	Central Receiver	Trough	CPC
Operating Temperature, °C/°F	900/1650	980/1800	425/800	225/440
Concentrator	0.89	0.74	0.74	
Tower Shading	---(1)	0.98	---(1)	---(1)
Atmospheric Attenuation	---(1)	0.98	---(1)	---(1)
Receiver	0.90	0.88	0.93	---(3)
Concentrator/Receiver Efficiency	(0.80)	(0.63)	0.69	(0.41)
Thermal Energy Transport	0.99(2)	0.99(2)	0.92	0.92
Electrical Energy Transport	0.96	---(1)	---(1)	---(1)
Power Conversion	0.47	0.50	0.36	0.22
Parasitic Power Losses	0.93	0.93	0.93	0.93
NET POWERPLANT SYSTEM EFFICIENCY	0.34	0.29	0.21	0.08

(1) Not applicable.
(2) Liquid metal, short length.
(3) This data is calculated within the ANL coding.

back-silvered surfaces achieving reflectivity values of 0.90 to 0.95 are employed. These estimates of reflectivity are based on the development of a thin, low-iron-content glass reflector technology, such as the fused glass process. Manufacturing techniques providing surfaces with small slope errors $\leq 0.1^{o}$ are assumed. Receiver losses are minimized by employing high-quality insulating materials.

Each of the different systems has an optimum operating temperature range. This range is determined via a tradeoff between receiver efficiency, which decreases with temperature (due primarily to re-radiation losses), and engine efficiency, which increases with temperature (Ref. 3). Two-axis tracking systems are able to obtain higher concentration ratios and correspondingly smaller receiver areas. In turn, these smaller areas permit the achievement of higher temperatures before re-radiation losses become dominant. Thus, as seen from Table 2, two-axis tracking systems have the highest design operating temperatures (in the range of 1500°F to 2000°F for the selected paraboloidal dish and central receiver systems). The one-axis tracking trough and fixed-orientation CPC attain lower concentration ratios and the selected designs for these configurations operate at lower temperatures of 800°F and 440°F, respectively.

The temperature level determines the theoretical upper-bound Carnot efficiency for the energy conversion system. Present heat engines achieve approximately 60% of Carnot, whereas the very advanced systems are projected to achieve values of 80% Carnot (Ref. 3). For the 1990-2000 timeframe, an advanced technology target of 70% Carnot was deemed to be appropriate, and this value was used for all systems.

Stirling engines were assumed for the paraboloidal dish system. Near-term development of these engines is focused on designs operating at $\sim$1500°F. A modest increase to 1650°F is projected for the 1990-2000 timeframe. An advanced Brayton/Rankine combined cycle was projected for the central receiver. To achieve the efficiency benefits of this particular combined cycle, high temperatures of $\sim$1800°F are desirable and 1800°F was used in the study. The parabolic trough employs either steam or organic Rankine power conversion. Advanced organic Rankine engines are best suited to the CPC.

Development of Stirling engines is concentrated on small sizes suitable for the paraboloidal dish system. Small Brayton engines are also candidates for dish systems since earlier studies (Ref. 2) indicate that performance reasonably close to that of the Stirling system can be achieved. For the large ($\sim$10MWe) engines needed for the central receiver concept, the Brayton/Rankine system was selected since these types of engines are available in this size range. Large Stirling engines, somewhat similar to large multi-piston diesel engines, are also candidates, but as mentioned above, current developmental activity is focused on the smaller sizes.

It is noted from Table 2 that power conversion efficiency decreases as operating temperature decreases. This follows the expected trend inferred from the Carnot efficiency variation with temperature. The power conversion efficiency also includes the effect of mechanical/gearbox and electric generator efficiencies. Lower mechanical-generator efficiencies are assumed for the small power units that are a part of the modular paraboloidal dish concept than are assumed for the other chosen concepts, which employ large centralized energy conversion units.

In terms of net or overall system efficiency, the optically more efficient two-axis tracking concepts achieve higher values than one-axis and fixed-orientation systems. However, it is emphasized that this greater efficiency is achieved at the price of greater complexity in the articulation of concentrating or reflecting surfaces. The paraboloidal dish appears to have the highest potential for efficiency, primarily due to its optical/tracking characteristics which avoid the cosine losses encountered to differing degrees by the other systems. Basically, the dish tracks so that the collector aperture is normal to the solar beam radiation whereas, for the other systems, the collector aperture cannot be maintained normal to the beam over the entire period of insolation availability.

Fixed-orientation systems, as represented by the CPC, employ relatively low concentration ratios of the order of five. The receiver is located at the base of the reflecting surfaces, as seen in Figure 2, and therefore can also absorb a portion of the diffuse radiation. The other systems only accept the direct beam radiation. When the direct beam radiation is blocked by cloud cover, these other systems cannot function. Systems, such as the CPC, which use some diffuse energy may still be able to function but, generally, when beam radiation is blocked, the entire level of insolation is low, and performance is correspondingly low.

Systems which convert diffuse solar energy could be advantageous for applications involving low-temperature heat, particularly in cloudy regions. When considering only power generation as in the present study, this advantage is greatly diminished. Although systems such as the CPC appear low in terms of performance potential in the context of the present study, it is emphasized that there is a wide range of solar thermal applications and that the CPC could be a strong candidate for some of these applications. Additionally, the CPC is at a more advanced stage of development and can be readily implemented for near-term applications.

As an additional point, it is noted in Table 2 that the net system efficiency applies to operation at design conditions where none of the energy passes through storage. To operate at high capacity factors (i.e., to deliver rated power for periods beyond the time of insolation availability), it is necessary to introduce energy storage. For the dish-Stirling system, advanced battery storage having a throughput efficiency of 75% is assumed. The other systems assume thermal storage with a throughput efficiency of 85%. The

effect of storage efficiency on total system performance is clearly a function of the amount of energy that passes through storage. The amount of energy passing through storage is determined by the desired capacity factor and the characteristics of the insolation. Thus, regional variations in insolation patterns will affect storage requirements and system performance.

The direct cost data for each of the selected systems is presented in Table 3. As determined from sensitivity studies, the key cost driver is unit concentrator cost. Since solar energy has relatively low intensity at the earth's surface, it is necessary to use collector fields of large area to capture and concentrate sufficient energy for applications such as electrical power generation. Since large areas are required, the cost per unit area must be small in order to achieve cost-competitive systems.

Projections of low-cost, advanced concentrators, as shown in Table 3, are predicated on high-volume mass production ($\sim 10^6$ units/year) of advanced designs specifically tailored for mass production. Most of the recent studies (e.g., Refs 6 and 7) concerned with high-volume mass production have treated the concentrator or heliostat of the central receiver system. Studies have encompassed the heliostat designed for the 10 MWe pilot plant being constructed near Barstow, CA, as well as advanced second-generation concepts. These studies indicate that a unit cost of $\$65/m^2$ (as shown in Table 3) is achievable for a completely installed system.

Table 3. Solar Subsystems Direct (1) Cost Data

• 10 MWE Power Plants • Year 2000 Startup • 1979 Base Year Dollars

Major Subsystems	Paraboloidal Dish	Central Receiver	Parabolic Trough	Compound Parabolic Concentrator
Operating Temperature °C/°F	900/1650	980/1800	425/800	225/440
Land, $/acre ($1000 - $5000)/acre	---(2)	---(2)	---(2)	---(2)
Concentrators, $/m^2	85	65	70(3)	50(4)
Cavity Receivers, $/m^2(5)	10	175 $/kWe(6)		
Energy Transport	40 $/kWe		60 $/kWt	50 $/kWt
Storage Structures/Medium(7)	30 $/kWe-h	26 $/kW-h	24 $/kW-h	21 $/kW-h
Heat Engine Equipment, $/kWe	60	60	60	60
Balance of Plant, $/kWe	85	85	85	85
Operations and Maintenance Costs, %(8)	1.0	1.25	1.0	1.0

(1) Direct costs do not include: spares/contingency (5%), indirect costs (10%), or interest during construction.
(2) Land costs are site dependent.
(3),(4) Estimated mass production costs: JPL, coordinated with Sandia, Albuquerque and Argonne National Laboratory.
(5) Receiver cost is normalized to concentrator aperture area.
(6) Includes tower, structure, receiver, and short piping transport in tower mounted power conversion system module.
(7) Based on 5-6 h of storage.
(8) Operations and maintenance (O&M) costs for the first year are assumed to be a percentage of the total capital investment cost;O&M costs escalate at the rate of 7% per year.

The values for unit cost shown in Table 3 were determined by using these studies as a point of reference in conjunction with goals established for the other systems. Generally, the paraboloidal dish employs doubly curved surfaces and is structurally more complex than the heliostat. Hence, it was assigned a unit cost of $\$85/m^2$, which is higher than the heliostat and within the established cost target range of 70-100 $\$/m^2$. Additionally, recent JPL contracted studies for dish systems projected installed costs in the 70-120 $\$/m^2$ range based on a mass production rate of 100,000 units per year.

Systems such as the one-axis tracking through and the CPC were judged to be simpler and less costly on a unit area basis. Laboratories directing the development of these systems, Sandia Laboratories, Albuquerque for the trough, and Argonne National Laboratory for the CPC, concurred with the judgment that troughs and CPS's should have lower costs than two-axis tracking heliostats and dishes. Since high-volume mass production studies comparable to those made for the heliostat have not been performed, there is uncertainty regarding the absolute magnitude but there is general ageeement regarding the trends.

Storage costs shown in Table 3 correspond to advanced technology projections. Since Department of Energy cost targets are in the process of being formulated updated, sensitivities to the assumed values are presented in Appendix C. Costs for the heat engine and associated conversion equipment are values based on large-volume mass production of small engines via techniques developed within the automotive industry. Thus, the costs shown in Table 3 of \$60/kWe strictly pertain to projections for the small heat engine employed in the paraboloidal dish concept. However, if the other systems are used for small power applications and if sizeable penetrations into the power market are made, some level of mass production manufacturing could also occur in their cases. Thus, it was decided to use the same energy conversion system unit cost for all systems, because it is believed that the equivalent unit costs of large engines could, at best, approach the mass production unit costs of the small engines.

Balance-of-plant and operations-and-maintenance costs (O&M) were based on detailed studies for the central receiver and EPRI estimates (Ref 8). These factors depend on detailed design considerations. Since detailed designs do not exist for the projected advanced systems, only approximate estimates could be made. Therefore, it was decided to use the same factors for all the systems.

As additional support for the use of the same factors, it is noted that there is no clear way to distinguish among the different systems without detailed study. For example, two-axis tracking systems are generally more complex than one-axis and fixed-orientation systems and would probably require more maintenance per unit area of collector field. However, the simpler but less-efficient systems will require a larger collector area to deliver the same power. These effects tend to be off-setting.

D. EFFECT OF REGIONAL INSOLATION ON SOLAR POWER PLANTS

Regional insolation characteristics have a significant impact on the design, performance and cost of solar thermal power plants. For a given plant output, the amount and intensity of the available insolation at a site are major factors in determining the size of the collector field and, hence, its cost. As noted previously, the collector field is the key cost driver for solar plants.

Based on performance potential, the southwest sunbelt is the best location for solar plants because it provides the greatest amount and intensity of insolation. However, depending on the performance level that they can achieve with prevailing insolation characteristics, there may be many potential applications for solar thermal systems outside the sunbelt.

The effect of insolation on solar power plant design and techno-economics was determined by using a previously developed performance/economics computer program (Ref. 9). The primary input of this program is hourly insolation data as supplied by SOLMET tapes. The performance portion of the program takes all the parametric characteristics of the power plant subsystems and links them into a simulation of a total system which operates according to specified control strategies; these strategies involve delivery of energy, storage of energy, and discharge of storage. Basically, the performance simulation determines the fraction of available insolation that is delivered as electrical energy.

Also, the required collector field area and energy storage requirements to deliver a specified level of energy are determined from the performance simulation. Component/subsystem unit costs as given in Table 3 are used to determine corresponding capital costs. The well-established economic methodology for determining levelized bus-bar energy costs for utility-owned power plants is then employed (Ref. B-10). A computer optimization technique is employed to delineate power plant configurations which provide minimum energy costs for a specified level of energy delivery (i.e. capacity factor). Further details are provided in Appendix B.

A set of three charts (Figures 3a, b, and c) summarizes the effect of regional insolation characteristics on solar power plant energy costs. In addition to expected overall trends of higher energy costs in regions of low insolation, some of the more subtle influences of differing regional insolation characteristics are delineated. The charts show energy cost as a function of annual average daily direct insolation (which is proportional to total annual direct insolation) for the selected advanced solar thermal power plants. The set of three charts is used to illustrate the effect of capacity factor (i.e., Figure 3a is for the capacity factor corresponding to zero storage whereas Figures 3b and 3c pertain to capacity factors of 0.4 and 0.55, respectively). For the latter two higher capacity factors, storage is required. The effect of regional insolation characteristics on storage and its influence on plant techno-economics is discerned by comparing the three charts.

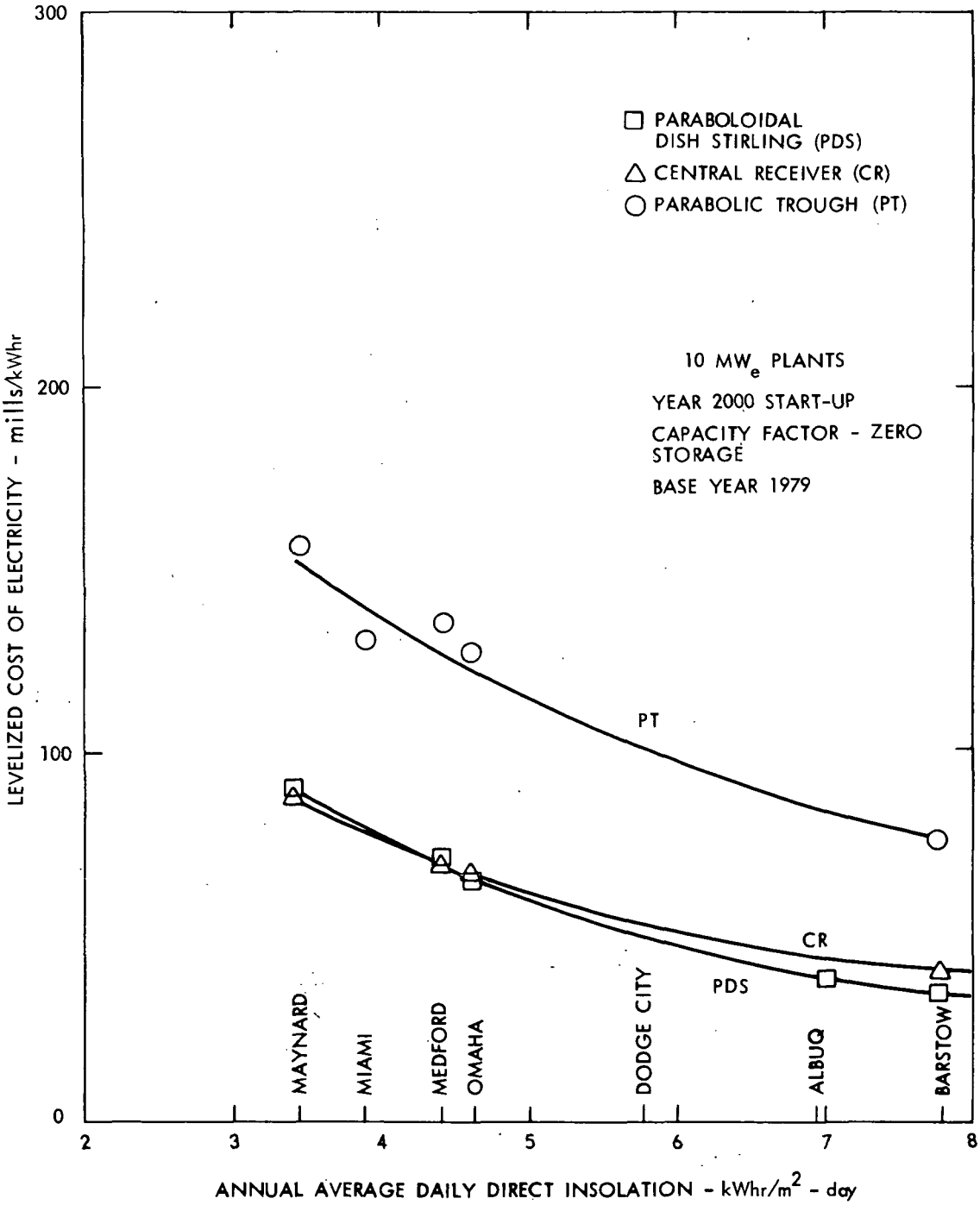

Figure 3a. Performance of Three Types of Solar Thermal Power Plants At Various Geographical Locations

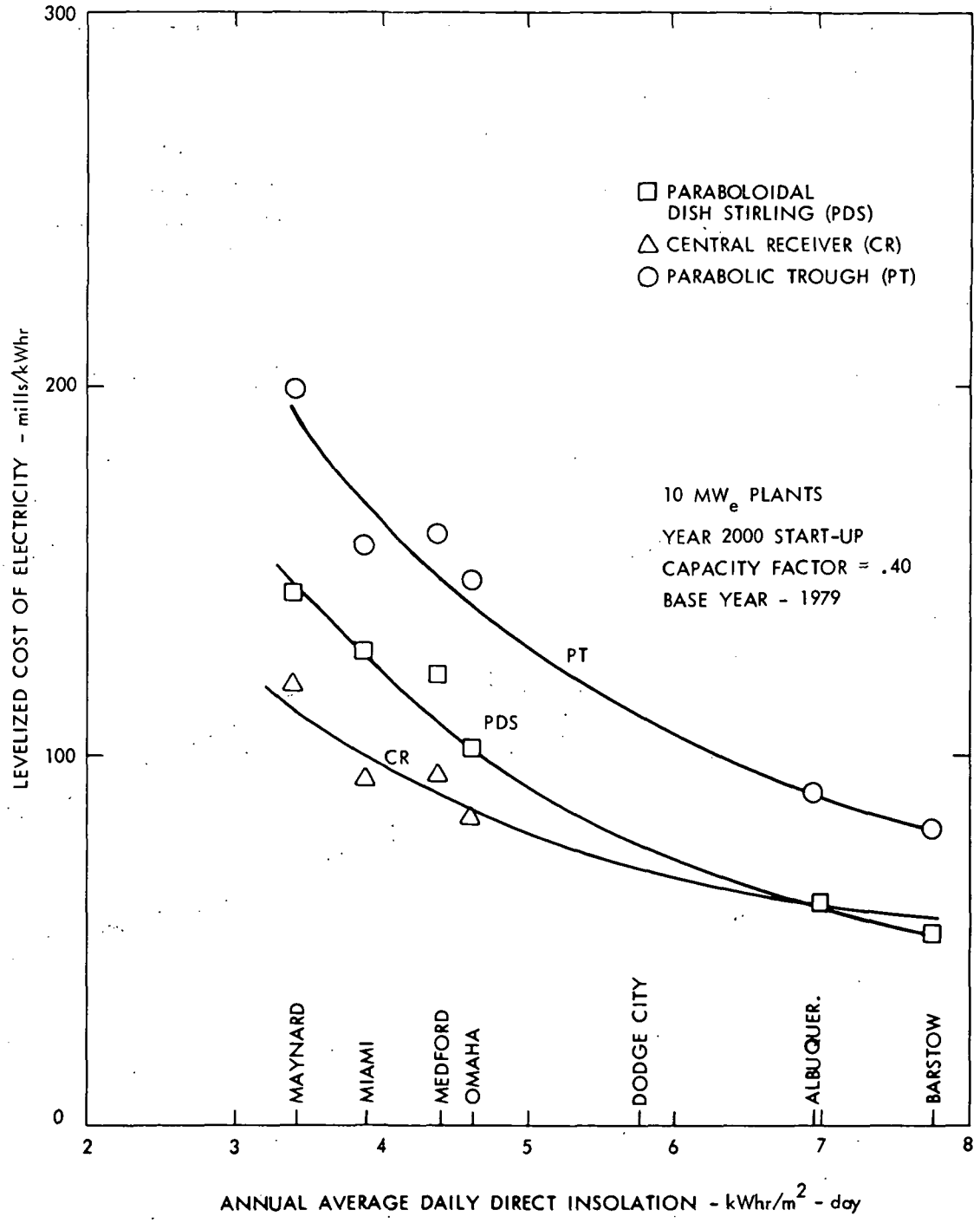

Figure 3b. Performance of Three Types of Solar Thermal Power Plants At Various Geographic Locations

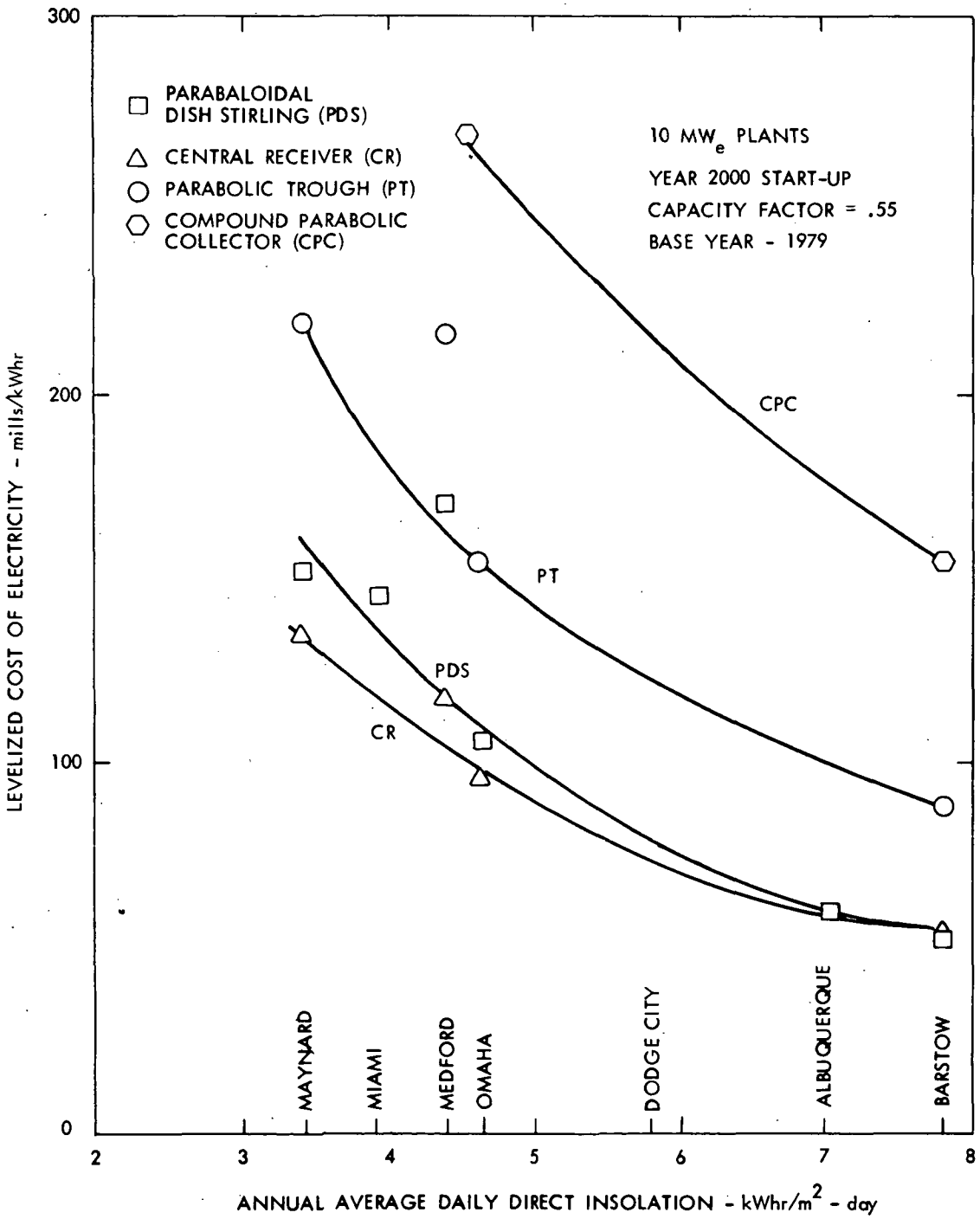

Figure 3c. Performance of Four Types of Solar Thermal Power Plants At Various Geographic Locations

When storage is not used, the collector field is sized to produce rated power during peak insolation periods and there is essentially no energy that is wasted. As shown in Figure 3a, the energy costs are lowest in the sunbelt region as represented by Albuquerque, New Mexico and Barstow, California. As the annual average daily direct insolation decreases, the levelized cost of electricity or energy cost increases.

There are particular perturbations about the overall trend that are caused by site-specific insolation characteristics. First, it is noted that, for the selected nominal designs, the central receiver has a slightly higher energy cost than the paraboloidal-dish-Stirling in the sunbelt and slightly lower costs in locations such as Medford, Oregon and Maynard, Massachusetts, where the insolation level is lower. This cross-over is explained in terms of differing off-load power conversion efficiency characteristics for the central receiver with combined Brayton/Rankine power conversion as compared to the parabolic dish with an advanced Stirling heat engine.

Closed-cycle Brayton engines typically have off-load curves with peak efficiency at 50-60% of rated load. This type of characteristic is therefore evident in the combined cycle system. The advanced Stirling engine used in the nominal designs achieves peak efficiency at rated power. Further, the engine located at the focal point of each dish was sized to handle peak insolation levels of the order of 1 kW/m^2 at all sites.

When a sizeable fraction of the available energy is furnished at near the peak insolation value, as in the sunbelt, engines with off-load curves having highest efficiencies near the rated peak design point provide higher performance. However, where a greater portion of the energy occurs at lower intensity levels, as in Maynard, MA or Medford, OR, off-load characteristics with maximum efficiencies occurring at partial load tend to be favored. This is one reason why the central receiver with Brayton/Rankine improves relative to the dish-Stirling in regions of low insolation.

The perturbations for the parabolic trough (as seen in Figure 3a) are also related to site-specific insolation characteristics which affect system performance by causing the engine to operate at different off-load settings for different amounts of time. The parabolic trough employs a Rankine conversion system with off-load characteristics similar to the Stirling engine (i.e., maximum efficiency at rated power).

The solar plant design can be perturbed and re-optimized to accomodate the perturbations and site-specific insolation characteristics noted above. For example, engine off-load curves could be altered through changes in engine design, (i.e., engine designs could be tailored to meet desired off-load characteristics). The design rating of the engine could be selected to match lower-than-peak insolation conditions in regions where the average insolation is low, and excess energy could be wasted or stored during the few peak insolation periods.

An attempt at such re-optimization was not made in the present study because re-optimization to tailor plants to site-specific regional insolation characteristics involves complex and detailed design trade-offs. Therefore, as a caveat, it is noted that values of energy cost lower than those shown could be achieved by further design optimizations.

Comparisons of Figures 3b and 3c with 3a reveal the influence of storage. First, the overall magnitude of energy costs shifts to slightly higher values as capacity factor and, hence, storage increase. This shift is attributed primarily to added capital costs for storage as well as the loss in energy associated with passing through storage. For the chosen nominal designs, the paraboloidal dish system is penalized relative to the other systems since an advanced battery storage throughput efficiency of 75% was used as compared to 85% for the other systems employing advanced thermal storage. There are indications that advanced battery systems such as the sodium-sulfur system may achieve efficiencies higher than 75% and thereby reduce differences between battery and thermal storage. The values used in this study are nominal projections, and results should be interpreted in this context.

The difference between the paraboloidal dish and central receiver is slightly greater at a capacity factor of CF = 0.4 (Figure 3b) as compared to a capacity factor of CF = 0.55 (Figure 3c). Here, higher capital costs for thermal storage systems are partially offsetting their efficiency advantages over battery systems. The effect of uncertainties in nominal storage cost values are presented in Appendix C because recent activities at NASA/LeRC have indicated lower thermal storage cost goals than were used in the present study.

In addition to an upward shift in energy cost levels with the addition of storage, it is seen that site-specific perturbations are greater. This trend is due to insolation characteristics which impact the storage system in different ways. Basically, the most desirable insolation pattern would be a cyclic (diurnal) variation that persists essentially unchanged over the entire year. The storage system could then be sized and optimized to meet this variation. However, seasonal variations in cyclic insolation characteristics can be very large, particularly for some regions outside the sunbelt. For example, there is a strong seasonal variation in Medford, OR, and it is seen that perturbations for Medford become very large at a capacity factor of 0.55 (see Figure 3c).

To achieve higher capacity factors, the collector field area is increased and the excess energy is stored and delivered during evenings or periods of insolation non-availability. Effective use of storage is difficult if the seasonal variations are such that there is one prolonged period of strong insolation and another prolonged period of poor insolation. During the period that strong insolation having regular diurnal insolation (cycles) is available, the field and storage size can be increased to the point where rated power is delivered during the full evening period. However, since this type of operation can occur for only a part of the year, the increase in capacity factor (based on annual energy delivered) will be proportional to the portion of the year for which strong insolation occurs. Storage will be largely under-utilized during the prolonged period of low insolation availability.

Depending upon seasonal insolation characteristics, there is a capacity factor corresponding to the condition where the energy during the strong insolation period is maximally utilized. If one attempts to achieve even higher capacity factors by further increases in collector field area and storage, there will be insufficient time to deliver all the stored energy by the next sunrise. To accommodate this buildup of excess energy, large seasonal storage must be supplied and/or energy must be wasted. Costs for long-duration seasonal storage become very large for the assumed thermal and battery storage systems and the computer optimization algorithm results in wasted energy. This results in a rapid increase in energy costs. Thus, sites such as Medford, OR having large seasonal variations in insolation characteristics will generally have a lower practical operating range of capacity factors.

These effects of seasonal variations in insolation are illustrated in Figure 4, where the relationship between collector area and capacity factor is shown for the paraboloidal dish system. Other systems show similar trends. For low capacity factors, the relation between collector area and capacity factor is essentially linear. This trend is reasonable since capacity factor is a measure of the energy delivered and the energy delivered is directly proportional to the energy collected and to the collector area.

Also, in the regions of low capacity factors, the sites with less total annual direct insolation (see Table 1) require more area to deliver a given quantity of energy. Here, a given quantity of energy delivery is denoted by a fixed value of capacity factor. This effect is apparent in the steep slopes for curves corresponding to sites having low insolation.

Departures from the linear relationship occur at higher capacity factors when storage is introduced. Since a portion of the collected energy is lost in storage, requirements for collector area increase and the slopes of the curves tend to be steeper as the level of storage increases. The rate at which the curves increase in slope is strongly affected by seasonal variations. For example, the slope for Medford, OR, increases sharply after a capacity factor of 0.4. The large area and storage at a capacity factor of 0.55 explains the reason for the large difference in energy cost for Medford, OR, as compared with other sites shown in Figure 3c.

It is noted that the fixed-orientation system, as represented by the CPC, is presented only on Figure 3c and only to show its general magnitude of energy costs relative to the other system. Generally it exhibits trends similar to the other systems. Its ability to use a portion of the diffuse energy does not provide a significant advantage at the operating temperature levels deemed necessary for power generation. If a given temperature level is maintained when insolation is low (large diffuse component), re-radiation losses from the receiver become a large fraction of the incoming energy and system efficiency drops. Engine performance suffers if a lower operating temperature is used to reduce re-radiation losses. Thus, it is difficult to generate power in any efficient way when insolation is low and in diffuse form. Diffuse solar energy may be more effectively utilized in low-temperature thermal applications.

Appendix B contains supporting detailed analyses which corroborate the findings discussed above.

E. REGIONAL COMPARISON OF SOLAR THERMAL WITH CONVENTIONAL ENERGY

As compared to performance in the solar-intensive Southwest sunbelt, the performance of solar plants will be degraded in regions such as the Northeast. However, the cost of electrical energy derived from conventional sources presently shows strong regional variation. Forecasts such as those of Data Resources Inc. (Ref. 9), indicate that relatively strong regional differences will persist through at least the year 2000. Moreover, regarding electrical costs from coal and gas turbine plants, there are large uncertainties that arise from potentially large variations in fuel prices coupled with capital cost increases that depend on the stringency of environmental control policies. Nuclear power also faces an uncertain future with regard to the nature and extent of the steps necessary to gain public acceptance for its expanded usage.

The projected energy costs for solar thermal plants with no storage are compared in Figure 5 with energy cost forecasts for conventional power plants. The ranges shown for gas turbine and coal plants were taken from the work of Anderson, Bowers, et al.(Ref. 12) of Oak Ridge National Laboratory. The basis of their projections is as follows:

	Fuel	Cost Range	Capacity Factor
Gas Turbine	Residual Oil	14 to 21 $/bbl	0.3
Coal Plant	Low Sulfur Coal	28 to 49 $/ton	0.6

Independent studies by JPL (Ref. 13) closely agree with the range determined by Anderson and Bowers.

The Data Resources Inc. (DRI) forecast (Ref. 11) is also shown on Figure 5. The band corresponds to worst and best case scenarios formulated by DRI. Since nuclear power was projected to have the lowest costs, the DRI forecast is predicated on a strong shift to nuclear power based on an econometric supply-demand model. As noted previously, the occurrence of a strong shift to nuclear power is presently a highly uncertain proposition.

For solar plants with no storage, which can be considered as the solar counterpart of the peaking gas turbine plants, energy costs equal to or less than the DRI forecast are projected for the central receiver and paraboloidal dish systems in the sunbelt region. For regions outside of the sunbelt, solar plant energy costs for the central receiver and dish are within about 40% of the DRI forecast. It is noted that the DRI forecast is for a mix of plants including old and new plants. New plants would tend to be more costly and have higher energy costs. When considering the implementation of solar plants, their energy costs should be compared with the energy costs of new conventional plants to be constructed in the same time period. Thus, a strictly one-to-one comparison with the DRI forecast cannot be made. Rather, the DRI forecast is regarded as a general reference level which is of particular value in illustrating regional variations in energy costs for conventional systems. Also, it is noted that no-storage solar plants are particularly suited for summer-peaking electrical demands where peak insolation and

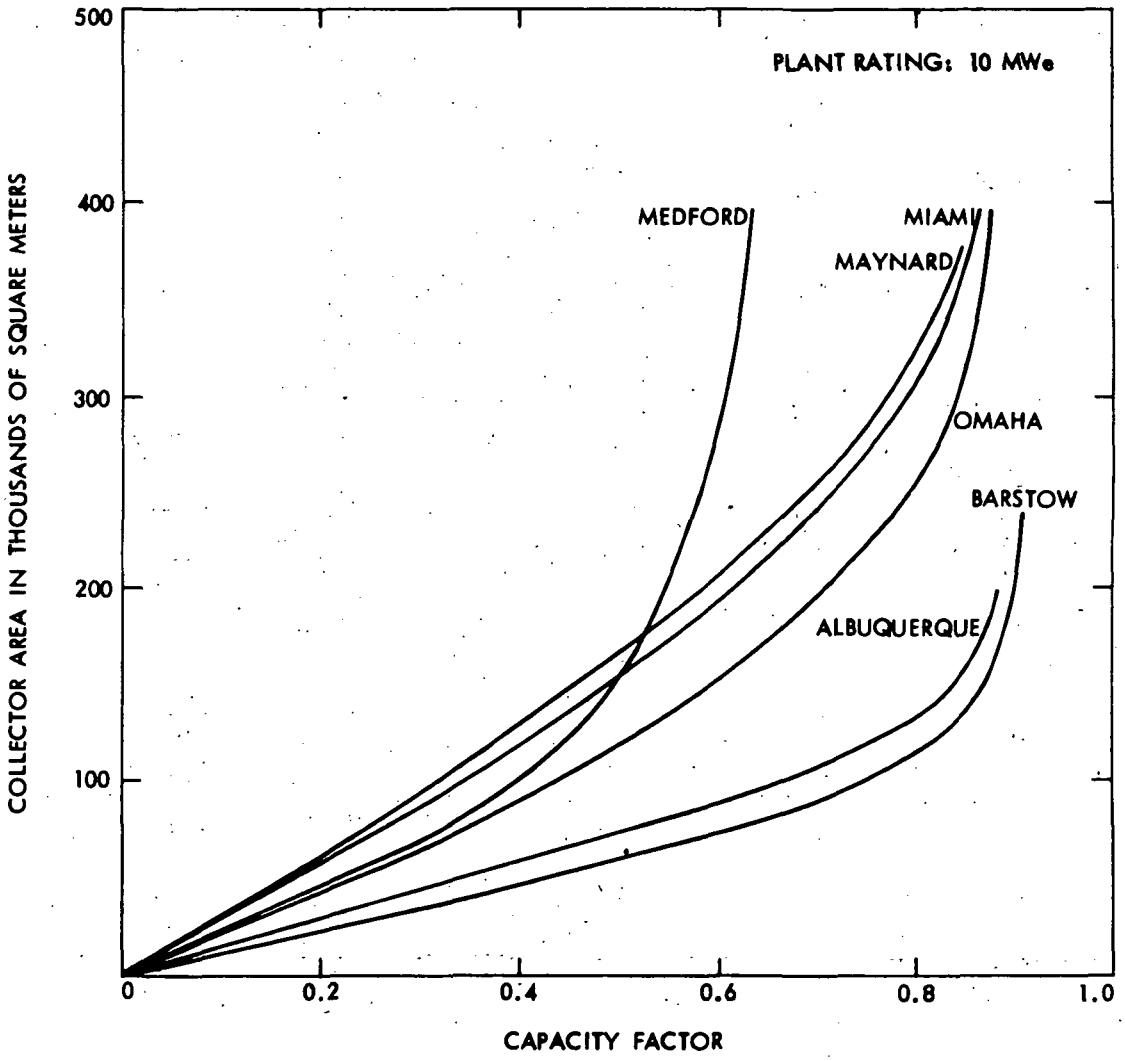

Figure 4. Collector Area As A Function of Capacity Factor For The 10 MW_e Paraboloidal Dish Stirling Solar Thermal Power Plant At Various Sites

peak demand are coincident. The matching of insolation characteristics with load demand curves and the integration of the solar plant into utility grid systems were beyond the scope of this study. Instead, this study focused on determining energy costs for a simple fixed-demand characteristic. Energy costs determined in this manner are regarded as a measure of potential attractiveness.

From Figure 5, it can be inferred that paraboloidal dish and central receiver solar thermal peaking (no storage) plants will achieve energy costs that are competitive with residual-oil, gas-turbine peaking plants for virtually all sites within the continental United States. The parabolic trough will be competitive in the sunbelt. To reach this competitive status will require advanced technology development, low-cost designs suited to mass production, and sufficient market penetration to achieve the high-volume production associated with low costs.

F. CONCLUSIONS AND RECOMMENDATIONS

The primary conclusion from this study is that the two-axis tracking solar thermal systems (namely the central receiver and paraboloidal dish systems) are potentially attractive for electric power generation in virtually all regions of the continental United States and the relative advantages of these systems over the other configurations hold for all regions. The most promising region is the Southwest sunbelt. However, in the context of large uncertainties regarding future energy costs from fossil and nuclear power plants, solar thermal power generation is potentially viable, even in the Northeast.

The parabolic trough could be competitive in the sunbelt for power generation. The fixed-orientation system does not appear to be competitive for strictly power generation applications. However, it is strongly emphasized that solar thermal systems are suitable for a wide range of applications requiring heat at different temperature levels. Thus, systems such as the trough could be used to supply both heat and electricity for total energy applications (the concept being pursued at Sandia Laboratories, Albuquerque), and the CPC could be developed to supply low-temperature heat. The present study does not address these possibilities, and the results should be interpreted in this context.

The present study is regarded as a first-order screening to assess the relative viability of using solar thermal power in different regions of the nation. For this purpose, a simple constant-demand load was assumed, where the solar plant delivered power during periods of insolation availability at levels equal to or less than rated power. When solar energy levels exceeded that needed to supply

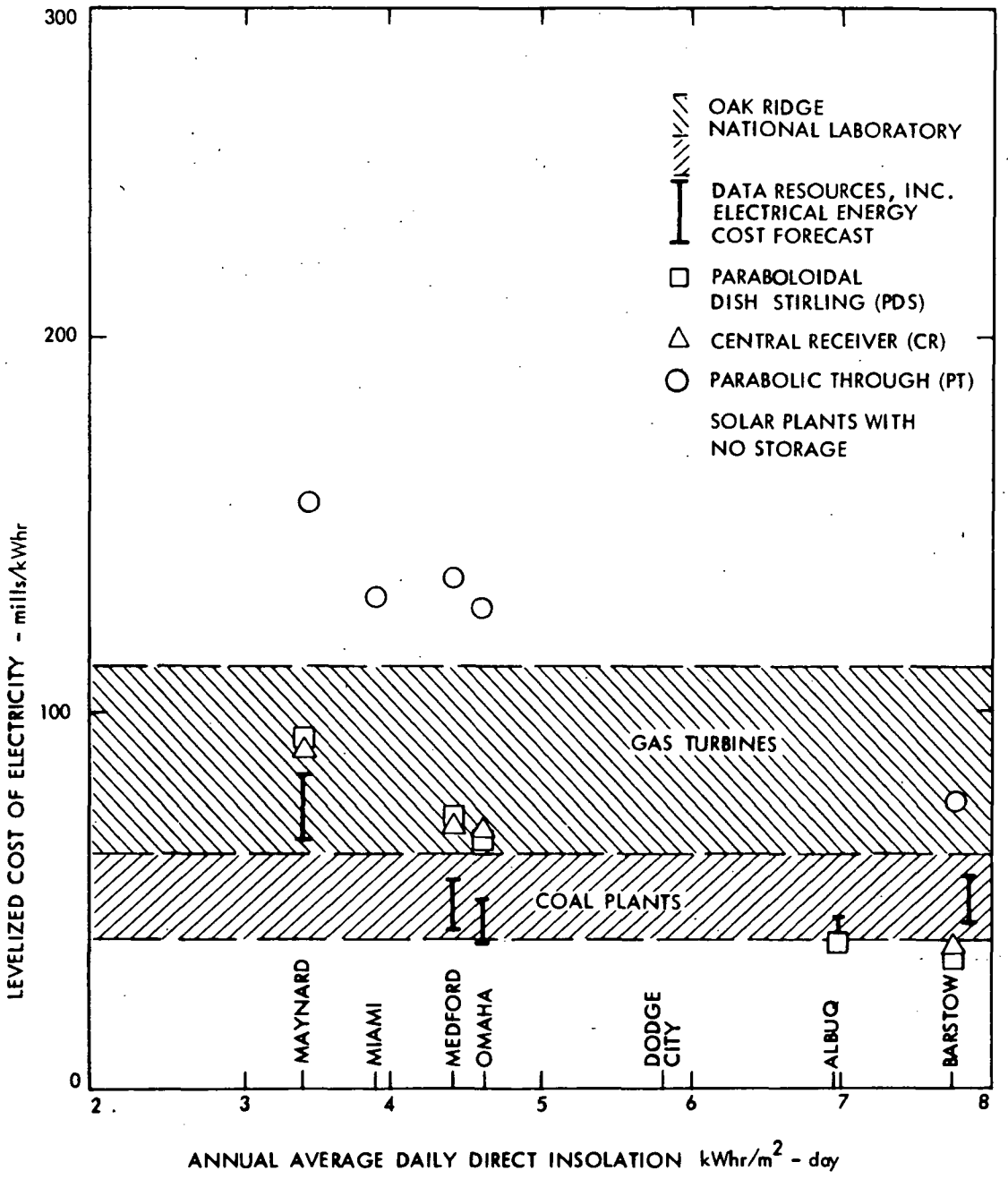

Figure 5. Projected Solar Thermal and Conventional Power Plant Energy Costs at Selected Sites

plant rating, energy was stored and delivered at rated power during periods when insolation was not available. If excess energy was available and storage was full, energy was wasted. It is recognized that there are strong site-dependent differences in load characteristics that will affect plant design, operation and energy costs. It is therefore recommended that following studies incorporate the effect of differences in regional demand characteristics and focus mainly on the two-axis tracking systems which have been shown from this study to be potentially attractive in all regions.

It is also recommended that a wide spectrum of solar thermal applications involving supply of heat over a range of temperatures be examined in the context of variations in regional insolation patterns. This is particularly important for systems requiring energy storage since it was shown that strong seasonal variations in insolation patterns have a severe impact on storage system requirements which, in turn, exert a major influence on plant operation and economics.

REFERENCES

1. "Recommendations for the Conceptual Design of the Barstow, California, Solar Central Receiver Pilot Plant," SAND 77-8035, UC-62, Sandia Laboratories, Albuquerque, NM, and Livermore, CA, October 1977.

2. Fujita, T.; El Gabalawai, N.; Herrera, G.; and Turner, G, "Projection of Distributed-Collector Solar-Thermal Electric Power Plant Economics to Years 1900-2000", DOE/JPL-1060-77/1(JPL Publication 77-79), Jet Propulsion Laboratory, Pasadena, CA, December, 1977.

3. Fujita, T.; Manvi, R.; Roschke, E. J.; El Gabalawi, N.; Herrera; G.; Kuo, T. J.; and Chen, K. H., "Techno-Economic Projections for Advanced Small Solar-Thermal Electric Power Plants to Years 1990-2000," DOE/JPL-1060-78/4 (JPL Publication 79-25), Jet Propulsion Laboratory, Pasadena, CA, November 1978.

4. Dudley, V. E., and Workhoven, R.M., "Summary Report:" Concentrating Solar Collector Test Results, Collector Module Test Facility," SAND 78-0815, Sandia Laboratories, Albuquerque, NM, May 1978.

5. Teagan, W. P. and Cunningham, D. R., "Conceptual Design and Analysis of a Compound Parabolic Concentrator Collector Array," ANL-K77-3855-1, prepared by Arthur D. Little, Inc., for Argonne National Laboratory, Argonne, IL, August 1977.

6. "Central Receiver Solar Thermal Power System, Phase 1, Pilot and Commercial Plant Cost and Performance," Preliminary Draft No. MDC G6776, Vol. VII, McDonnell-Douglas Astronautics Company, Huntington Beach, CA, May 1977.

7. Powell, J. C., "Solar Pilot Plant Phase I, Preliminary Design Report, Pilot Plant Cost and Commercial Plant Cost and Performance," Report No. F3419-DR-302-III, Vol. VII, Honeywell Energy Resources Center, Minneapolis, MN, June 7, 1977.

8. "Technical Assessment Guide," EPRI PS-866-SR, Electric Power Research Institute, Palo Alto, CA, June 1978.

9. El Gabalawi, N; Hill, G., Bowyer, J. M.; and Slonski, M. L., "A Modularized Computer Simulation Program for Solar Thermal Power Plants," JPL Internal Report 5102-80, Jet Propusion Laboratory, Pasadena, CA, July, 1978.

10. Doane, J. W., et. al, "The Cost of Energy from Utility-Owned Solar Electric Systems, a Required Revenue Methodology for ERDA/EPRI Evaluations," Internal Report 5040-29, ERDA/JPL-1012-7613, Jet Propulsion Laboratory, Pasadena, CA, June, 1976.

11. "The Data Resources Energy Review, Spring and Autumn 1978", Data Resources Inc., Lexington, MA, 1978.

12. Anderson, T.D.; Bowers, H. I.; Delene, J. G.; et al., "Summary Report, An Exploratory Study of Cost Targets for Solar Electric Power Plants," ORNL/TM-5787, Oak Ridge National Laboratory, Oak Ridge, TN, March 1977.

13. Garfield, R., and Davis, C., "Electric Energy Costs of Southwest U.S. Utilities to the Year 2000," Internal Document 5103-62, Jet Propulsion Laboratory, Pasadena, CA., June, 1979.

APPENDIX A

INSOLATION DATA

FOR

SOLAR THERMAL POWER SYSTEMS DESIGN

AND

ECONOMIC STUDIES

CONTENTS

Figures

Tables

I. INTRODUCTION

The evaluation of different thermal power plant design concepts requires a knowledge of the solar insolation available across the continental U.S. This appendix summarizes the various aspects of insolation that must be considered in such evaluations, analyzes the current status of the data relating to these aspects with respect to accuracy and completeness, and discusses the basic information necessary to compare the technical and economic feasibility of various solar thermal power systems.

II. THEORY OF INSOLATION

A. BASIC CONCEPTS

In addition to the actual magnitude of the insolation values, the two aspects of insolation which are of major importance in evaluating solar thermal power systems are its directional and temporal properties.

The radiance of the solar radiation field at a given point in space, $R(\ )$, represents the power per unit area normal to a specified direction, per unit solid angle, and is a function of the direction specified. Outside the earth's atmosphere this radiance has a value of

$$R(\theta) = 1.988 \times 10^4 \quad \frac{kW}{m^2 \text{ steradian}}$$

in the direction of the solar disc, and is essentially zero for other directions.* This value is independent of the sun-earth distance and does not therefore have an annual time dependence. Being a measure of intrinsic solar properties it is also believed to be constant in time over very long periods, although recent studies have suggested possible variations of a few percent over the past few decades.

The solar constant is obtained from the above radiance by integrating over the solar disc at a sun-earth distance of one astronomical unit and has the value of 1.354 kW/m^2. This value is also constant in time and does not depend upon direction.

In contrast to the simple conditions outside the earth's atmosphere, scattering and absorption phenomena result in a much more complex situation for locations at or near the earth's surface. These effects may be summarized by comparing the radiance at the earth's surface with that outside the earth's atmosphere, and such a comparison is shown in Fig. A-1. It is seen that the terrestrial plot of $R(\theta)$ differs from the exoatmospheric plot in having a smaller value across the solar disc (1.5×10^4 kw/m^2 - steradian) and non-zero values for angles away from the disc.

*This is an average value across the solar disc and ignores limb darkening.

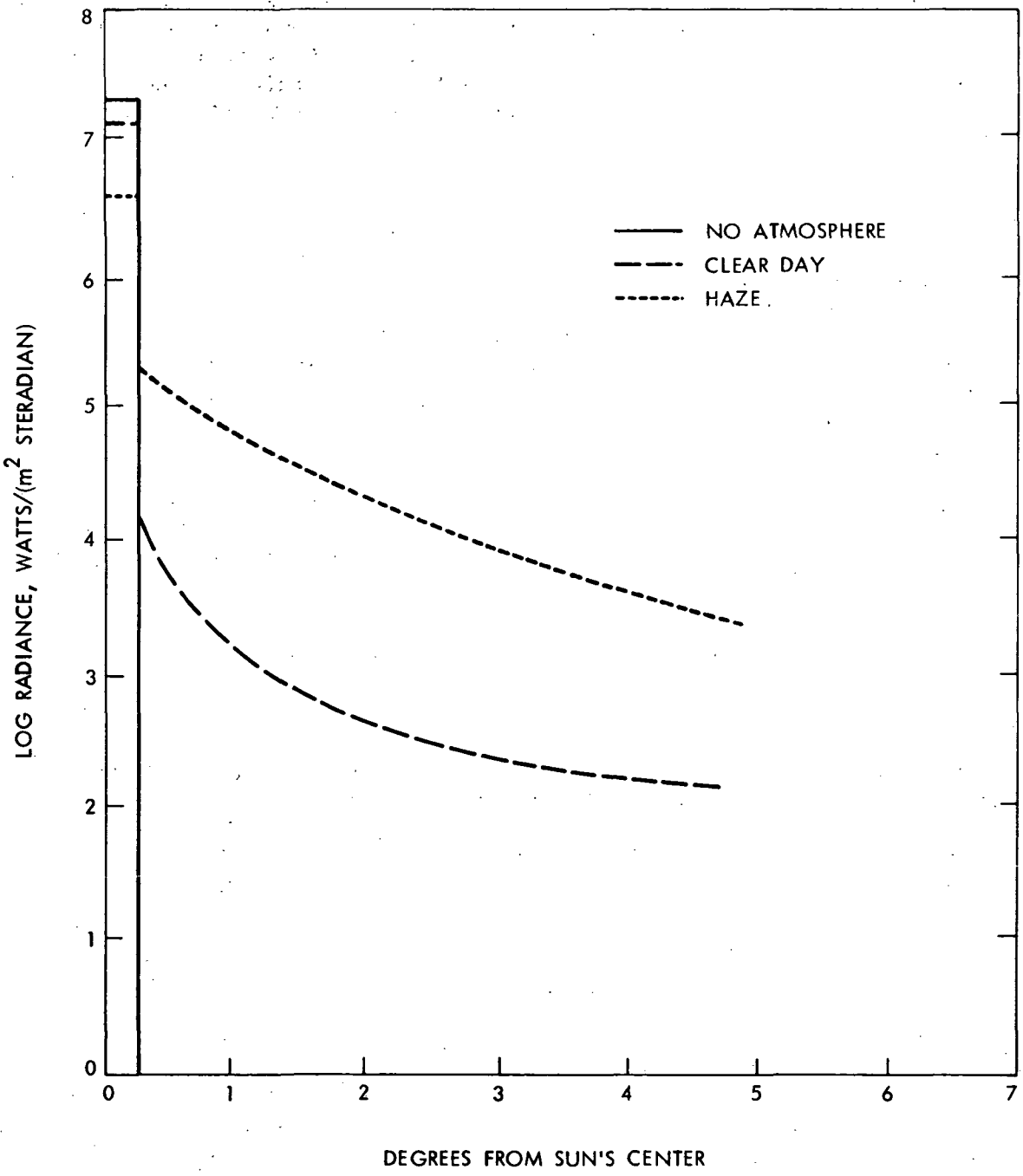

Figure A-1. Radiance of the Sky on and in the Region Surrounding the Solar Disc

The above discussion has dealt with the total power integrated over all wavelengths. Not shown in the comparison of Fig. A-1 is the fact that scattering and absorption produce a wavelength dependence (the sun is yellow, the sky is blue). Also not shown is the fact that the plot has a strong temporal dependence as well as a dependence upon the location on the earth's surface where the measurements are made. The temporal and spatial variations of R( ) are of great importance to solar thermal power system operation and will be discussed in greater detail in Section A-III.

B. INSOLATION MEASUREMENTS

Radiation measuring instruments (radiometers) are designed to measure power levels integrated over some fixed area and solid angle determined by the instrument geometry. The quantity they specify is the power per unit area normal to a specified direction, i.e., the irradiance over the given solid angle.

Insolation instruments differ in the solid angle used and the orientation of the instrument axis relative to the sun's center. They fall into two categories depending upon the values of these parameters.

The pyrheliometer has a relatively small field angle (typically 5^{o}-15^{o}), and is maintained with its axis directed towards the sun by means of a clock-driven equatorial mount. The quantity thus measured is called the direct normal insolation and is related to the radiance shown in Fig. A-1 by the following expression,

$$\int_{\Omega} I_{DN} = \quad R(\theta)\, d\Omega ,$$

where is the solid angle corresponding to the instrument's field angle.

The pyranometer has a 180^{o} field angle and hence measures the insolation over a solid angle of 2 steradians. The orientation of the instrument axis is fixed relative to the local vertical direction and is usually parallel to this direction. In this case, the resulting measure is called the total horizontal insolation or total hemispheric insolation, I_{TH}. Since the direction to the sun's center relative to the local vertical direction has a complex temporal dependence which, in turn, depends upon the geographical location, the relationship between I_{TH} and $R(\theta)$ is no longer simple.

The pyranometer is sometimes used with a shade ring which is mounted so as to prevent the direct radiation from the sun from reaching the instrument's entrance pupil. In this case the instrument measures the diffuse horizontal insolation, I_{dH}.

As can be seen from Fig. A-1, a pyrheliometer with a total field angle of several degrees will measure not only the direct radiation from the sun (field angle $1/2^{o}$), but also a certain amount of diffuse radiation coming from the sky. While generally small, this diffuse radiation which enters the pyrheliometer (called the circumsolar insolation, I_{cs}) can be significant in the presence of strong

atmospheric scattering by water vapor. The dashed curve in Fig. A-1 corresponds to a hazy atmospheric condition and illustrates the strong atmospheric scattering power of water vapor and submicron-size water droplets.

If the irradiance measured by a pyrheliometer with a $1/2^{o}$ field angle is defined as the true direct normal component, I_{DNO}, then the quantities defined above are related as follows:

$$I_{DN} = I_{DNO} + I_{cs},$$

$$I_{TH} = I_{DN} \cos Z + I_{dH}$$

$$= (I_{DNO} + I_{cs}) \cos Z + I_{dH},$$

where: Z = zenith angle of sun.

III. TEMPORAL AND SPATIAL VARIATIONS OF THE INSOLATION OBSERVED AT THE EARTH'S SURFACE

There are a number of different phenomena which produce temporal and spatial variations in insolation, and these will be treated individually in the following sections.

A. EARTH'S ORBITAL ECCENTRICITY

The earth-sun distance varies between 1.47×10^{8} km (perihelion - Jan. 3) and 1.52×10^{8} km (aphelion - July 5) causing the apparent diameter of the solar disc to vary from 32.55' to 31.48'. A focusing collector with a field angle slightly larger than the former value, aimed at the disc's center will thus detect an annual variance in irradiance of about $\pm$ 3.4% from this cause.

B. DIURNAL VARIATION

In the absence of an atmosphere, a focusing collector continuously aimed at the solar disc would measure a nearly rectangular time dependence for the irradiance from sunrise to sunset. The effect of the atmosphere is twofold. First, atmospheric refraction extends the length of a day by about 4.5 minutes in the continental U.S., and second, atmospheric absorption and scattering round off the rectangular shape to produce typical clear-day curves such as those shown in Fig. A-2 for the direct-normal component.

C. LATITUDE AND SEASONAL EFFECTS

In the absence of atmospheric effects, the direct normal irradiance integrated over an entire year would be the same anywhere on earth, neglecting the aforementioned orbital distance effect. Long summer days would be balanced by short winter days. However, since the average zenith angle for the sun is greater at higher latitudes, absorption and scattering are more pronounced at such locations. This effect alone causes the annual average clear-day values of direct-normal irradiance in the northern part of the country to be some 20% lower than those in the southern part [A-1].

The geometrical relationship between the sun's position in the sky and the latitude of the observer also leads to greater extremes in the number of daily hours of possible sunshine in northern latitudes than in southern latitudes. Thus, for example, the extreme lengths of summer and winter days at 35°N latitude are approximately 14 and 10 hours respectively, while at 42°N latitude they are about 15 and 9 hours; cf. (a) and (b) of Figure A-2.

D. ATMOSPHERIC TURBIDITY

Absorption and scattering processes in the earth's atmosphere may be classed conveniently into essentially constant effects and time and position dependent effects. The former include absorption and scattering due to dry air and ozone and the latter, that due to water vapor and dust.

The term turbidity refers to the amount of absorption and scattering by aerosols, and includes effects due to dust particles at both high and low altitudes. Both water vapor and low-altitude dust concentrations show marked annual as well as geographical variations. In each case, the concentration is higher in summer than in winter. Water vapor concentration is high for the southeastern states and low for the non-coastal northwestern, while low-altitude dust concentrations tend to be high in the eastern part of the country and low in the western [A-1].

Superimposed on this is the effect of high-altitude dust particles. The primary source of these is volcanism, and their concentration has shown considerable variation over the years.

Variations in lower atmospheric turbidity cause direct-normal irradiance values in the east to be some 20% lower than those in the west, while water vapor concentration variations result in variations of only a few percent [A-1].

Upper atmospheric turbidity variations caused by volcanic activity result in overall average direct-normal irradiance variations of approximately 5-10% with some changes amounting to greater than 30% (Krakatoa) [A-1].

E. CLOUD COVER

Cloud formation and distribution show strong temporal and geographical variations and clouds result in a major reduction of the direct-normal component. In the absence of clouds, the cumulative effect of the phenomena discussed above is a reduction of the average clear-day direct-normal component by about 25-30% in going from the southwest to the northeast. The lower percentage of sunshine due to clouds results in the values in the northeast that are less than half those in the southwest and drastically alters the geographical and temporal distributions of insolation over the United States.

Variations in average cloud cover at various locations throughout the country show both short term (monthly) and long term features. Typically, the former amount to some ±15% while variations over periods of a few years are about 10% [A-1].

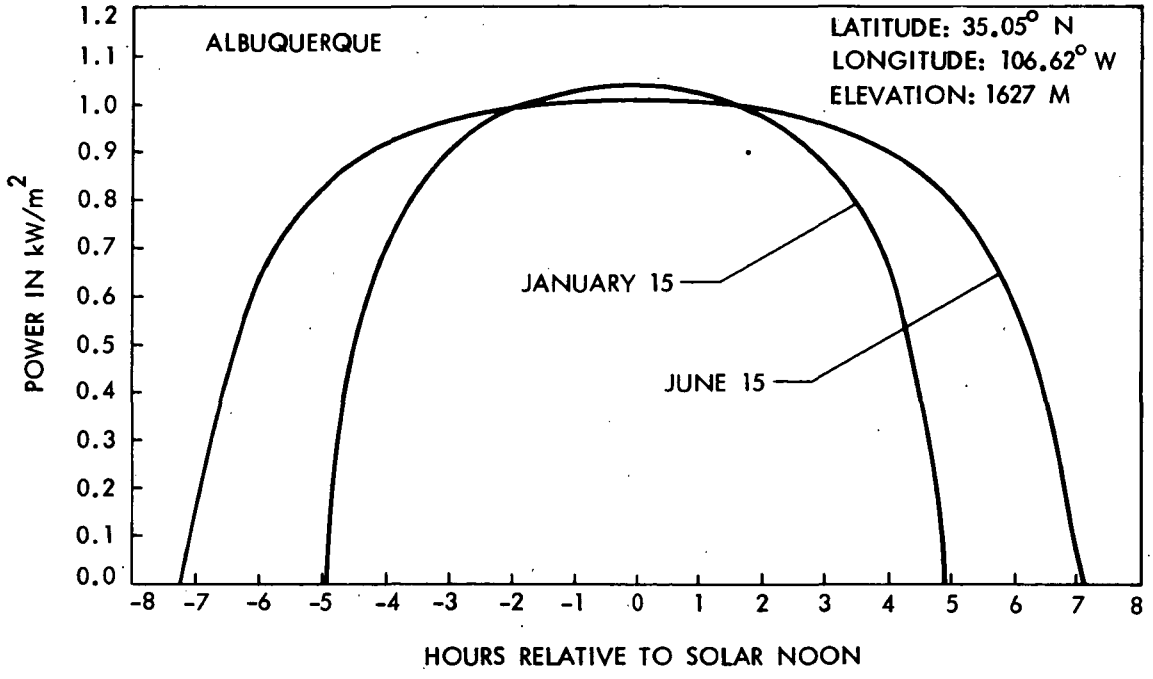

(a)

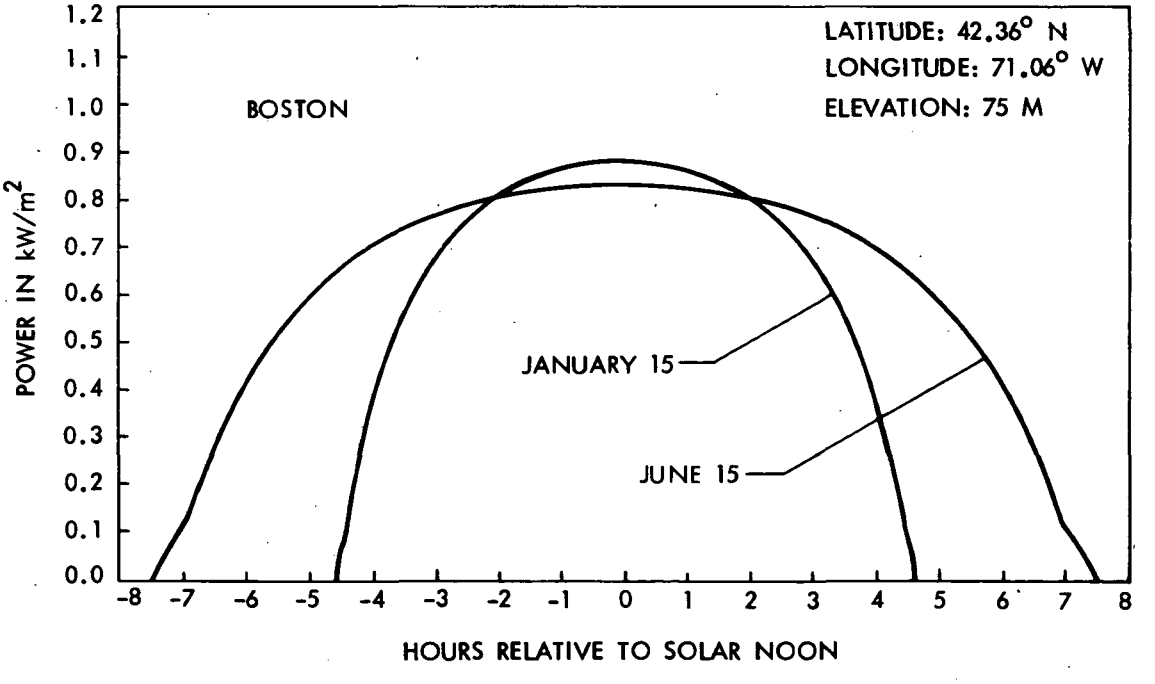

(b)

Figure A-2. Typical Temporal Variation of Solar Insolation on Selected Clear Days at Two Different Sites

F. DISCUSSION

Owing to the nonstationary nature of the statistics inherent in the I_{DN} versus time curve, it is not possible to determine true averagesfor any finite time interval because such average values will depend in a random way upon the time selected. Accordingly, caution must be exercised in using data based upon averages formed during a particular time interval because they may not be representative of those formed during a different interval.

One may nevertheless consider the I_{DN} curve to have certain characteristic time dependences resulting from the phenomena described in the previous sections, and an understanding of these is essential in considering the influence of solar insolation on solar thermal power plant operation.

Figure A-3 shows a typical I_{DN} curve for thirty days of one month. The non-stationary nature of the statistics is evident in this figure.

IV. INSOLATION DATA

A. INTRODUCTION

Although many insolation measurements have been made at a large number of sites across the United States and over a period of many years, very few data of the kind and accuracy required for the engineering analysis of solar thermal power plants are available. The main reason for this circumstance is that very few measurements of I_{DN} exist; in the past, agricultural and other land use considerations favored the measurement of I_{TH} rather than I_{DN}.

This situation has been further compounded by the fact that large errors have been found to exist in much of the total horizontal insolation data [A-2] and some of the limited direct-normal data available [A-3].

The following sections summarize the current situation with respect to these data.

B. DIRECT NORMAL INSOLATION DATA

Since high-efficiency operation of a solar thermal plant dictates the achievement of high receiver temperatures with the concomitant need for precise focusing of the direct-normal term, there exists a need for reliable I_{DN} data at many locations across the country.

The measured data which exist may be divided into those which have been gathered by the National Weather Service and archived by the National Climatic Center (NOAA data*) and those gathered by other sources.

*NOAA - National Oceanic and Atmospheric Administration, Dept. of Commerce

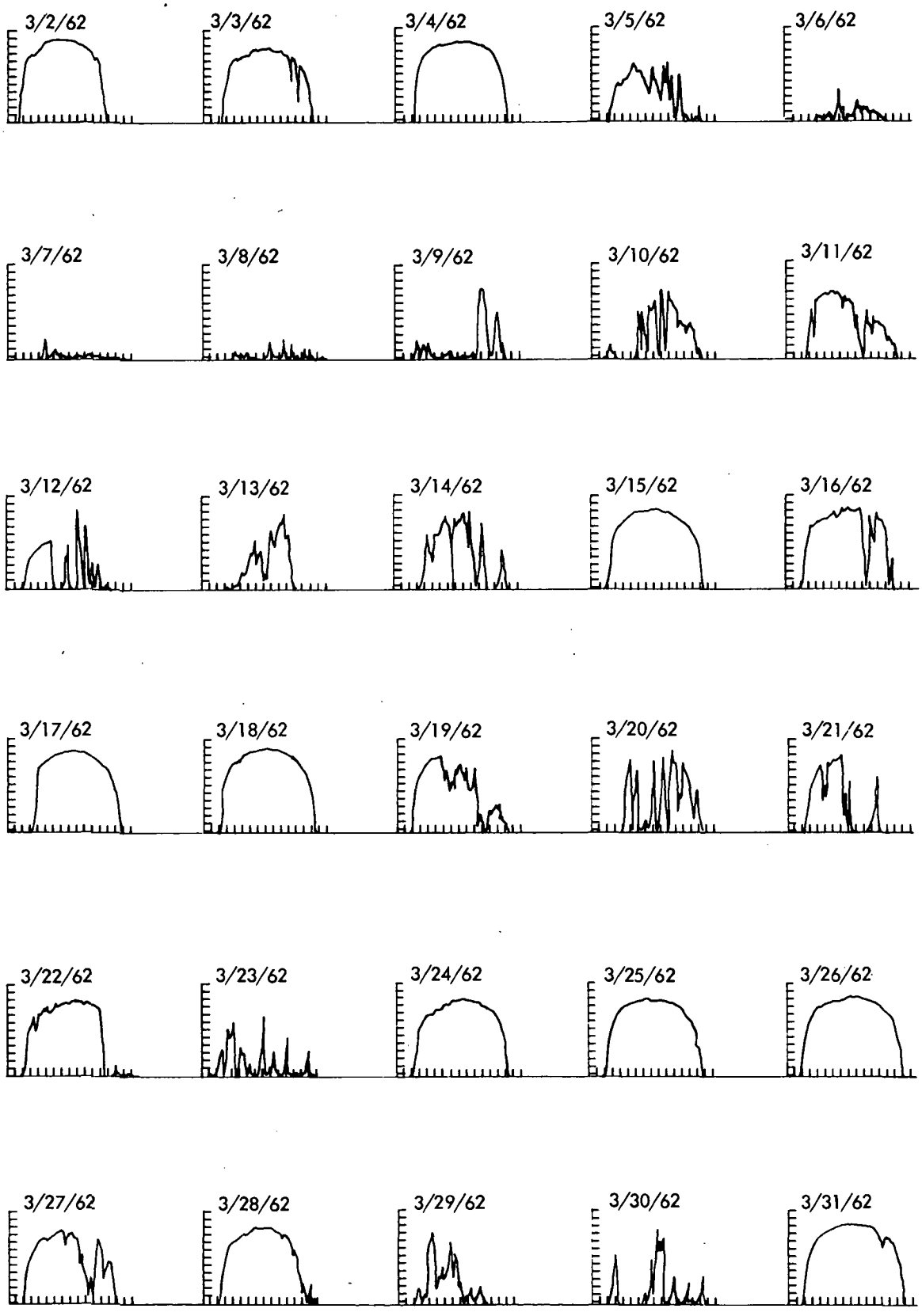

Figure A-3. Direct Normal Solar Insolations as a Function of Time During January 1962 at Albuquerque, NM

In addition to the NOAA network stations, there are some 80 locations where total horizontal measurements are being taken by various governmental, state, and private organizations. Some of these data are being archived by the NCC, but most are not, and individual sources must be contacted in order to obtain information [A-4].

V. INSOLATION MODELS

A. INTRODUCTION

The paucity of adequate high-quality data has prompted a number of workers to develop insolation models based upon different assumptions and different kinds of data. In spite of the complexity of the problem and the limited measured data available, certain of these modeling techniques are quite successful and, in fact, provide what is probably the best means presently available for determining accurate insolation values on an hourly basis at various locations throughout the country. An indication of the success of these modeling methods is the fact that one of them is currently being used by the NWS in its quality control program for the NOAA network data. Thus, if measured data are found to differ from the model predictions by more than 5%, the data are re-examined for errors [A-5].

The following paragraphs give brief descriptions of the bases for several of these models and assess their usefulness with respect to solar thermal power plant design and economic studies.

B. WATT MODEL

Watt Engineering, Ltd., has constructed an insolation model for the direct, total, and diffuse components which is relatively simple and quite accurate [A-6]. It is based upon an analysis of the physical processes involved in the scattering and absorption of radiation by the earth's atmosphere and takes into account all of the phenomena felt to be significant in determining the actual values of insolation received at a given location at a given time.

The model relies upon a minimum of assumptions and, aside from basic data on dry-air scattering and absorption, exoatmospheric radiance, and geometrical factors, utilizes as input only data on upper and lower atmospheric turbidity, water vapor and cloud cover.

One of the strongest features of the model, aside from its excellent agreement with measured average insolation values, is that it can be used to generate accurate clear-day I_{DN} versus time curves for the analysis of solar thermal systems. With the addition of a more refined handling of cloud statistics, it could also produce such curves for cloudy days. Such an approach would enable the construction of a realistic data input for any location in the country at any given time and, hence, could provide the best means of system evaluation for different sites.

Another strong point is that it does not rely on total insolation data of questionable accuracy in order to compute the direct normal component. It does, however, rely upon monthly averages for water vapor and turbidity data and does not therefore take into account more rapid fluctuations in these quantities.

Figures A-4, A-5, and A-6 present respectively the results obtained by Watt Engineering, Ltd. for direct normal, diffuse horizontal, and total horizontal insolation. These figures have been reproduced from Ref. A-1. A comparison of the annual average daily direct normal insolation characteristics tabulated as Table 1 in the body of this report (and reproduced here as Table A-1) with Figure A-4 shows a fairly close agreement of corresponding values.

C. AEROSPACE MODEL

Randall and Whitson [A-6] have constructed a model for determining hourly direct-normal insolation values from hourly data regarding total horizontal insolation. While the procedure works quite well, it suffers from the generally poor quality of the available I_{TH} data used as the input.

The procedure is based upon a statistical analysis of the correlation between hourly direct-normal measurements and simultaneously measured values of total horizontal insolation. The data used to construct the model enable the calculation of annual average direct normal insolation values from total insolation data with an accuracy of 4%, provided the input data are at least this good.

However, when applied to the rehabilitated NOAA data for 24 locations in the U.S., the uncertainty in the results is believed by the authors to be 10%. Like the Watt model described above, the Aerospace model permits the calculation of statistically correct I_{DN} versus time curves for both clear and cloudy days and, hence, may also be used for solar thermal system analysis. It is these computed hourly values of I_{DN} which appear on SOLMET tapes produced since April 1978 for the six NWS stations listed in Table A-1.

Figure A-7 presents a comparison of annual average daily direct insolation contours as determined by the Aerospace Model with those determined by the Watt Model. This figure vividly illustrates the magnitude of the currently existing uncertainties in an input parameter that is critically important to proper site selection and subsequent evaluation of the solar thermal power system whose operation is estimated at that site. The existence of geographic subregions in which annual average daily direct insolation levels are especially favorable or unfavorable is suggested by Figure A-7, but the figure clearly shows that much better definition of these subregions is urgently needed.

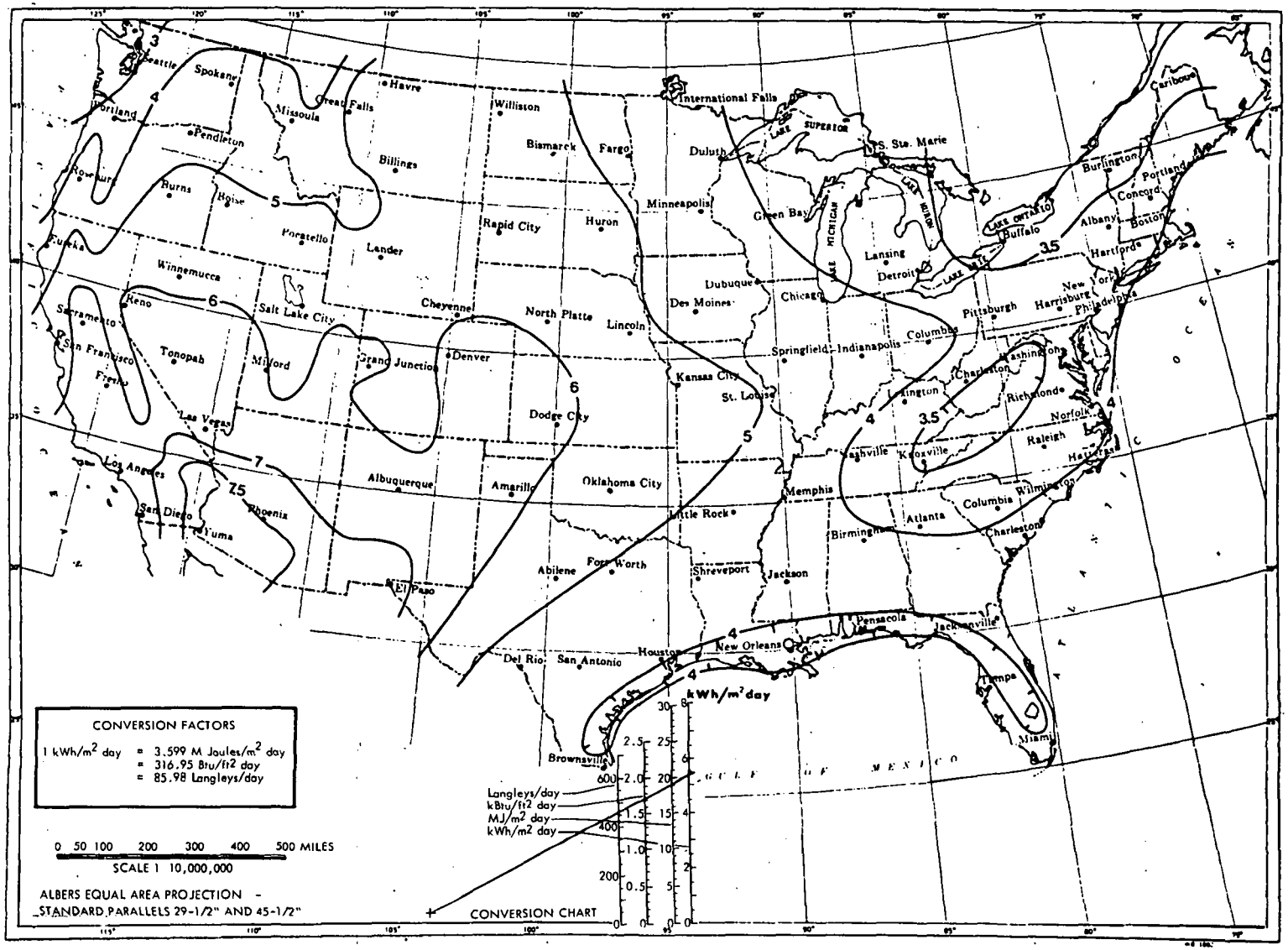

Figure A-4. Annual Average Daily Direct Normal Insolation in the United States as Presented by Watt Engineering, Ltd.

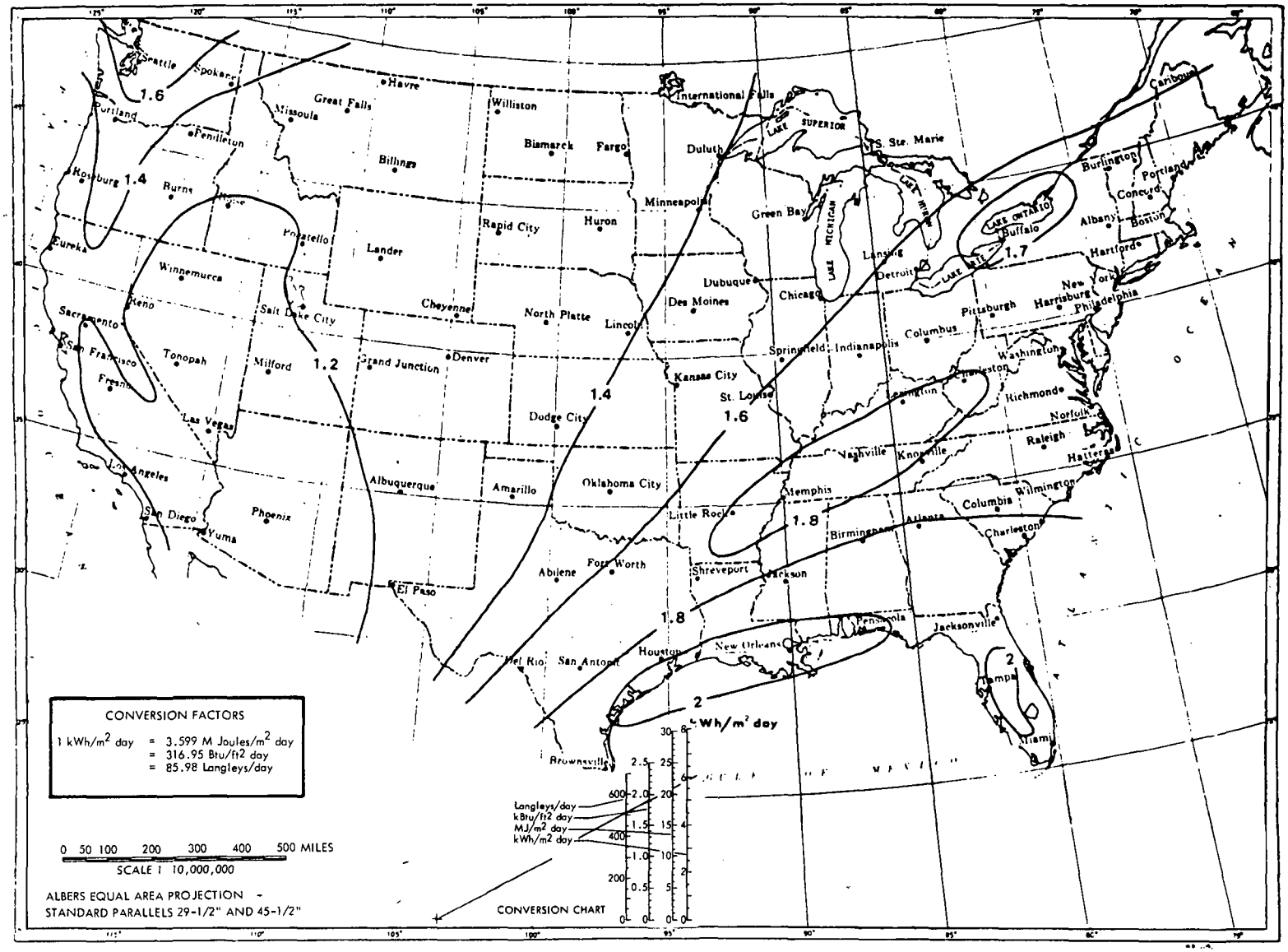

Figure A-5. Annual Average Daily Diffuse Horizontal Insolation in the United States as Presented by Watt Engineering, Ltd

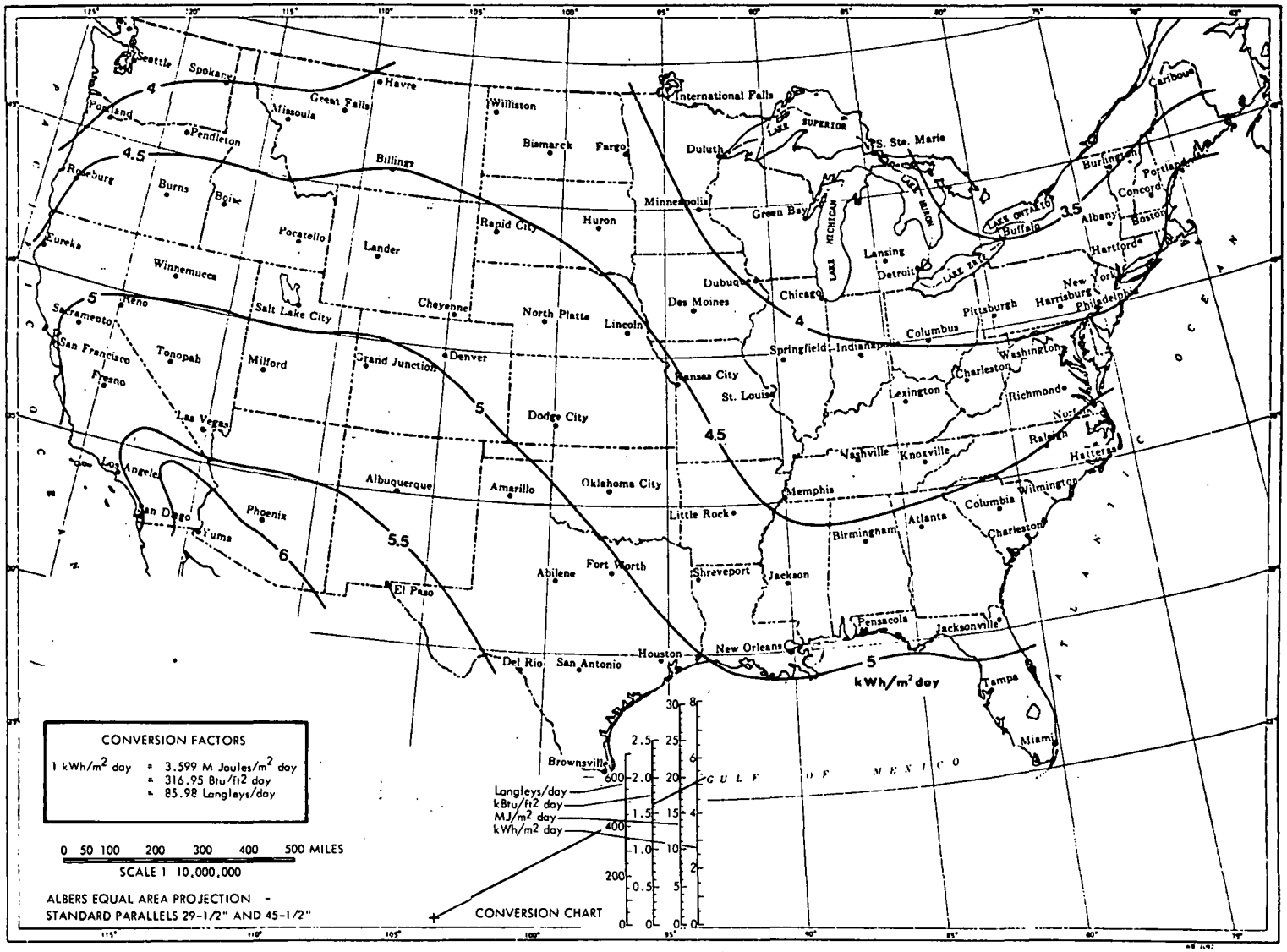

Figure A-6. Annual Average Daily Total Horizontal Insolation in the United States as Presented by Watt Engineering, Ltd

Table A-1. Insolation Characteristics of Chosen Sites

Location (year)*	Annual Total Direct Insolation kWh/(m^2y)	Annual Total Hours of Direct Insolation h/y	Annual Average Daily Direct Insolation kWh/(m^2d)	Annual Average Hourly Insolation (Based on Hours of Direct Insolation) kW/m^2
Barstow, CA (1976)	2848	4494	7.781	0.6337
Albuquerque, NM (1975)	2538	4300	6.953	0.5902
Omaha, NB (1974)	1688	4263	4.625	0.3960
Medford, OR (1973)	1602	4326	4.389	0.3704
Miami, FL (1975)	1424	4138	3.901	0.3442
Cape Hatteras, NC (1973)	1421	4094	3.893	0.3471
Madison, WI (1971)	1298	4143	3.556	0.3132
Maynard, MA	1253	2813	3.433	0.4456

*Year in which insolation data was taken.

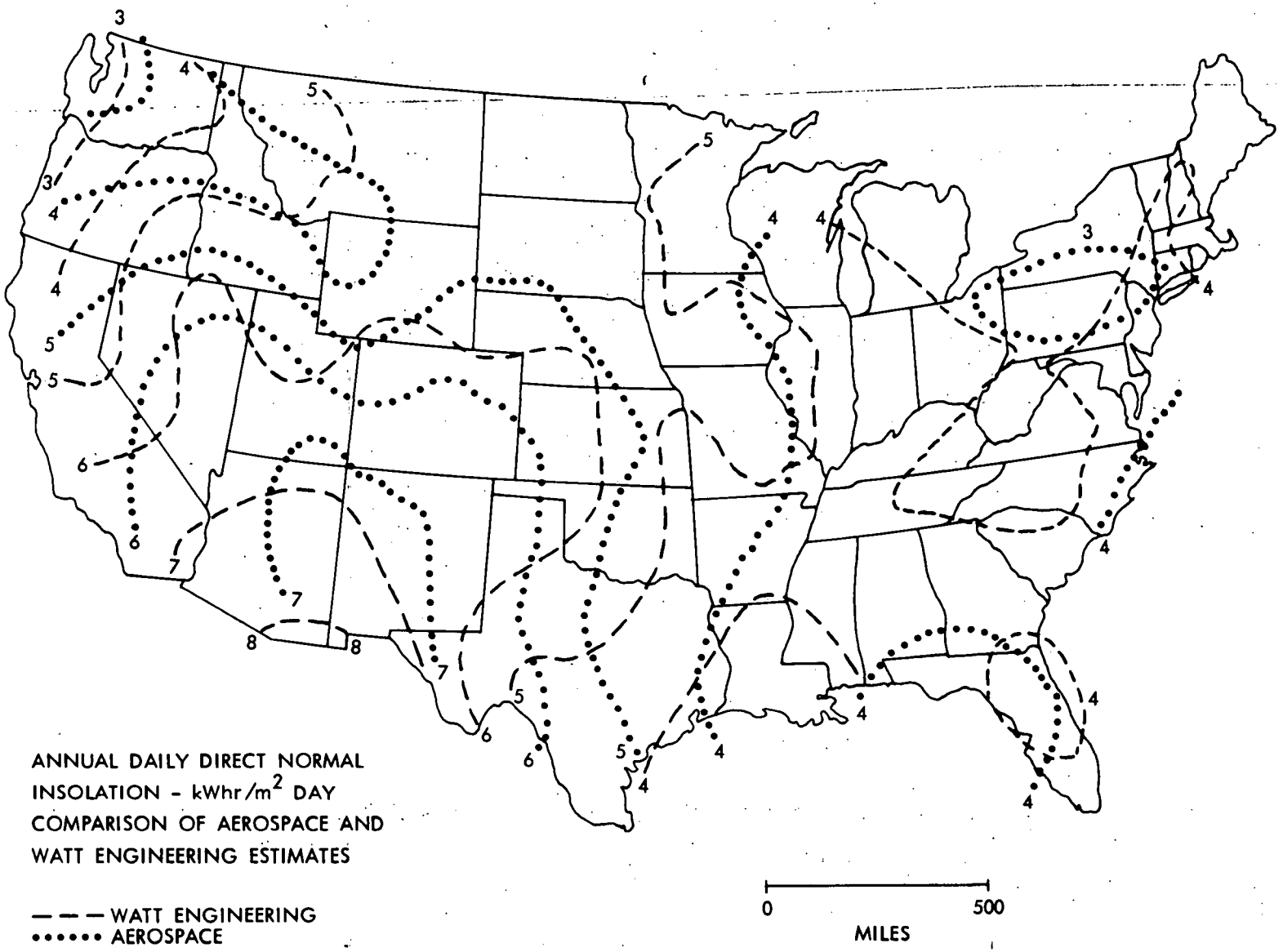

Figure A-7. Annual Average Daily Direct Insolation Contours as Determined by the Aerospace Model and by the Watt Model

D. LIU AND JORDAN MODEL

In the Liu and Jordan approach, observed statistical correlations between monthly average values of the daily diffuse horizontal and daily total horizontal insolation values, betwen hourly diffuse radiation and solar time, and between hourly total radiation and solar time, are used to calculate average hourly values of direct, diffuse, and total insolation on surfaces of arbitrary orientation. The input data to the model are observed monthly average daily total horizontal insolation values for the specific location considered [A-7].

While the model yields hourly data, these data are for average days and, hence, do not reproduce the temporal effects due to clouds. Also, it is subject to the same limitations as the Aerospace model through its dependence upon observed I_{TH} values. Thus, while the hourly time dependence is not realistic enough for system dynamic analysis, the data may be averaged to yield insolation maps for various time periods.

E. THE HOYT MODEL

Hoyt [A-8] has recently published model calculations similar to but more detailed than those of Watt. These calculations use measurements of turbidity, precipitable water vapor, and surface albedo of the earth as input data, and result in clear day solar noon total hemispheric insolation values that agree with calibrated pyranometer readings to within 2.7%. The agreement between the model and the measurements is well within the instrumental error of. ±5%.

These calculations have been used by NOAA to rehabilitate the total insolation data from 26 NWS stations in the network and, as mentioned in the introduction to this section, are also used as a means of quality control of the data.

The model has also been used to calculate daily average clear-day values of I_{TH} as well as monthly mean values of I_{TH} (including clouds). In all cases the agreement with measured values is within the pyranometer error.

While the model has good accuracy, it does not permit the calculation of hourly values of I_{TH}, either with or without clouds, nor does it permit the calculation of I_{DN}, although it could be modified in such a way as to include these cases.

F. METHODS FOR GENERATING CONTOUR MAPS

The question of the effect which different interpolation schemes have on contours produced from a given data set does not appear to have been considered by those presenting such maps because little or no mention is generally made as to which of the many possible methods for generating contours has actually been used. The discussion which follows presents some of the basic problems that should be considered and provides a number of specific examples which demonstrate the

rather large variations that can be obtained by using different methods for the generation of contour maps. At present, there does not appear to be any generally accepted criterion which would clearly indicate which method should be chosen to the exclusion of all others.

Two basic approaches may be used to generate contours from a given set of randomly distributed points at which z-values are specified. In the first, the points are interconnected to form a net of triangles and points on the contour lines are determined by linear interpolation of the z-values along each of the sides of each triangle. Common z-value points are then joined by a smooth curve. The second approach begins by fitting a smooth surface to the z-values given, and then drawing the contours.

In the first approach, there is ambiguity in the choice of interconnections in that there is no unique way to join a set of randomly distributed points to form triangles. Thus, different sets of triangles will result in different contours. Also, any of several different methods can be used to draw smooth curves through the common z-value points found by interpolation and, generally speaking, each different method will result in a slightly different set of contours.

In the surface fitting approach, all of the ambiguity is concentrated in the surface fitting algorithm since, once a smooth surface is obtained, the contours are unique.*

The number of ways a smooth surface can be fitted to a randomly distributed set of z-values is virtually unlimited. Some common methods employ splined cubic functions while others adapt an iterative approach in which the surface is constrained by some simple partial differential equation (Poisson's equation, the biharmonic equation). Even with a given method, the resulting surface and, hence, the contours depend upon the exact manner in which the algorithm is applied. For example, one method of fitting a splined cubic function involves the initial formation of a triangular net, as in the linear interpolation scheme described earlier. Since the polygon formed in the (x,y) plane must be convex in this method, one must usually supply additional data points to accomplish this, and since these points must themselves be determined by some method of interpolation or estimation, an additional uncertainty is introduced into the final contour map. Actual computer runs show that such schemes tend to produce questionable edge effects which depend upon the exact choice made for assigning z-values to the extra points.

Another important consideration that enters into the surface-fitting problem is the extent to which the final surface actually coincides with the original data points. Many techniques of smoothing introduce departures from a perfect fit unless the algorithm

*Actually, one may view the triangle method as a crude surface fit which would produce a unique set of linearly segmented contours.

explicitly prevents this by constraining the surface to pass through the original points as the iteration proceeds. Such departures may or may not be desirable depending on the data and the purpose for which the contours are to be used. For example, if, as is often the case, the existing data constitute a severely under-sampled set, a smoothed surface which does not necessarily provide a perfect fit might be more representative of average trends than one which does. For example, a random sampling that happens to select adjacent high and low z-values would lead to unrepresentative contours if the surface were constrained to pass through these points.

The above discussion suggests an approach to surface fitting based upon Fourier theory analogous to that used when the data points form a periodic lattice. Such an approach is briefly described in the following paragraphs.

A given set of randomly distributed z-values may be represented by the following sum,

$$z(x,y) = \sum_{i=1}^{N} z_i \; \delta(x - x_i) \; \delta(y - y_i),$$

where:

z_i = value of Z(x,y) at the point (x_i, y_i),
$\delta(x)$ = Dirac delta function,
N = number of data points.

The Fourier spectrum of this set of weighted -functions is:

$$\tilde{z}(\kappa_x, \kappa_y) = \int\int_{-\infty}^{\infty} \left[\sum_{i=1}^{N} z_i \; \delta(x - x_i) \; \delta(y - y_i) \right] e^{-i(\kappa_y \chi + \kappa_y y)} dxdy$$

$$= \sum_{i=1}^{N} z_i e^{i(\kappa_x \chi_i + \kappa_y y_i)} \quad ,$$

where:

κ_x = spatial frequency in x-direction,
κ_y = spatial frequency in y-direction.

If the average separtion between data points in the x-direction is Δx, and that in the y-direction is Δy, and we choose to construct a surface z'(x,y) such that the given points constitute an average Nyquist sampling of this surace, then the maximum spatial frequencies that the Fourier spectrum of the surface can have in the x and y directions are:

$$\kappa_{xm} = \frac{\Pi}{\Delta x} \quad , \kappa_{ym} = \frac{\Pi}{\Delta y} \; .$$

Thus, if we apply a low pass filter $F(\kappa_x, \kappa_y)$ having cutoff frequencies of κ_{xm} and κ_{ym} to the spectrum of our original set of weighted -functions, we obtain:

$$\tilde{z}'(\kappa_x,\kappa_y) = \tilde{F}(\kappa_x,\kappa_y)\ \tilde{z}(\kappa_x,\kappa_y),$$

and taking Fourier transforms we find:

$$z'(x,y) = \sum_{i-1}^{N} z_i F(x - x_i,\ y - y_i),$$

where:

$$F(x,y) = \text{Fourier transform of } \tilde{F}(\kappa_x,\ \kappa_y).$$

We are thus left with a surface formed by replacing each original x-value by the spatial domain filter F(x,y) multiplied by that z-value. For example, if $F(\kappa_x, \kappa_y)$ is a Gaussian function, then F(x,y) is also a Gaussian, and the surface z'(x,y) is a weighted sum of Gaussians. Clearly, our filter should be chosen so that these overlap as little as possible if the surface is to pass through the original z-values, and we must also choose our filter such that F(0,0) = 1, that is, we must demand that

$$\frac{1}{4\Pi 2} \int_{-\infty}^{\infty}\int \tilde{F}(\kappa_x,\ \kappa_y)\ d\ \kappa_x d\kappa_y = 1$$

and

$$F(x_n - x_i,\ y_n - y_i) << 1, \text{ for all } i,\ n.$$

The above procedure can be expected to provide a representative surface fit provided there is no clustering of points in the (x,y) - plane. A clustering will cause strong overlap of the functions $F(x - x_i,\ y - y_i)$, resulting in abnormally high values in the region where the clustering exists. Also, the choice of a filter function must be made so as to avoid ringing on the one hand ($F(\kappa_x, \kappa_y)$ too steep near cutoff) and a non-smooth surface on the other (F(x,y) a box filter, for example). A Gaussian function appears to be a natural choice. The clustering problem can be handled by departing from linear filter theory and directly applying a spatially dependent filter in the spatial domain by means of convolution. Then, each point will have its own filter chosen so as not to overlap those of neighboring points, thus giving explicit recognition to the fact that the sampling represented by the original data set is non-uniform, i.e., some regions contain more information than others.

In order to assess the confidence that one should have in an insolation contour map produced from a given set of data by a given surface fitting/contouring technique, a series of maps has been prepared from two different data sets by a number of different techniques so that the reader may compare these and judge for himself what limits to place on conclusions drawn from one map or another.

The two data sets used in the study are the Watt Engineering Ltd. estimates of direct normal insolation, and the Aerospace Corp. estimates of direct normal insolation, cf., Sections B and C above. Annual averages based on approximately 25 years of recent data have been used in producing both the Watt and Aerospace contour maps. Figures A-8 and A-9 show a comparison of contours produced from Watt and Aerospace data by means of simple linear interpolation. Although the general trends are similar, the two maps differ considerably in detail. Figures A-10 and A-11 show contours produced from the same two data sets by fitting a splined cubic function to the given data points. Again, there is considerable difference in the contours. A comparison of Figure A-8 with A-10, and Figure A-9 with A-11 shows the different effects which these two contouring methods have on the results, and while the differences are smaller than those due to the different data sets, they are still quite apparent.

Figures A-12, A-13, and A-14 present the results of applying various low pass filters to surfaces produced from the Watt data by a growth procedure wherein a discontinuous surface is first produced by assigning to each (x, y) point the z value corresponding to the nearest data point. It is seen here that one may obtain significantly different contours depending upon the degree of smoothing provided by the filter. The intermediate filter (Fig. A-13) corresponds approximately to an average Nyquist sampling, and the problem associated with clustering has been handled by applying low pass filters to the discontinuous surface produced by the growth procedure rather than to the set of weighted δ-functions represented by the original data. This prevents excessively high values from appearing in the final surface and permits the use of a simple box filter.

Figures A-15, A-16, and A-17 show the results of applying the same technique to the Watt data, where Figure A-16 corresponds to an average Nyquist sampling. The effect of the higher sampling rate of the Watt data is clear from a comparison of Figures A-12, A-13, and A-14 with Figures A-15, A-16, and A-17.

The maps shown in Figure A-12 to A-17 were generated at the Image Processing Lab (IPL) at JPL, and illustrate the power of this facility in producing such contoured surfaces. An additional benefit provided by IPL techniques can be seen in the continuous gray scale representation shown in the figures; this gray scale provides a graphic display of the surface, and, hence, of the actual insolation values represented by the filtered data. Such contour maps can be generated quickly and inexpensively once the original U.S. map has been produced and stored; thus, new data may be incorporated readily into new maps.

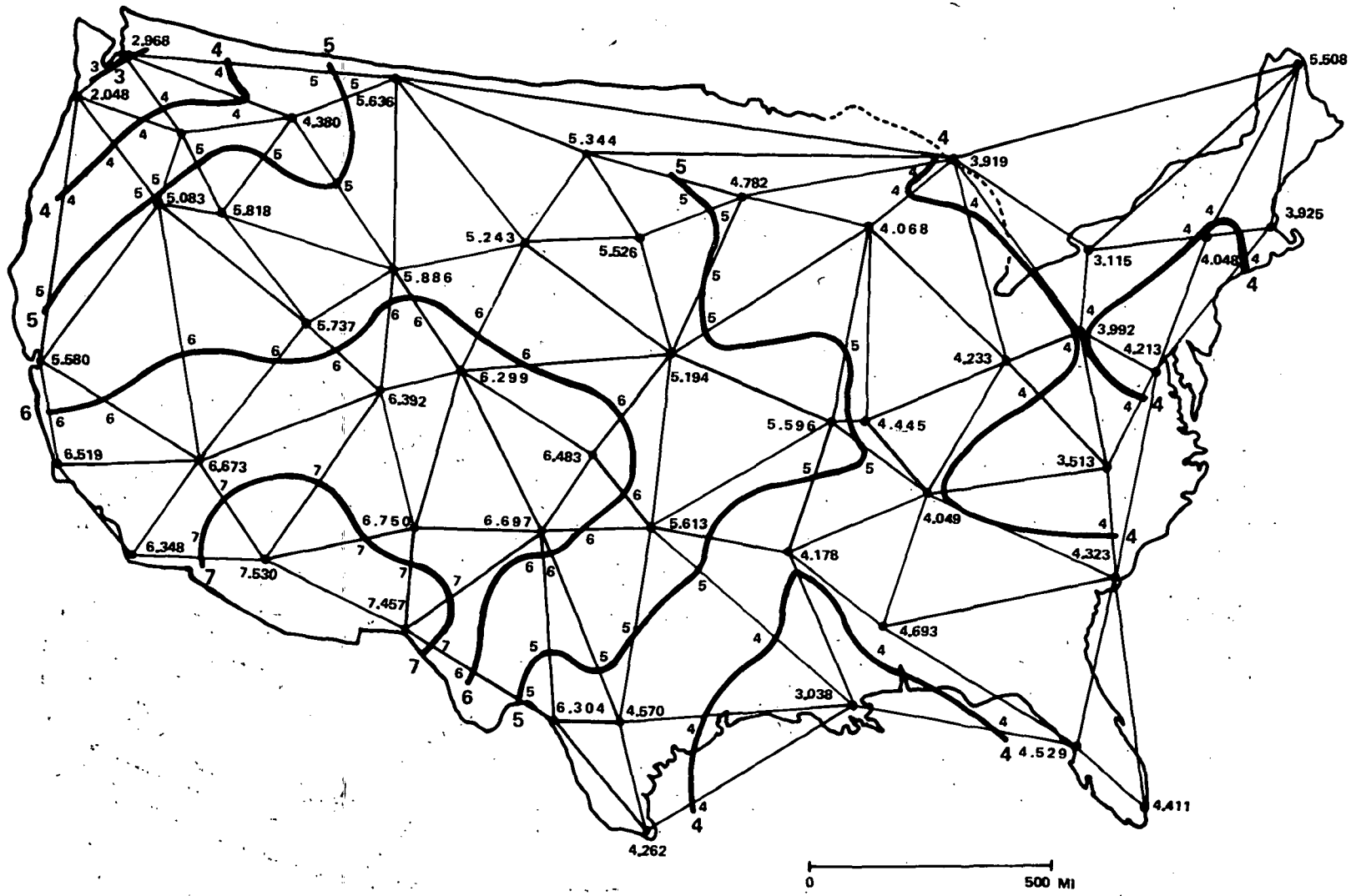

Figure A-8. Annual Mean Daily Direct Normal Insolation
(Watt data, linearly interpolated)

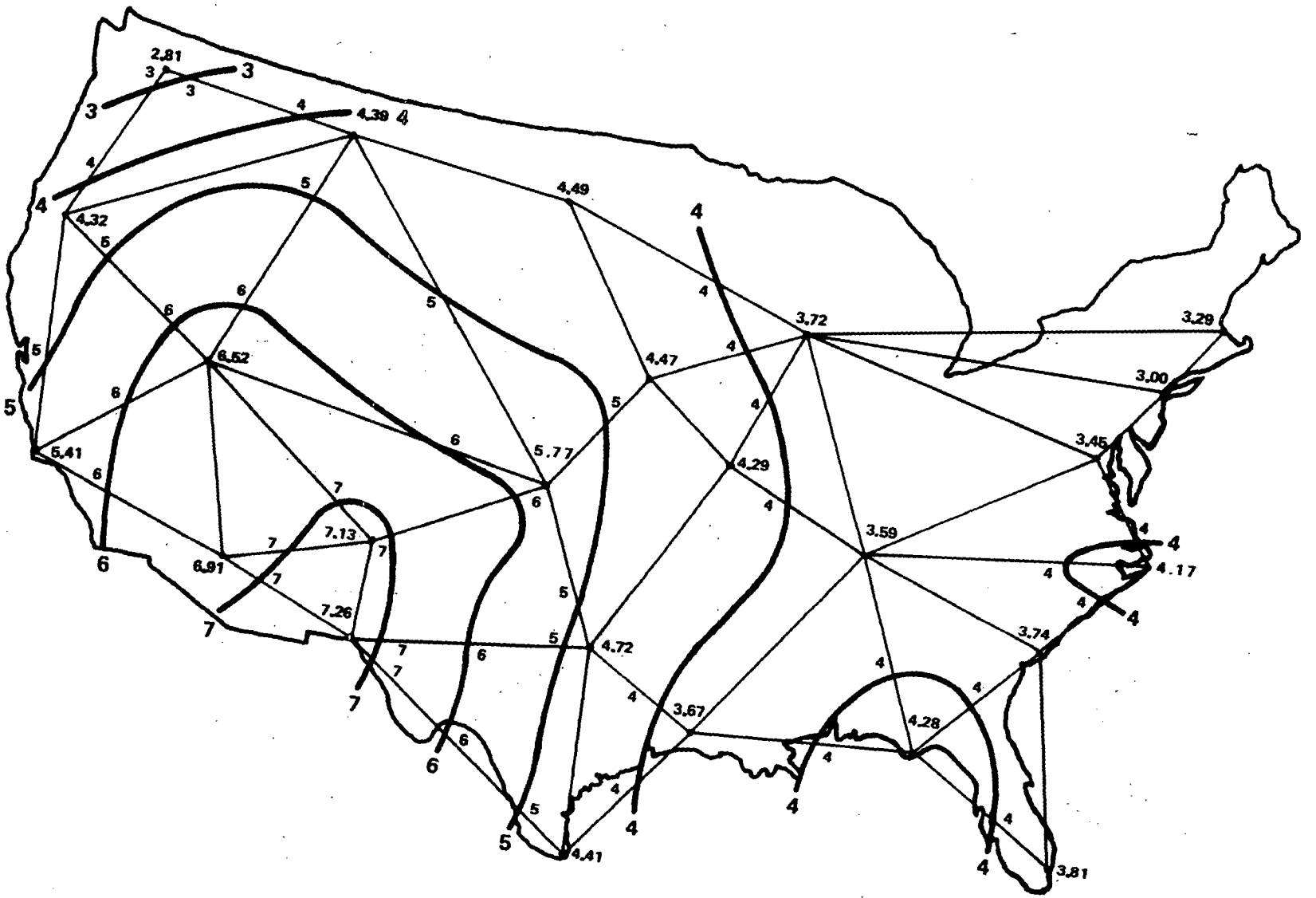

Figure A-9. Annual Mean Daily Direct Normal Insolation (Aerospace data, linearly interpolated)

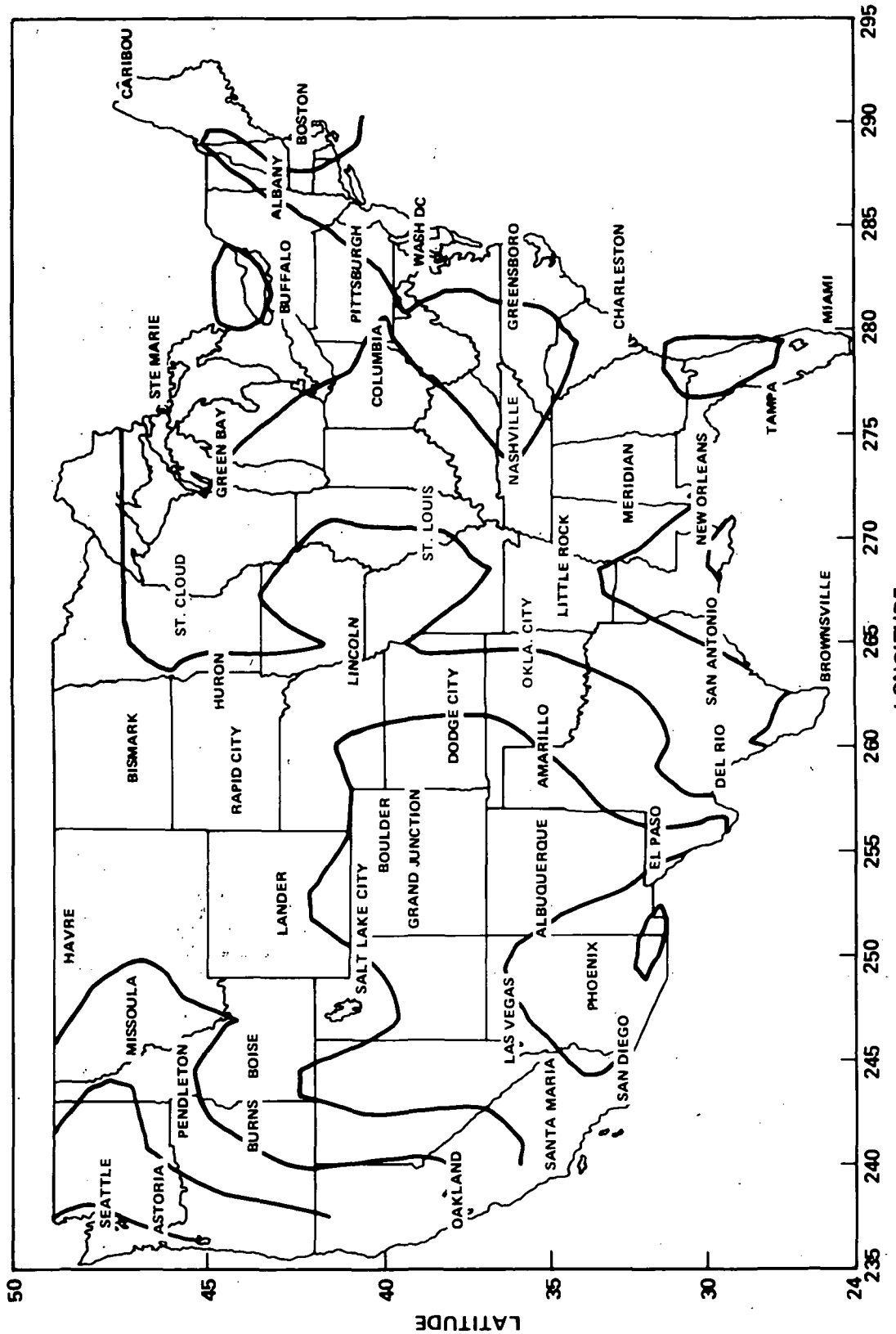

Figure A-10. Annual Mean Daily Direct Normal Insolation (Watt data, cubic spline fitted)

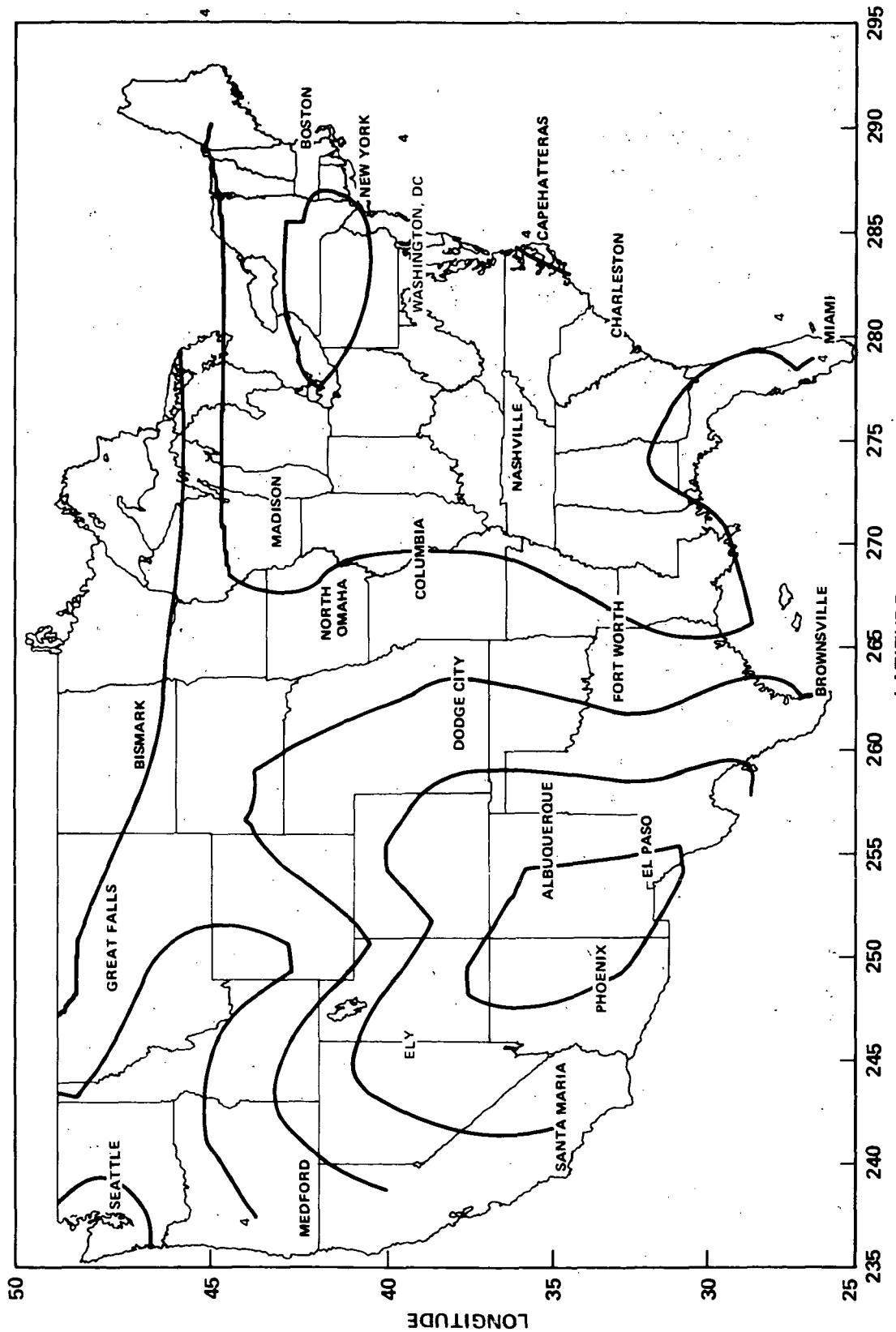

Figure A-11. Annual Mean Daily Direct Normal Insolation (Aerospace data, cubic spline fitted)

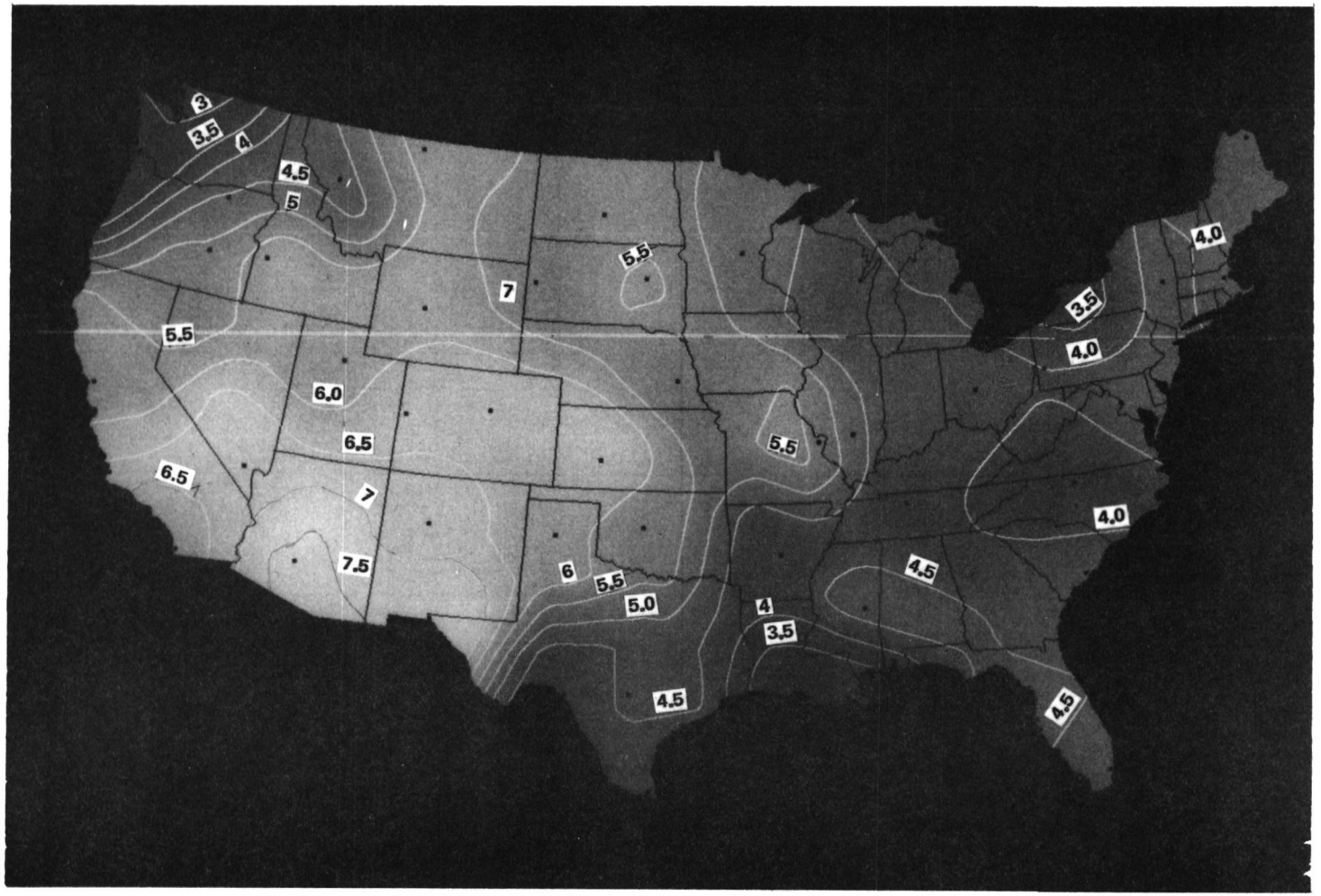

Figure A-12. Data Based on Watt Engineering, Ltd. Estimate of Direct Normal Insolation. The Degree of Smoothing of the Surface Increases in Going from Figure A-12 to Figure A-14, Figure A-13 Corresponding Approximately to an Average Nyquist Sampling (See Text).

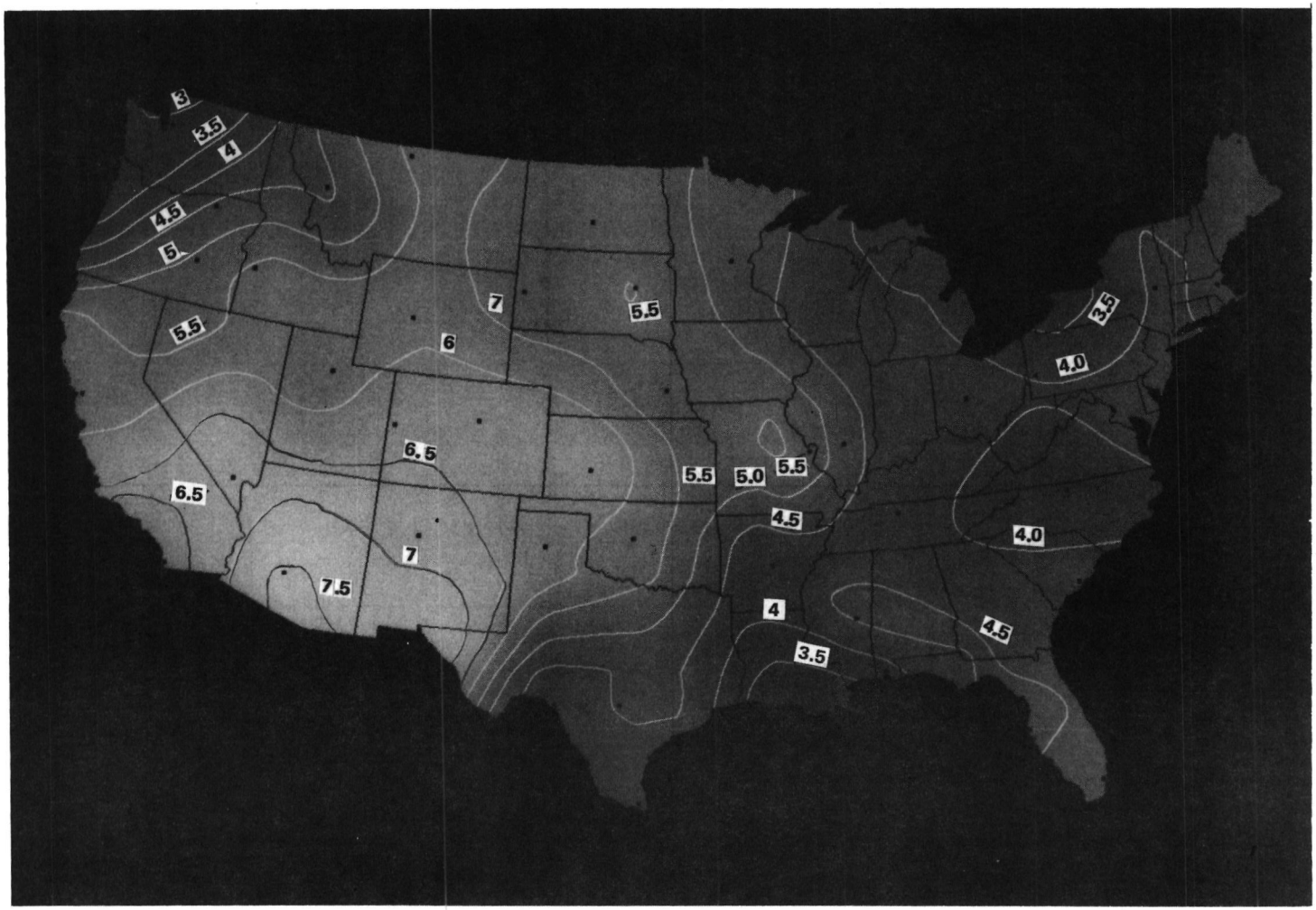

Figure A-13. Data Based on Watt Engineering, Ltd. Estimate of Direct Normal Insolation. The Degree of Smoothing of the Surface Increases in Going from Figure A-12 to Figure A-14. Figure A-13 Corresponding Approximately to an Average Nyquist Sampling (See Text).

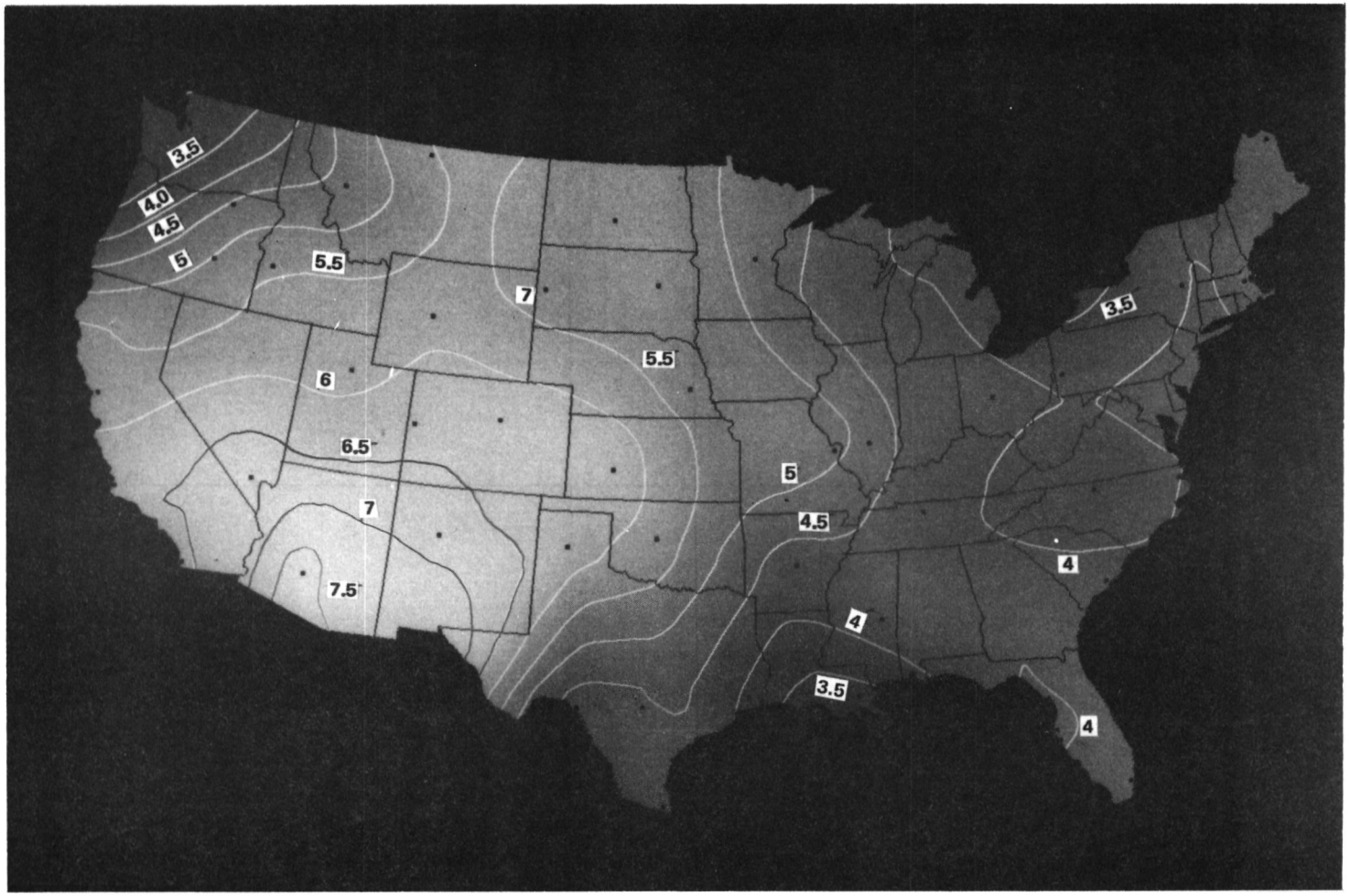

Figure A-14. Data Based on Watt Engineering, Ltd. Estimate of Direct Normal Insolation. The Degree of Smoothing of the Surface Increases in Going from Figure A-12 to Figure A-14, Figure A-13 Corresponding Approximately to an Average Nyquist Sampling (See Text).

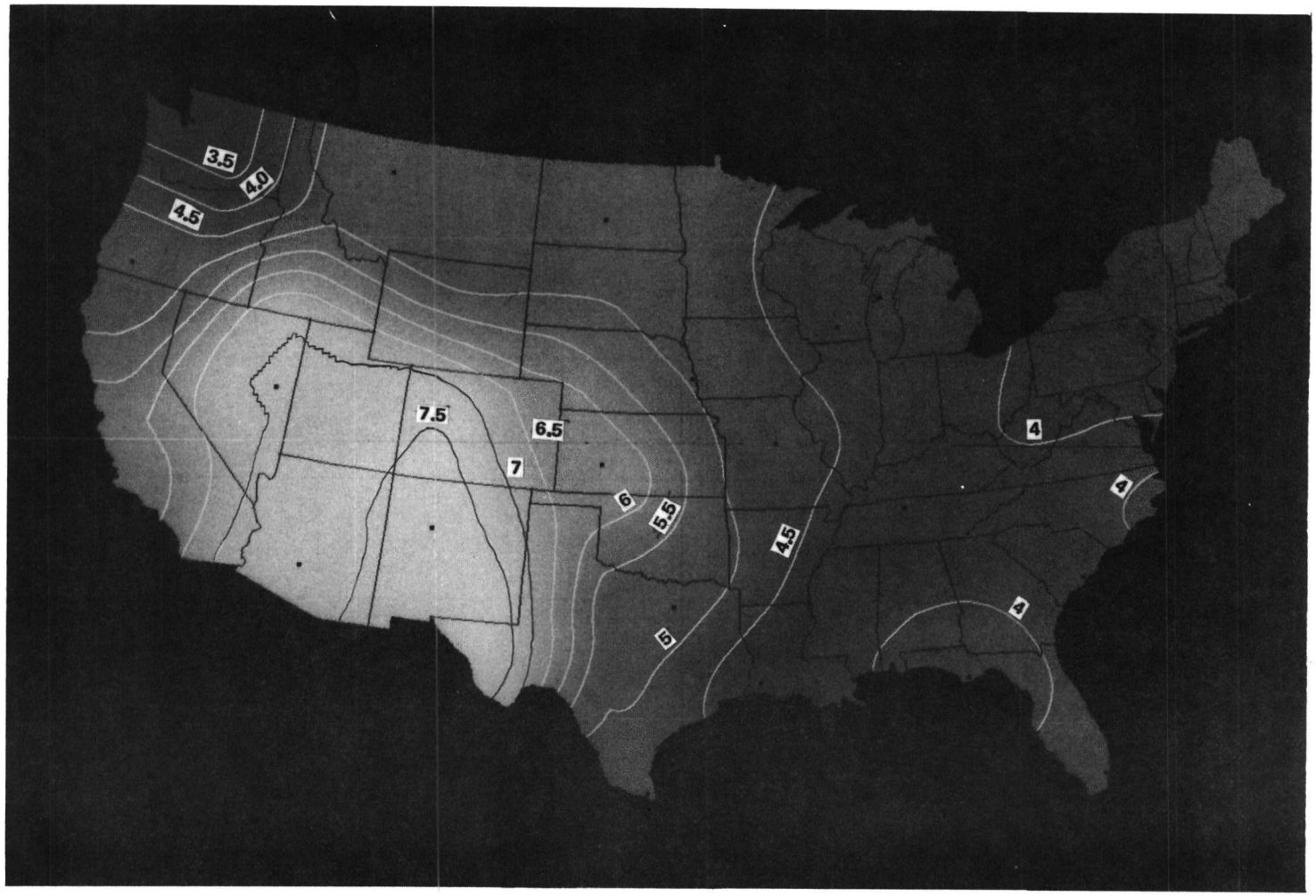

Figure A-15. Data Based on Aerospace Corp. Estimates of Direct Normal Insolation. The Degree of Smoothing of the Surface Increases in Going from Figure A-15 to Figure A-17. Figure A-16 Corresponds Approximately to an Average Nyquist Sampling (See Text).

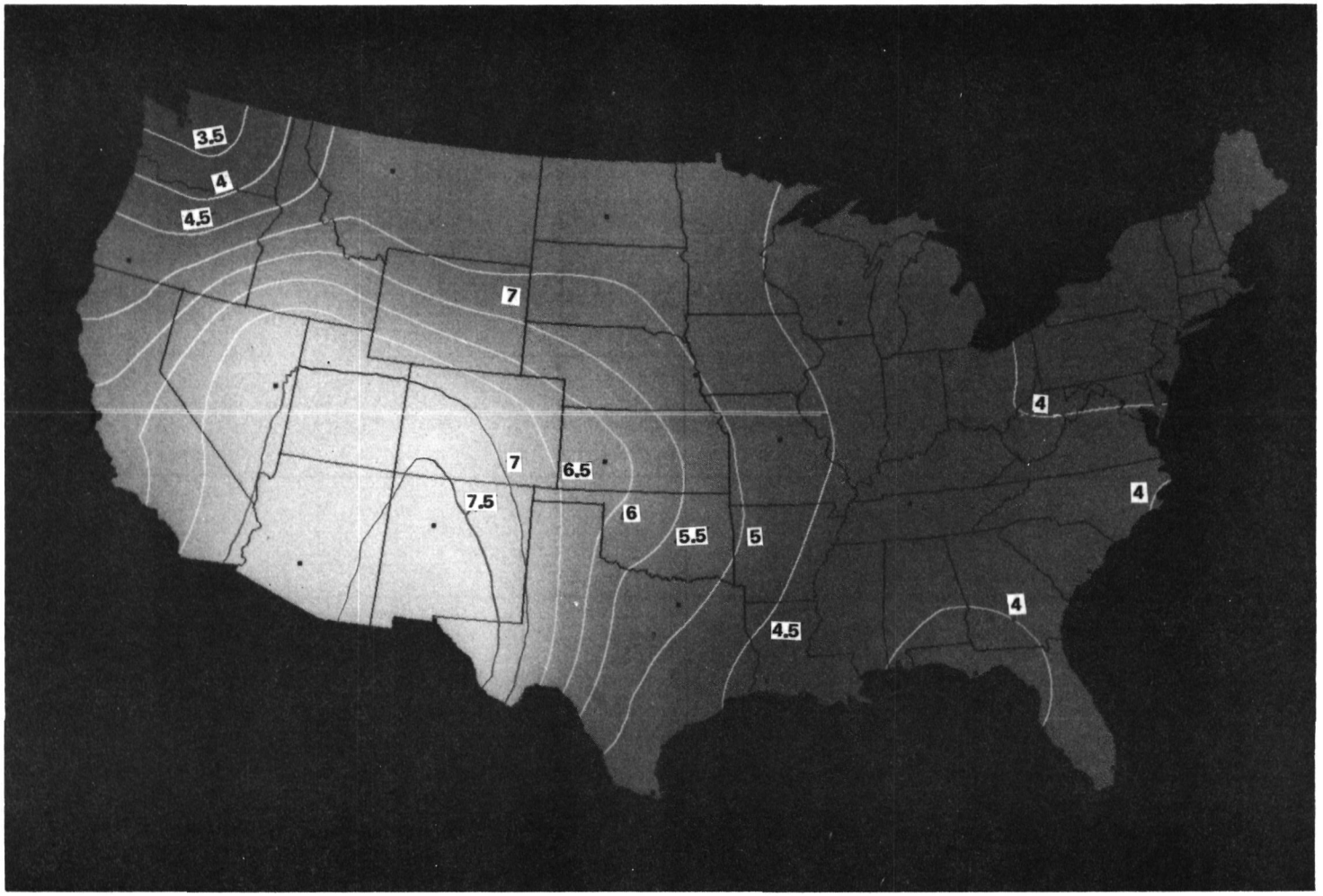

Figure A-16. Data Based on Aerospace Corp. Estimates of Direct Normal Insolation. The Degree of Smoothing of the Surface Increases in Going from Figure A-15 to Figure A-17. Figure A-16 Corresponds Approximately to an Average Nyquist Sampling (See Text).

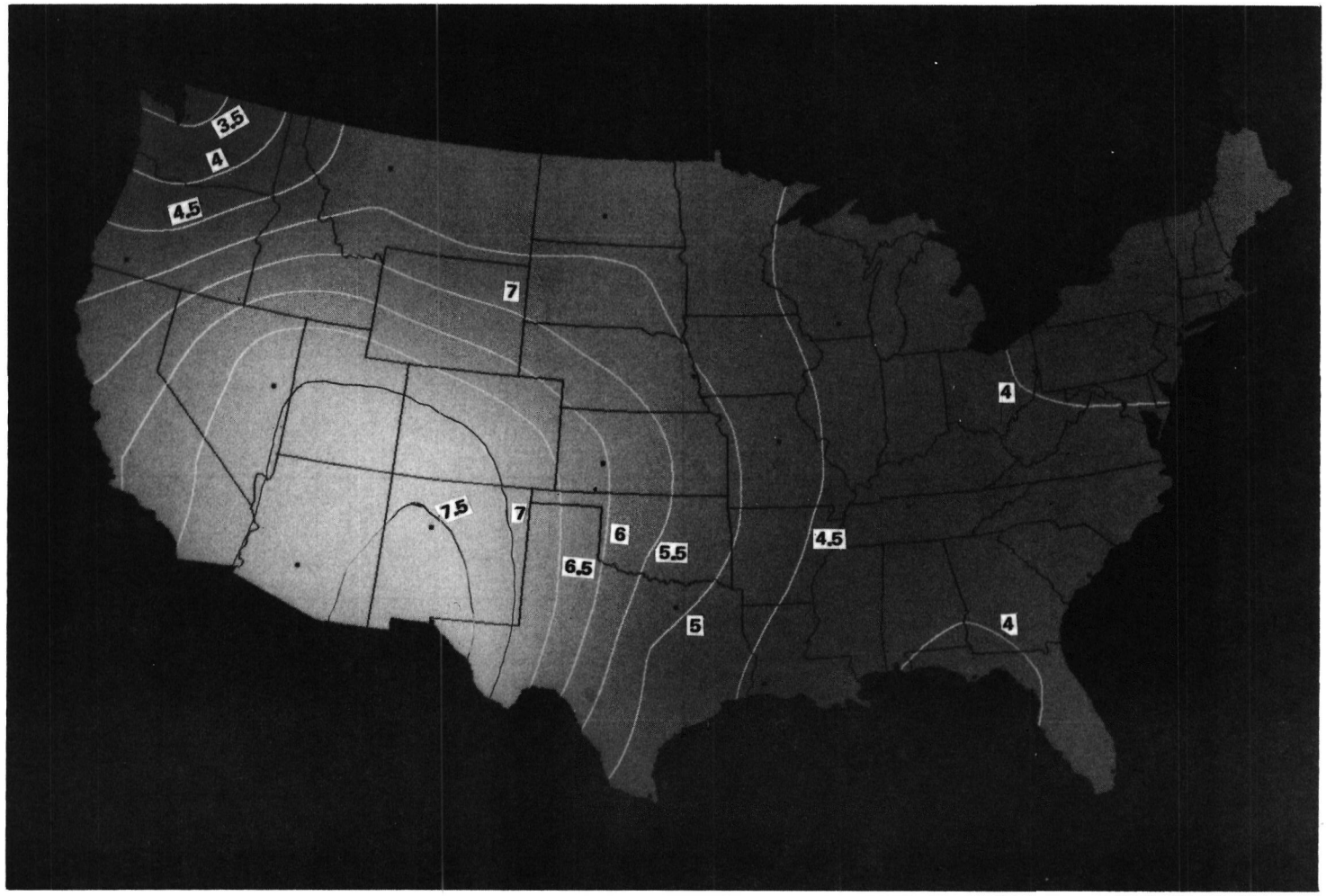

Figure A-17. Data Based on Aerospace Corp. Estimates of Direct Normal Insolation. The Degree of Smoothing of the Surface Increases in Going from Figure A-15 to Figure A-17. Figure A-16 Corresponds Approximately to an Average Nyquist Sampling (See Text).

G. DISCUSSION

The above is not an exhaustive discussion of existing insolation models; nevertheless, it provides an indication of the range and accuracy of the calculations that have been made and indicates which approaches are most useful for solar thermal power systems analysis.

In this connection, one must consider two distinct needs requiring two essentially different kinds of data. On the one hand, systems analysis, either engineering or economic, requires at least hourly data which simulate the actual insolation values (I_{DN} or I_{TH}) with correct statistics for given locations. On the other hand, site selection considerations require the construction of insolation maps based upon longer term averages (monthly, annual), with provision for estimating long-term variations. Thus, somewhat different approaches must be used in each case.

Figure A-18 is included to show the very different distribution in monthly average daily direct insolation that may exist at one site as compared with another, even though the annual average daily direct insolations for the two sites may be nearly the same. At each site, a particular recent year was selected on the bases that (a) the data were recent enough to insure reasonably accurate measurement and (b) the annual and monthly average daily direct insolation values were close to the corresponding long-term averages. Referring to Figure A-18, the distributions of monthly average daily direct insolation at Medford, OR and Miami, FL are drastically different. During June, July, and August, average daily direct insolation at Medford, OR is virtually equal to that at Albuquerque, NM.; during November, December, and January, average daily direct insolation at Medford, OR ($\overline{I}_{DN} \approx .9$ kWh/day) is several times lower than that at any of the other sites for which data are presented here. On the other hand the monthly average daily direct insolation is virtually constant throughout the year at Miami, FL.

Figure A-19 presents, for each of the sites shown in Figure A-18, the number of hours during the selected year that hourly average direct insolation was between specified intensity limits defined by increments of .05 kW/m^2. These histograms complement the results presented in Figure A-8. The relatively even distributions of intensity at Miami and Maynard reflect the climatological character of the Eastern coastal climate. Madison, as well as Miami and Maynard, shows a sharp decrease in incidence of the higher intensity levels ($.85 \leq I_{DN}$), this is attributed to the high relative humidity established at these sites by surrounding bodies of water and frequent rainfall whenever the local weather is warm. On the other hand, the histograms for Barstow and Albuquerque reflect the large proportion of days that are clear and during which, because the surrounding regions are relatively arid, the relative humidity is low. These characteristics, coupled with low latitudes, appear to be the chief factors contributing to the relatively much higher performance of solar thermal power systems located in the Southwest as compared with these same systems located in other regions of the contiguous United States.

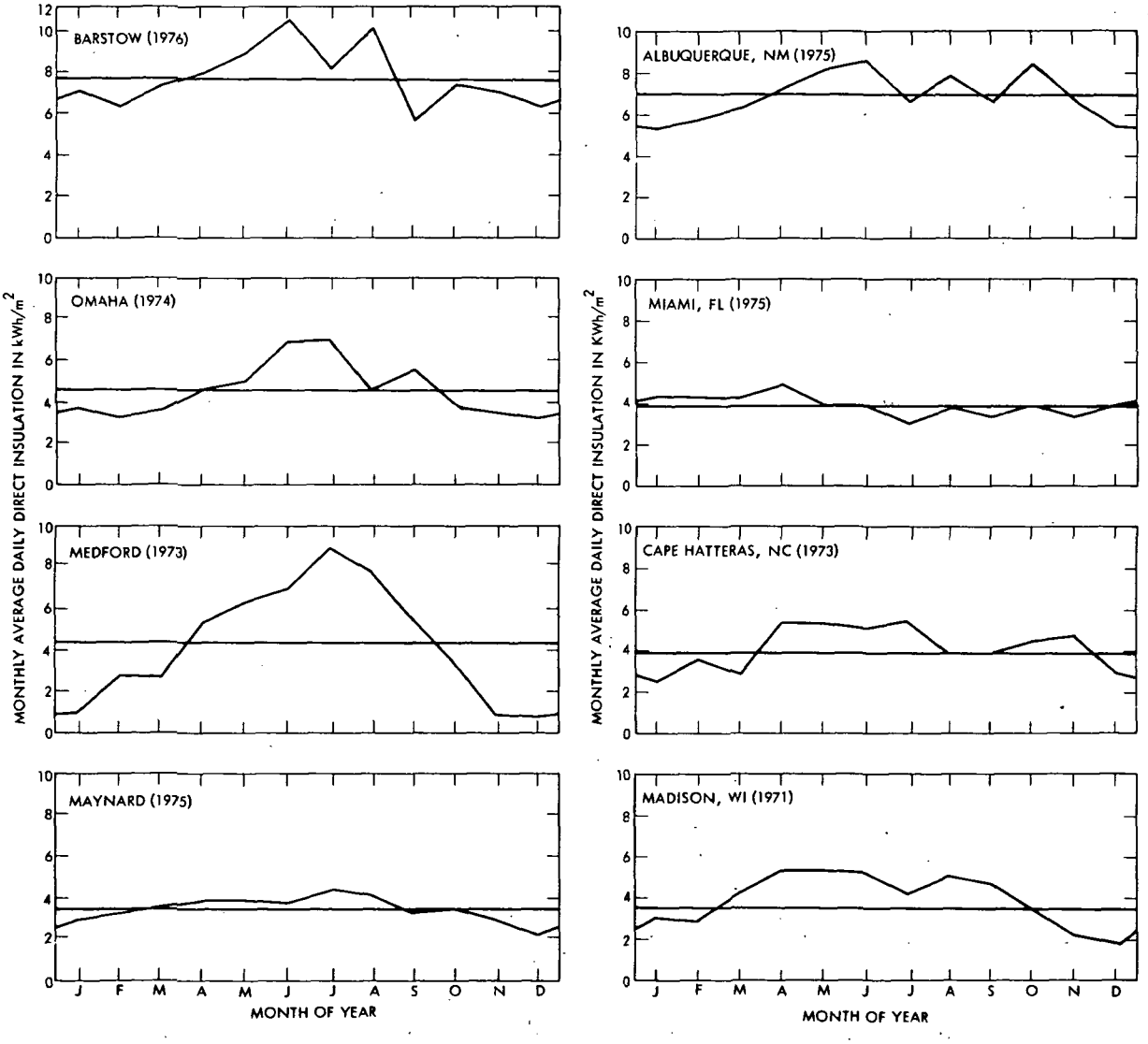

Figure A-18. Monthly Average Daily Direct Insolation for a Typical Year at Each of Several Sites Within the United States

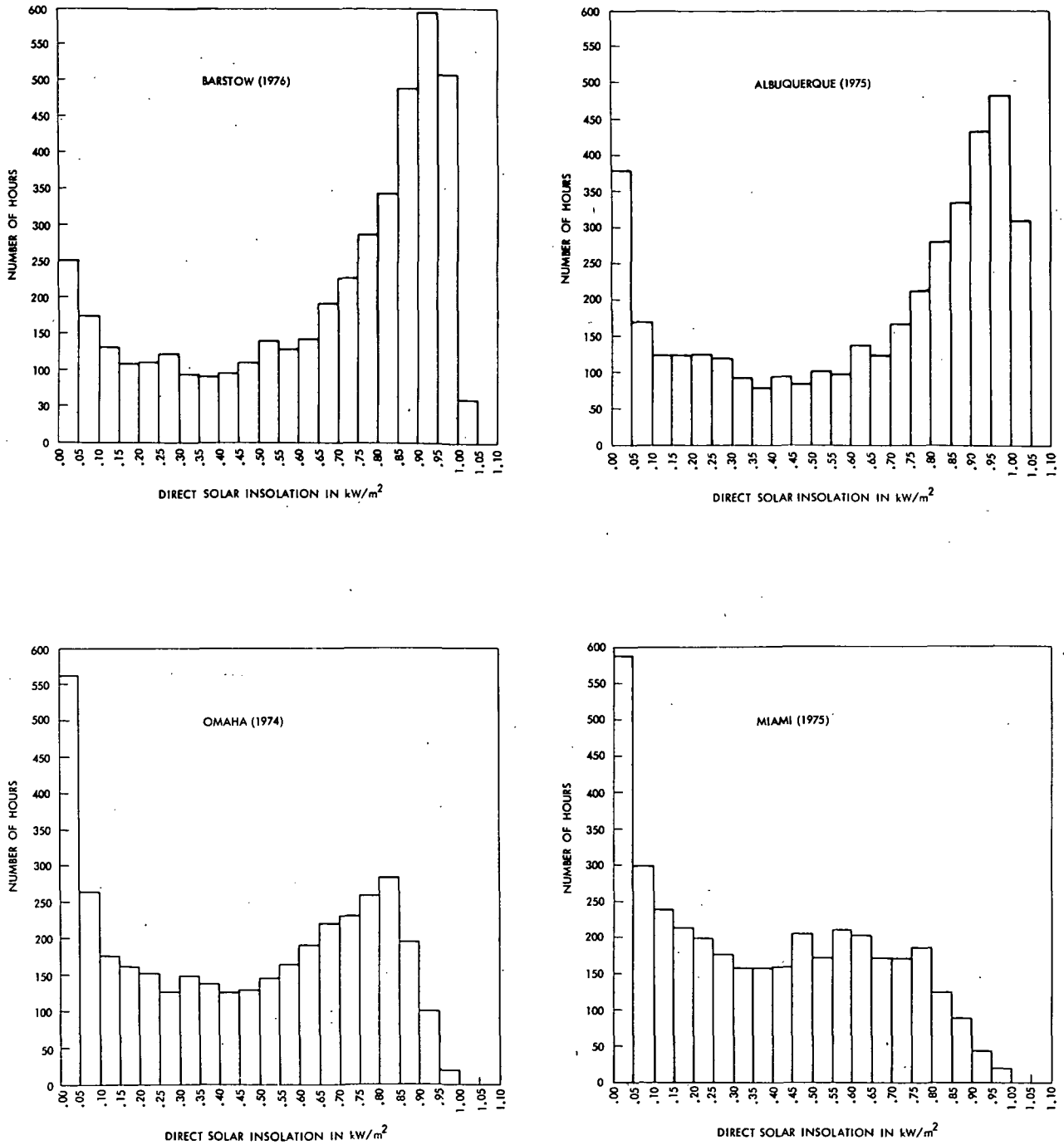

Figure A-19. Histograms of the Annual Hourly Average Direct Insolation for the Same Years and for the Same Sites Presented in Figure A-18.

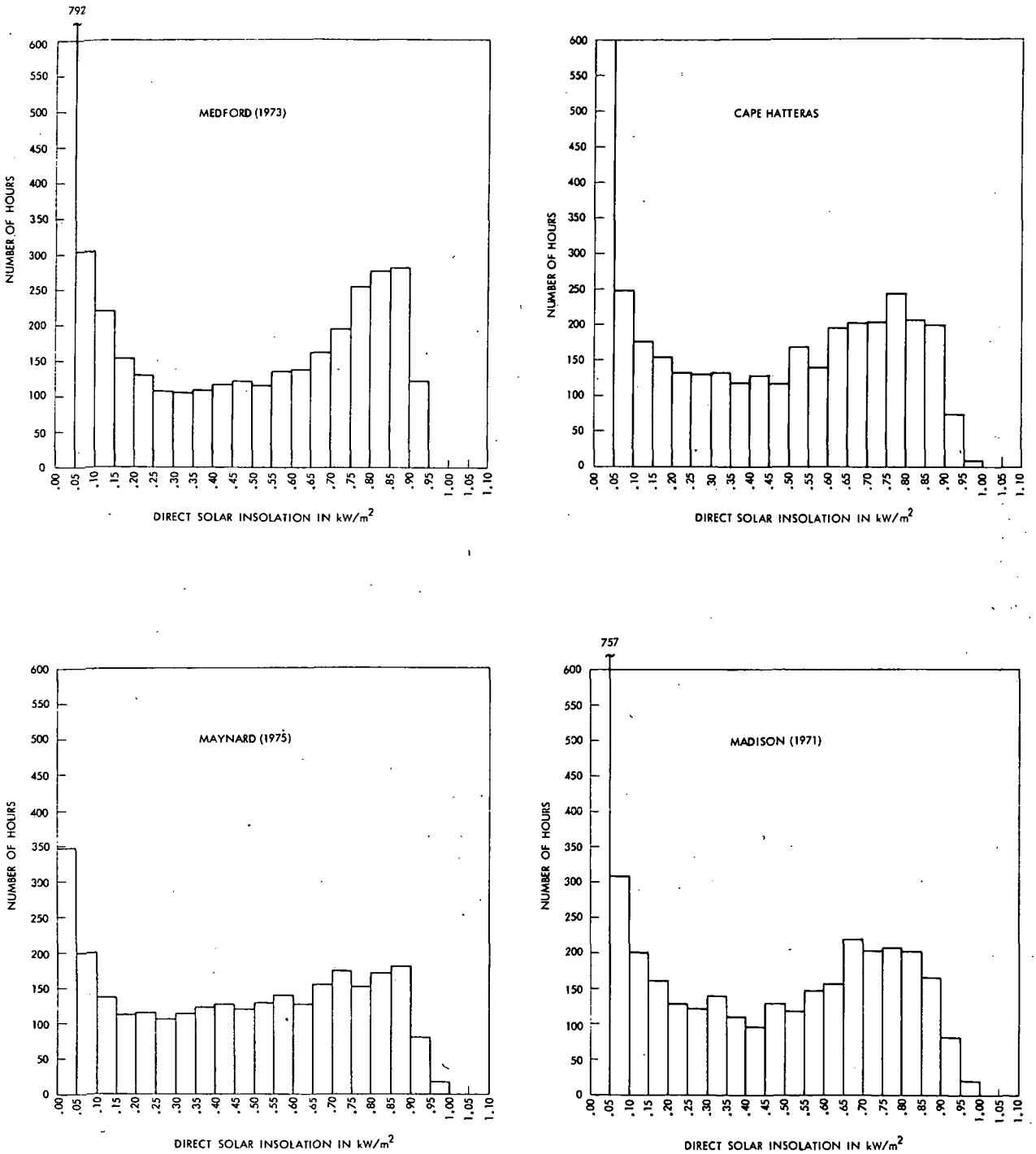

Figure A-19 (cont'd) Histograms of the Annual Hourly Average Direct Insolation for the Same Years and for the Same Sites Presented in Figure A-18.

VI. SUMMARY

The basic physical considerations relevant to insolation have been presented, including a discussion of the quantities measured and the basic instrumentation used for such measurements.

Various factors influencing the temporal and geographical variation of insolation values have been analyzed, and estimates of the variations caused by these factors have been given. Across the contiguous United States, these include a north-south variation of 20% due to zenith angle effects, an east-west variation of 20% due to atmospheric turbidity variations, and a 2-to-1 southwest-northwest variation in average cloud cover. In addition, the fact that the dominant long-term effect of upper atmospheric turbidity caused by volcanic activity can result in changes in northern hemispheric insolation values of more than 30% within a year or so, has been emphasized.

According to recent studies (Ref. A-9), insolation measurements have nominal error bands of about 3%. For coastal regions at extreme northern latitudes (e.g., Seattle, Washington, and Caribou, Maine), it appears that actual direct insolation could be of the order of 20% higher than is indicated by SOLMET insolation tapes. This would tend to improve performance of solar plants in these extreme northern coastal regions, but would not materially affect the comparisons among plant types. Moreover, performance in these northern, low-insolation regions would still be lower than that in the Southwest and other lower-latitude regions.

The existing insolation data base in the United States has been analyzed with respect to accuracy, completeness, and type of data, and it has been pointed out that this data base is not completely adequate in each of these respects for every solar thermal study.

The current status of model calculations has been investigated and the conclusion reached that certain of these models, individually or in combination, are adequate for calculating any type of insolation at any location and for any given time frame. Thus, they are suitable for both quasi-steady-state systems analysis and site selection studies.

VII. CONCLUSIONS

From the above it is clear that, in the future, the evaluation of solar thermal systems must depend upon accurate model calculations. None of the existing models are entirely satisfactory for this task at the present time, but, taken as a whole, they provide a basis upon which a suitable model can be constructed. A more nearly ideal model would

1. permit the calculation of I_{DN}, I_{TH}, and I_{dN} values;

2. allow such calculations to be made at any specific site within the continental United States;

3. allow such calculations to be made for any given time period and to any practical time resolution (time interval for integration);

and

4. do all of the above with correct statistics.

In order to construct such a model, the following steps need to be taken:

1. Improved and more extensive measured data must be acquired.

2. The existing models must be analyzed and compared for overall suitability in terms of accuracy and flexibility.

3. One or more of these must be selected as a basis for further modification to allow the proper inclusion of the dynamic effects of clouds.

4. The resultant model must be checked for accuracy and evaluated with respect to sensitivity to input data. This would involve surveying the existing sources of such data as turbidity, water vapor, and albedo and determining the errors in insolation values introduced by errors in these parameters.

REFERENCES

A-1. "On the Nature and Distribution of Solar Radiation," DOE Report HCP/T2552-01. Watt Engineering Ltd., (Mar. 1978).

A-2. "Solar Radiation Data Sources, Applications and Network Design," DOE Report HCP/T5362-01. University of Alabama, pp. 1-18, (Apr. 1978).

A-3. Robert W. Durrenberger and Anthony J. Brazel, "Need for a Better Solar Radiation Data Base," Science 19, 1154-5, (Sept. 1976).

A-4. Carter, E. A., Wells, R. E., and Williams, B. B., "Solar Radiation Observation Stations with Complete Listing of Data Archived by the National Climatic Center, Asheville, N.C., and Initial Listing of Data not Currently Archived," Center for Environmental and Energy Studies, the University of Alabama, Huntsville, Nov. 1976 - prepared for ERDA, Div. of Solar Energy, under contract NA58-31293.

A-5. Ward Seguin, National Weather Service, (private communication).

A-6. "A New Procedure for Estimating Hourly Direct-Normal Insolation from Hourly Total-Hemispheric Insolation," C. M. Randall and M. E. Whitson, Aerospace Report, (Draft - 1978).

A-7. "Hourly Solar Radiation Data for Vertical and Horizontal Surfaces on Average Days in the United States," T. Kusuda and K. Ishii, NBS Building Science Series 96, U.S. Dept. of Commerce, (April, 1977).

A-8. Douglas V. Hoyt, "A Model for the Calculation of Solar Global Insolation," Solar Energy 21, 27-35, (1978).

A-9. Rapp, D., "A Critique on Rehabilitation Procedures Used by NOAA for Solar Data,' to be published in Energy Conversion Journal (1979).

APPENDIX B

PERFORMANCE AND COST CHARACTERISTICS OF ADVANCED SOLAR THERMAL POWER PLANTS

CONTENTS

FIGURES

APPENDIX B

INTRODUCTION

This appendix first describes the rationale and procedures used to determine the performance and cost characteristics of the four selected advanced solar thermal power plants.

- Paraboloidal Dish (PD)
- Central Receiver (CR)
- Parabolic Trough (PT)
- Compound Parabolic Concentrator (CPC)

Then, selected results based on computer simulations of these systems operating in regions with differing insolation patterns (Appendix A) are presented. These results provide details which supplement and amplify the primary findings summarized in the body of this report.

II. SYSTEM CHARACTERIZATION

The four selected systems were characterized in terms of performance and cost data pertaining to the subsystems/components comprising each system. The ground rules used in determining performance and cost characteristics were:

- Subsystem/component advanced technology development was projected to the 1990-2000 timeframe.
- High-volume mass production (~10^6 units/year) was assumed for modular components (e.g., concentrators).

These ground rules are closely related to those used in determining solar thermal program targets. Thus, a basic source of information regarding the desired projected data is program planning documents (e.g., Refs. B-1 and B-2). These planning documents were used as the starting point. In general, the information available was not adequate for the detailed system characterization required for computer simulation methods employed in the study. Therefore, it was necessary to generate much of the detailed subsystem/component performance and cost data base. The basic approach was to work with specialists from Government Laboratories and industry who are actively involved in developing the four selected systems and their components.

A. PERFORMANCE DATA

The performance of the selected power systems is presented in Figure B-1. It shows the design-point efficiencies of components in the primary power train that captures solar energy and converts it to

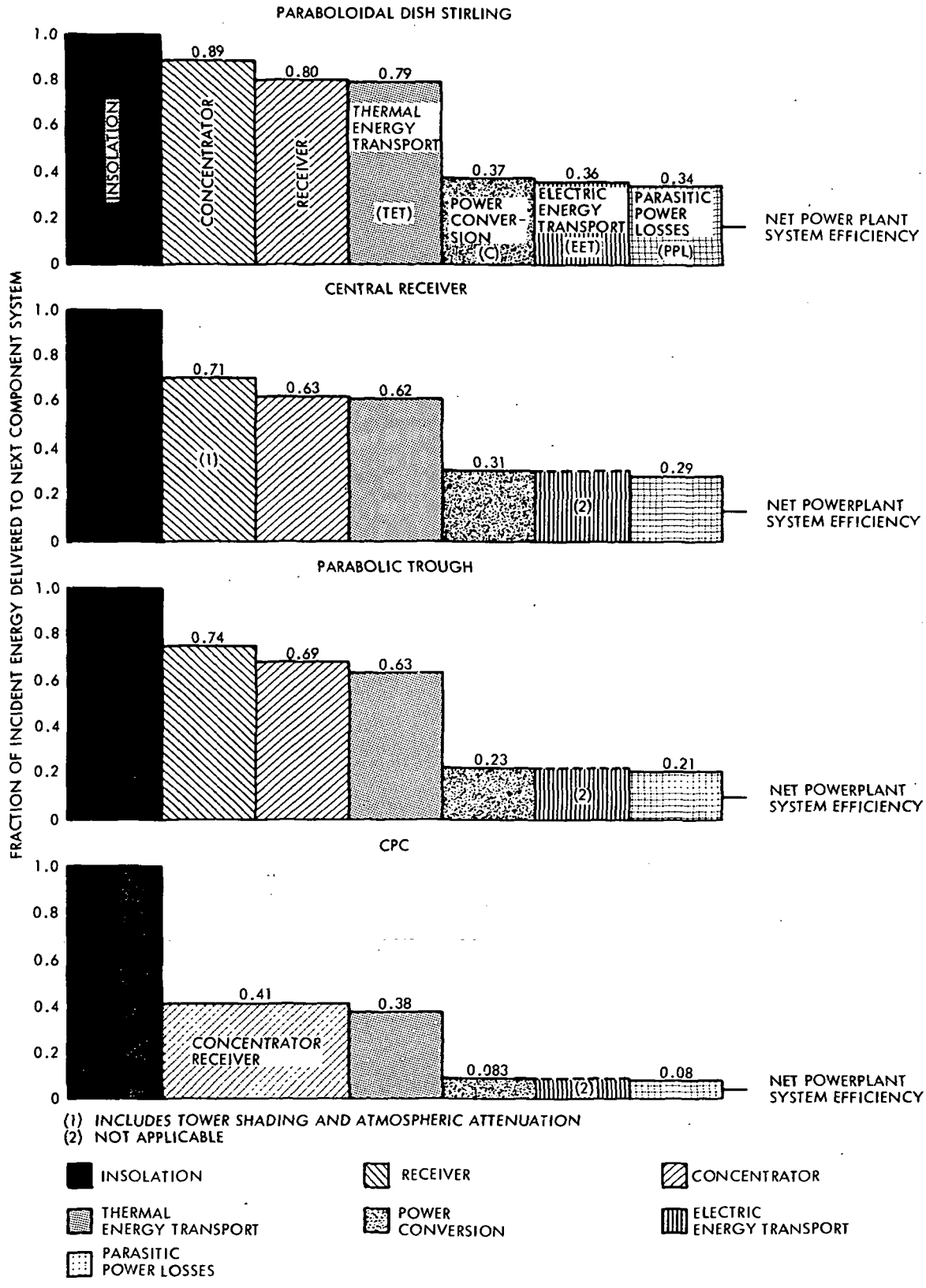

Figure B-1. System Design Efficiency Train

electricity. This electricity is then delivered to the grid or application site. It is shown that the two-axis tracking systems represented by the parabolodial dish and central receiver achieve higher design point system efficiencies than the one-axis parabolic trough. The paraboloidal trough has a higher efficiency than fixed or periodically adjusted orientation systems such as the Compound Parabolic Concentrator.

These basic trends explain the motivation behind efforts to develop tracking concentrator systems. Tracking permits a greater fraction of the available insolation (solar flux) to be captured. This solar flux can be highly concentrated at the receiver, particularly in the case of two-axis tracking systems. The result is higher temperatures and correspondingly higher conversion efficiencies as seen in Figure B-1.

For all systems, the reflective surface was taken to be a back-silvered, thin, low-iron content glass produced, e.g., by the fused glass process. Based on laboratory tests at Sandia Laboratories, Albuquerque, (Refs. B-3 through B-6) reflectivities in the range of 0.90 to 0.95 are projected.

In addition to reflectivities, each of the systems requires the specification of key design parameters. Slope errors for the paraboloidal dish of ±0.1 are assumed for the mirrored reflective surface. Low slope errors yield high concentration ratios with small spillage of flux outside the receiver aperture. The result is efficient capture of solar flux for operation at high temperatures in the range of 1500°F to 2000°F. These temperatures are deemed appropriate for power generation from paraboloidal dish systems (Ref. B-7).

A major consideration for the central receiver is the layout of the heliostat field with respect to the tower. The highest optical efficiencies for the latitudes encompassing the contiguous United States (Refs. B-8 and B-9) are provided, by a north-field arrangement, wherein the heliostat field is located north of the tower. However, the north-field requires a higher tower for the receiver than do field arrangements where the tower is more centrally located within the field. As the power rating and size of the field are reduced, the tower height decreases. Tower design complexity and costs then diminish and north-field designs appear to be preferable for small central receiver systems. In the present study, an efficient north-field arrangement was assumed even for a 10 MW plant. The higher cost of the north-field tower was offset by projecting development of advanced high-temperature liquid metal or molten-salt heat transport systems to carry energy from the tower-mounted receiver to the energy conversion system. The heat transfer characteristics of liquid metals like sodium allow construction of lighter weight receivers and the use of smaller pipe diameters as compared to steam or gas systems. This results in the projections of lower tower costs according to estimates by Sandia Laboratories, Livermore (Ref. B-10).

Minimization of receiver heat losses is required for high efficiency operation of the parabolic trough. For a reflective surface with a small slope error ($\leq$0.1), the reflected solar flux

will be concentrated in a narrow strip impinging on the linear receiver. To minimize heat losses, it is necessary to insulate the receiver; on the other hand, a thick insulation will block a portion of the insolation from hand, the concentrating surface. Thus, sophisticated insulation techniques as, for example, evacuated jackets in conjunction with advanced insulation materials will be required. Performance projections for the trough are predicated on evolutionary development of this technology as supported by activities at Sandia Laboratories, Albuquerque. These projections indicate that the next generation of parabolic trough systems will perform much more efficiently than do present systems (Ref. B-11).

The CPC system (Refs. B-12 and B-13) is less critically dependent on reflective surface accuracies and can capture a portion of the diffuse radiation. A key parameter for this system is the concentration ratio. As the concentration ratio is increased by enlarging the reflecting surfaces, higher operating temperatures are practicable. However, as the sun passes over the fixed reflecting surfaces of the CPC, only the direct insolation falling within the acceptance angle or field-of-view is concentrated on the receiver. The acceptance angle becomes smaller as the concentration ratio is increased. Based on guidance from Argonne National Laboratory, a concentration ratio of 3 to 5 was employed in this study. Sensitivity to concentration ratio, particularly for CPC systems operating in regions with high percentages of diffuse radiation, is discussed further in Appendix C.

The efficiency of transporting energy is high (>90%) for all systems, even though widely different approaches are represented. The modular paraboloidal dish relies primarily on electric transport, whereas the central receiver employs optical transfer of energy from the field. The parabolic trough and CPC use thermal transport of steam and organic fluids, respectively via pipelines. The central receiver, with an optical atmospheric attenuation loss of only ~2% for a 10 MWe plant, has the highest projected transport efficiency. The assumed values for electrical and thermal transport efficiencies could theoretically be improved, e.g., by using larger diameter wires to reduce electrical resistance losses and larger diameter pipes with thicker insulation to reduce friction and heat losses. However, these measures would increase costs. Efficiency values are therefore a function of engineering trade-offs. For this study, values consistent with current electrical and pipeline networks were used since they reflect engineering trade-off considerations.

A spectrum of energy conversion systems is employed in the selected advanced systems. For the paraboloidal dish, a Stirling engine operating at 1650°F is employed. For the central receiver, an 1800°F combined-cycle Brayton/Rankine system is used. The parabolic trough employs a Rankine cycle steam power system operating with steam at 800°F amd the CPC employs an organic Rankine system. Current engines generally achieve about 60 percent of the corresponding Carnot efficiency. Carnot efficiency is the maximum achievable for specified conditions. With the development of advanced designs and the incorporation of features such as reheat and intercooling, it is possible to improve the efficiency of all the engine types above.

Trade-offs between improved efficiency, added cost, and complexity will dictate the extent to which efficiency is improved. For solar thermal plants, the achievement of high efficiency is extremely attractive since the collector field area can be reduced as the efficiency increases. System trade-offs favor development of efficient engines and, in this context, it is projected that values of about 70 percent of Carnot cycle efficiency will be attained in the 1990-2000 timeframe. Since Carnot efficiency increases with operating source temperature, the higher source temperature system has higher conversion efficiencies, as seen in Figure B-1.

A value of about 70 percent Carnot cycle efficiency is the practical maximum design efficiency for the energy conversion systems. The basic types of engines have differing part-load efficiencies as shown in Figure B-2. All the systems have excellent part-load performance in that they maintain high efficiencies over a wide load-range (Ref. B-7). The Brayton/Rankine achieves its peak efficiency at a power less than its design power rating. It is important to understand that, only at its maximum normalized efficiency of about 1.02 (occurring at approximately 0.7 of design power output), does the Brayton/Rankine power conversion system associated with the CR achieve its practical design maximum corresponding to 70% of Carnot cycle efficiency. This curve is characteristic of closed-cycle, recuperated, Brayton engines (Ref. B-14).

B. COST DATA

Each of the four selected advanced power plants was separated into the following cost elements:

- Land
- Concentrators
- Receivers
- Energy Transport
- Storage Structure/Medium
- Heat Engine Equipment
- Balance of Plant
- Operations and Maintenance

Unit cost data for each of these elements was determined by (1) using cost target data from planning documents, (2) synthesizing results from mass-production studies, and (3) conferring with personnel from other Government Laboratories who are responsible for developing the selected systems. Data for the paraboloidal dish Stirling (PDS) system were determined within the Jet Propulsion Laboratory (JPL). For the central receiver (CR) data inputs, Sandia Laboratories, Livermore, the Electric Power Research Institute (EPRI), McDonnell

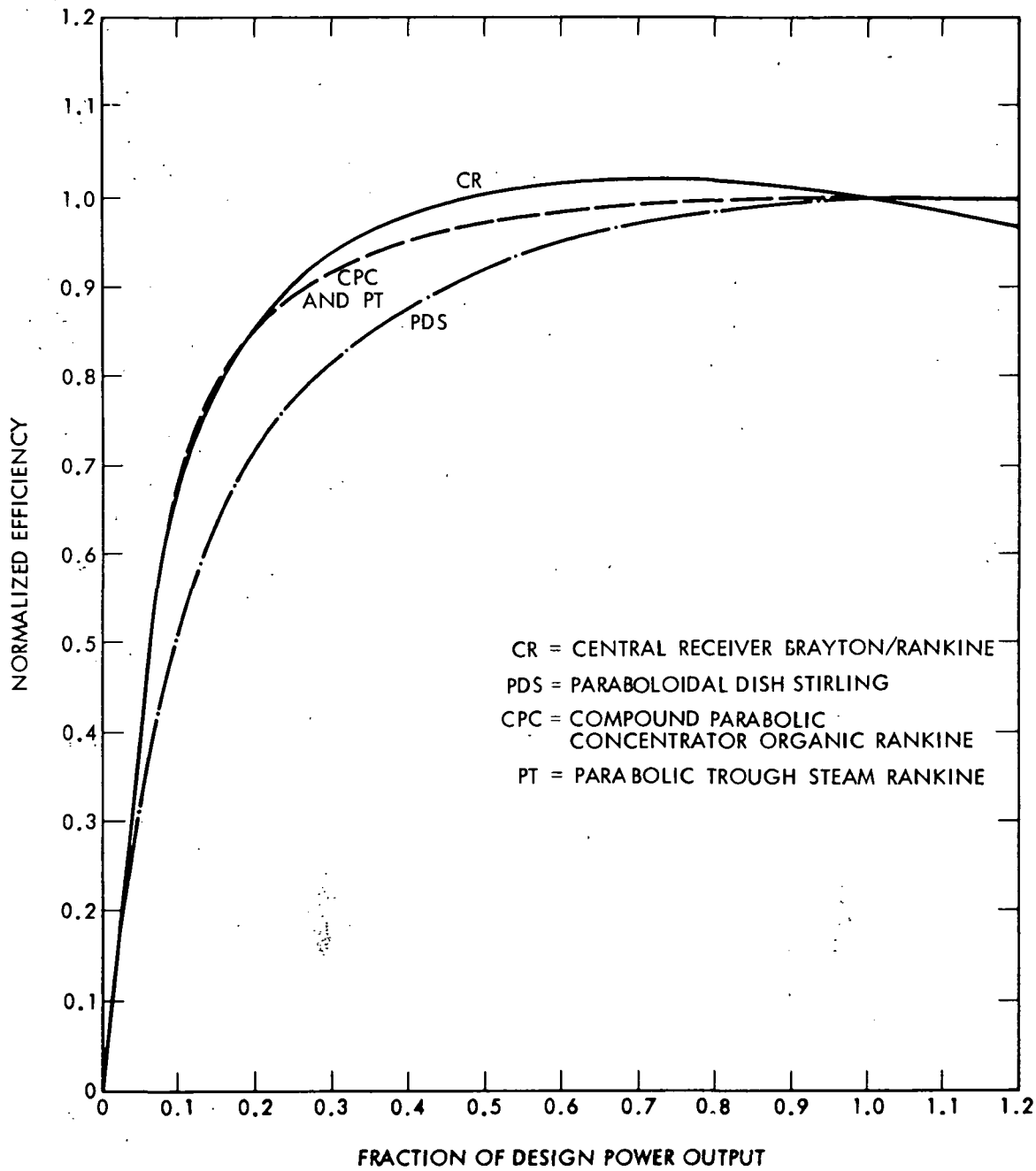

Figure B-2. Part Load Engine Efficiencies

Douglas Astronautics, Inc. (MDAC), the University of Houston, and the NASA Lewis Research Center (LeRC) provided valuable assistance to JPL. Similarly, Sandia Laboratories, Albuquerque (SLA) and the Argonne National Laboratory (ANL) gave helpful assistance to JPL in the data for the parabolic trough and the compound parabolic collector (CPC) respectively.

With regard to land costs, it is tacitly assumed that solar plants will not be located on premium real estate since large areas are required. Instead, it is considered likely that solar plants will be located on low cost land ranging from $1000/acre to $5000/acre. The lower cost of $1000/acre is assumed for the arid sunbelt which contains large areas of low-cost desert land.

High-volume mass production studies have only been conducted for the central receiver system (Refs. B-15 and B-16). Comparable studies at the same production rates are not available for the other systems. Therefore, the central receiver studies were used as a baseline. In general, existing cost estimates for the collectors of both the PT and CPC under limited mass production were higher than those for the CR. However, both of these systems were judged to be simpler to manufacture and assemble than is the two-axis tracking central receiver. Both SLA and ANL concurred with this judgement. Thus, lower collector unit costs were used for the trough and CPC, with the CPC having the lowest unit cost since it does not require tracking mechanisms.

The paraboloidal dish system, on the other hand, was judged to be more complex than the heliostat (concentrator) of the central receiver. The dish requires doubly curved reflective surfaces and additional structure to support the receiver/engine-generator assembly at its focal point.

The following nominal collector costs are used to define collector costs as the sum of the concentrator and receiver costs.

System	Collector Cost, $/m^2
Paraboloidal Dish Stirling	95
Central Receiver	75
Parabolic Trough	70
Compound Parabolic Conc.	50

These nominal values are considered to be reflective of relative cost trends. The effect of uncertainties in projecting these nominal values is evaluated via sensitivity analyses in Appendix C.

For energy transport, the central receiver employs a relatively short length of pipe for transporting thermal energy in the tower, whereas the parabolic trough and CPC use extensive piping networks to bring thermal energy from the collector field to a centrally located energy conversion unit. The paraboloidal dish system uses an electrical network to collect the energy generated by the small power conversion units that are located at the focal point of each dish concentrator.

Transport costs for the central receiver are included in the receiver/tower subsystem. Costs for the thermal piping networkds of the parabolic trough and CPC were estimated on the basis of piping layouts for designs being evaluated and studied by SLA and ANL, respectively. A pipe network optimization code developed at JPL was used as an aid in selecting nominal costs (Ref. B-17). Activities are underway at JPL to update electrical network transport costs for the paraboloidal dish system. However, this effort is not yet complete; therefore, values from earlier studies (Ref. B-7) have been used wherever these values are considered to be representative nominal values.

Storage costs were inferred from studies (Refs. B-18 through B-22) which investigated storage systems in the context of advanced technology developments. The advanced battery costs of ~$30/kWeh for the PDS system is consistent with advanced technology projections in Ref. B-19. Thermal storage costs are based on projections for advanced latent heat systems. Since the trough and CPC employ lower temperature storage than the central receiver, lower storage costs are assumed. Containment material problems are generally less at reduced temperature levels. Recent thermal storage cost goals based on NASA/ LeRC activities yield lower cost goals than used in this study and therefore Appendix C treats systems sensitivity to storage cost uncertainties.

Based on high-volume mass production practices as employed in the automotive industry, a nominal target cost for the power conversion system has been set at 60 $/kWe (Ref. B-7). Automotive industry practice pertains to small engines as used in the paraboloidal dish system. For the larger 10 MWe plants used in the other systems, the same level of mass production will not be achieved if the same overall level of market penetration is assumed for each system. Further, procedures for mass-producing large power systems are not well established.

However, in the context of a significant market penetration in the 1990-2000 timeframe, production of large power systems could benefit to some extent from increased production. In view of these possibilities, it is believed that, as an ultimate goal, large engine system costs could approach those of smaller engines. Therefore, the same cost of $60/kWe was used for these engines. The increase in energy cost that would result if these ultimate values for large engines are not met is presented in Appendix C as part of the sensitivity analysis.

Balance-of-plant includes items such as buildings, electrical plant equipment, and master controls. The cost of all these items will depend on detailed plant design considerations. For nominal projection purposes, the same value of ≈$85/kWe determined by recent central receiver studies has been assumed to hold approximately for all the systems. For systems with large central engines, the plant and engine rating are the same but, for the PDS systems using battery storage, total system engine rating exceeds plant rating. For the present study, the balance-of-plant costs were based on total system engine rating for the PDS system. For dish systems having high capacity factors and correspondingly large field areas, total system engine rating is significantly larger than plant rating. At large capacity factors, this results in much larger balance-of-plant costs

for PDS systems This treatment of balance-of-plant costs is considered to be conservative for the dish system since some balance-of-plant items, such as buildings, probably will not increase in proportion to total system engine rating.

Moreover, one basis of analysis used for the PDS system in this report is to assume that any power produced in excess of plant rating must be stored or wasted. Thus when storage is filled, this basis results in the wastage of electrical energy. On an alternate basis, the wastage would be fed to the associated electrical distribution network and could therefore be credited to the PDS system.

The estimation of Operation and Maintenance (O&M) costs is presently subject to considerable uncertainty. Based on EPRI studies (Ref. B-23), a value of about 1% of capital costs is assumed for plant operation and maintenance during the first year of operation. The effect of variations in O&M costs is treated in the sensitivity analysis of Appendix C.

C. FINANCIAL FACTORS

The energy cost for solar power plants is determined by using a levelized cost methodology developed for utility systems (Ref. B-24). This methodology requires financial inputs. Recently, a set of financial factors has been adopted for solar thermal comparison studies being performed by the Solar Energy Research Institute (SERI), Battelle Pacific Northwest Laboratories (BPNL), and JPL. These factors listed haved been used in this study.

Utility Description Data

System Operating Lifetime	30 years
Annual "Other Taxes" as a fraction of capital	0.02
Annual Insurance Premiums as a fraction of capital	0.0025
Effective Income Tax Rate	0.40
Ratio of Debt to Total Capitalization	0.50
Ratio of Common Stock to Total Capitalization	0.40
Ratio of Preferred Stock to Total Capitalization	0.10
Annual Rate of Return on Debt	0.08
Annual Rate of Return on Common Stock	0.12
Annual Rate of Return on Preferred Stock	0.08

General Economic Conditions

Rate of General Inflation	0.06
Escalation Rate for Capital Costs	0.06
Escalation Rate for Operating Costs	0.07
Escalation Rate for Maintenance Costs	0.07
Base Year for Constant Dollars	1979

Nominal Intermediate Outputs

Cost of Capital to (and internal rate of return in) a Utility	0.086
Capital Recovery Factor	0.0939
Annualized Fixed Charge Rate	0.1568

III. OPERATION IN REGIONS WITH DIFFERING INSOLATION

Computer simulation results for the selected four advanced solar thermal power systems operating in regions with differing insolation characteristics are determined by using the performance and cost values of the previous section as inputs. First, the computer methodology of simulating solar thermal power plants is described. Then, selected results from the computer simulation are presented.

A. COMPUTER SIMULATION METHODOLOGY

The structure of the power plant computer simulation program is illustrated in Figure B-3. Detailed documentation for this program is given (Ref. B-25). The basic input to the program is hourly insolation data which are provided in the form of SOLMET tapes for a number of sites within the Continental United States (see Appendix A). Plant power rating and performance characteristics of subsystems/components are the basic inputs to the plant performance simulation subprogram. Performance is specified in terms of the design efficiency train of Figure B-1 and off-design characteristics, e.g., engine part-load efficiency as given in Figure B-2.

Component cost characteristics comprise the basic input to the plant capital costs subprogram. These cost characteristics are generally unit costs normalized to concentrator area or power rating as presented in the previous section. To determine plant capital costs, these unit costs are multiplied by collector area, storage capacity, and relevant power levels (thermal or electrical) within the plant as determined by the performance subprogram.

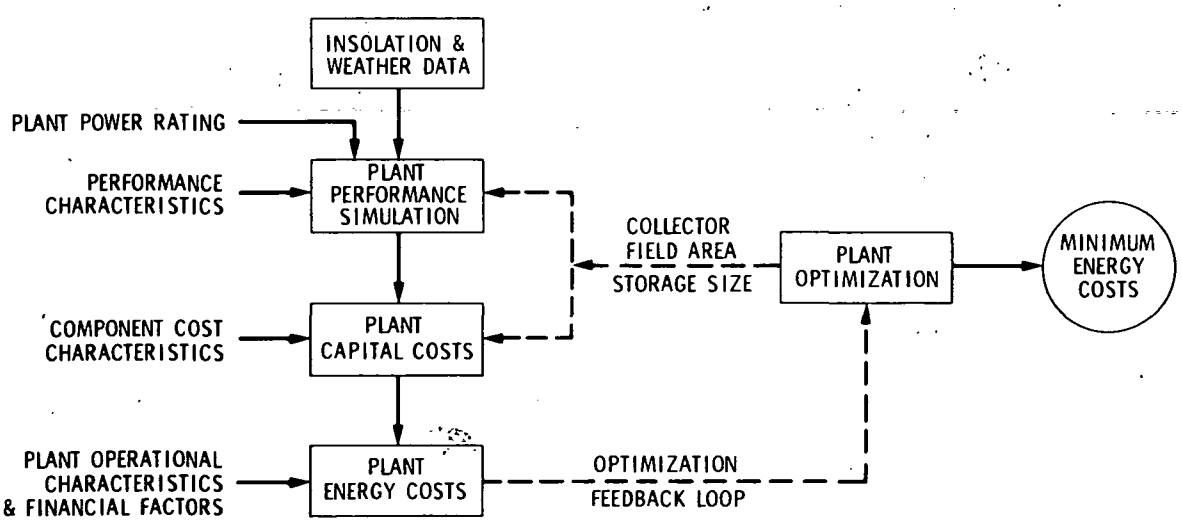

Figure B-3. Structure of Power Plant Simulation Computer Program

Capital costs as determined by the capital cost subprogram and capacity factor from the performance subprogram are inputs for the plant energy costs subprogram. The capacity factor is the ratio of the actual energy delivered throughout a year of operation to the energy that the plant could have delivered it if had operated continuously at rated plant power during the year. Other required inputs to the energy cost program include operational characteristics such as O&M costs and plant life. Financial factors including considerations such as escalation rates, taxes, and insurance as presented in the previous section are also needed as inputs to the energy cost subprogram.

As seen from Figure B-3, the computer program contains an optimization feedback loop which determines minimum energy costs as a function of collector field area and storage capacity. A collector field area is first chosen and the storage size is increased until the minimum energy cost is reached. Since energy in excess of plant rating must be either wasted or stored according to the adopted operational groundrules, increasing storage reduces waste energy which, in turn, increases system efficiency and capacity factor. This reduces energy cost until the storage size reaches a value where further increases are no longer effective in reducing waste energy. After this point is reached, the added cost of further storage increases the energy cost.

There is a particular capacity factor at the storage size corresponding to minimum energy cost. Selection of another collector area and a repetition of the process of increasing storage capacity, will provide a different minimum energy cost at a different capacity factor. By systematically varying collector field area and repeating the process, a curve of minimum energy costs as a function of capacity factor is determined. This constitutes the primary output of the computer power plant simulation program.

B. MINIMUM ENERGY COST ENVELOPES

Minimum energy cost envelopes are presented in Figures B-4, B-5, and B-6 for the paraboloidal dish, central receiver, and parabolic trough, respectively. For this set of three charts, envelope curves for five sites representative of major regions in the Continental United States are shown. The selected sites are:

	Region
• Barstow, CA	Southwest
• Omaha, NE	Midwest
• Miami, FL	Southeast
• Maynard, MA	Northeast
• Medford, OR	Northwest

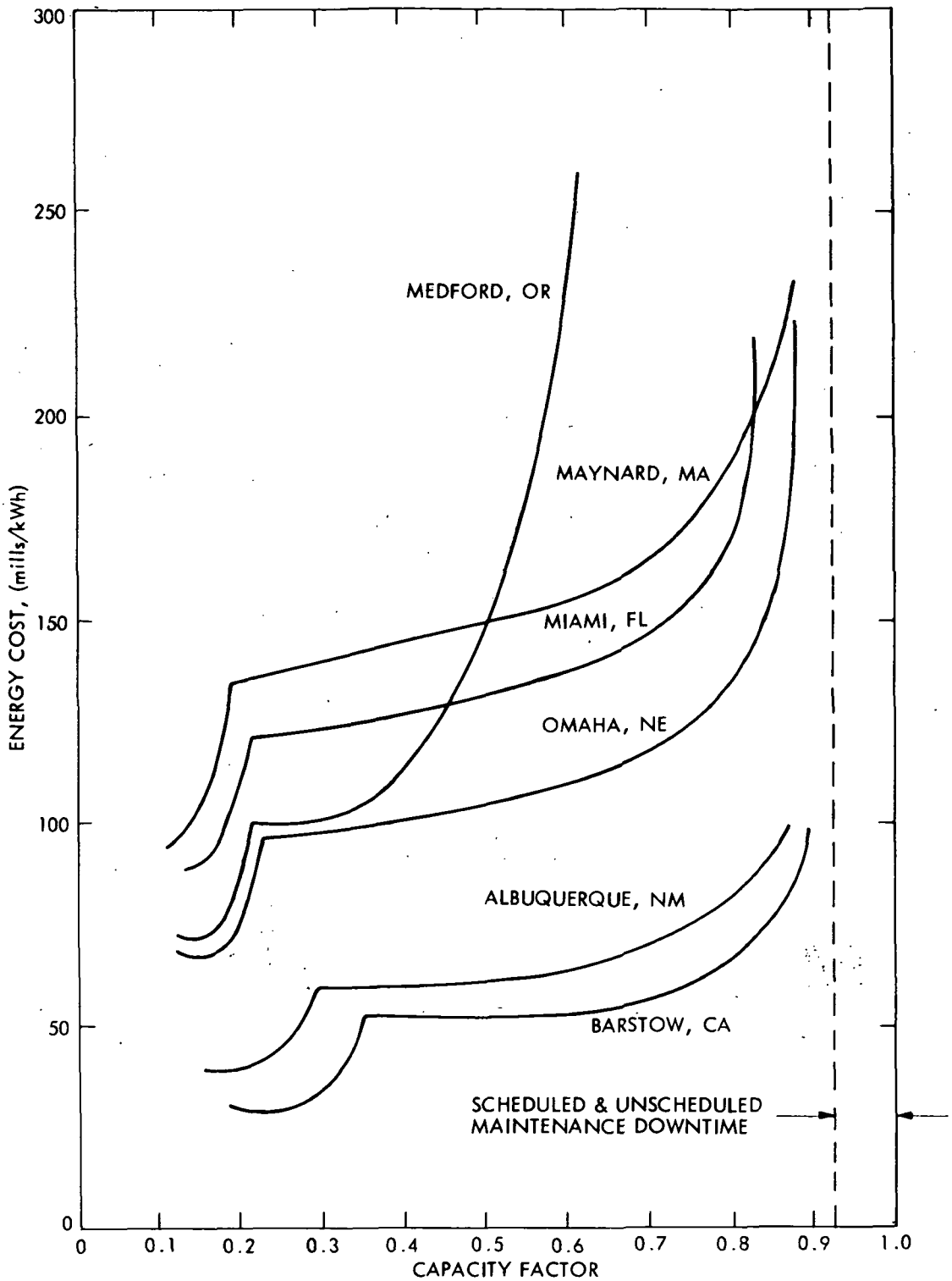

Figure B-4. Minimum Energy Cost Envelopes for the Paraboloidal Dish Stirling System

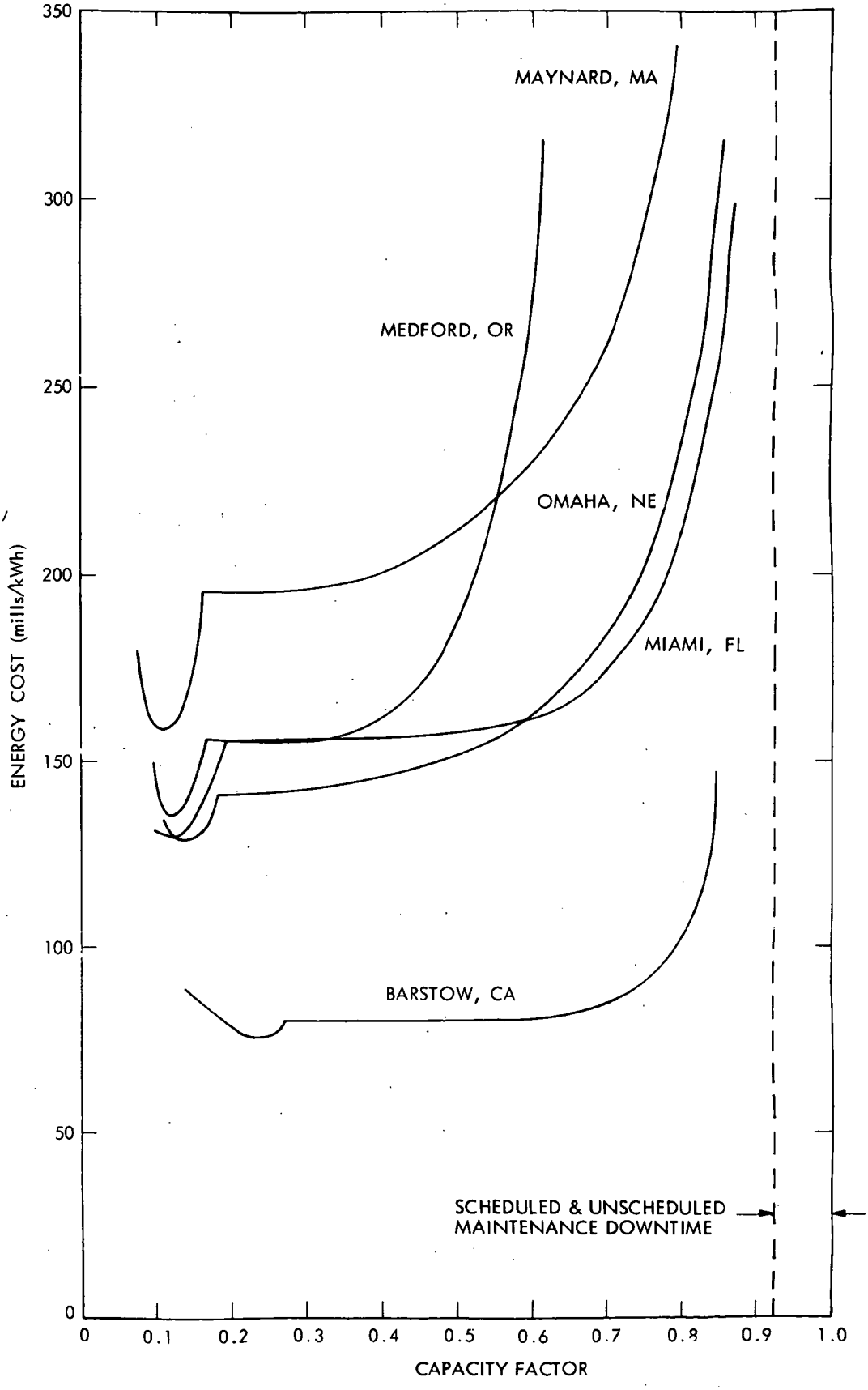

Figure B-5. Minimum Energy Cost Envelopes for the Central Receiver System

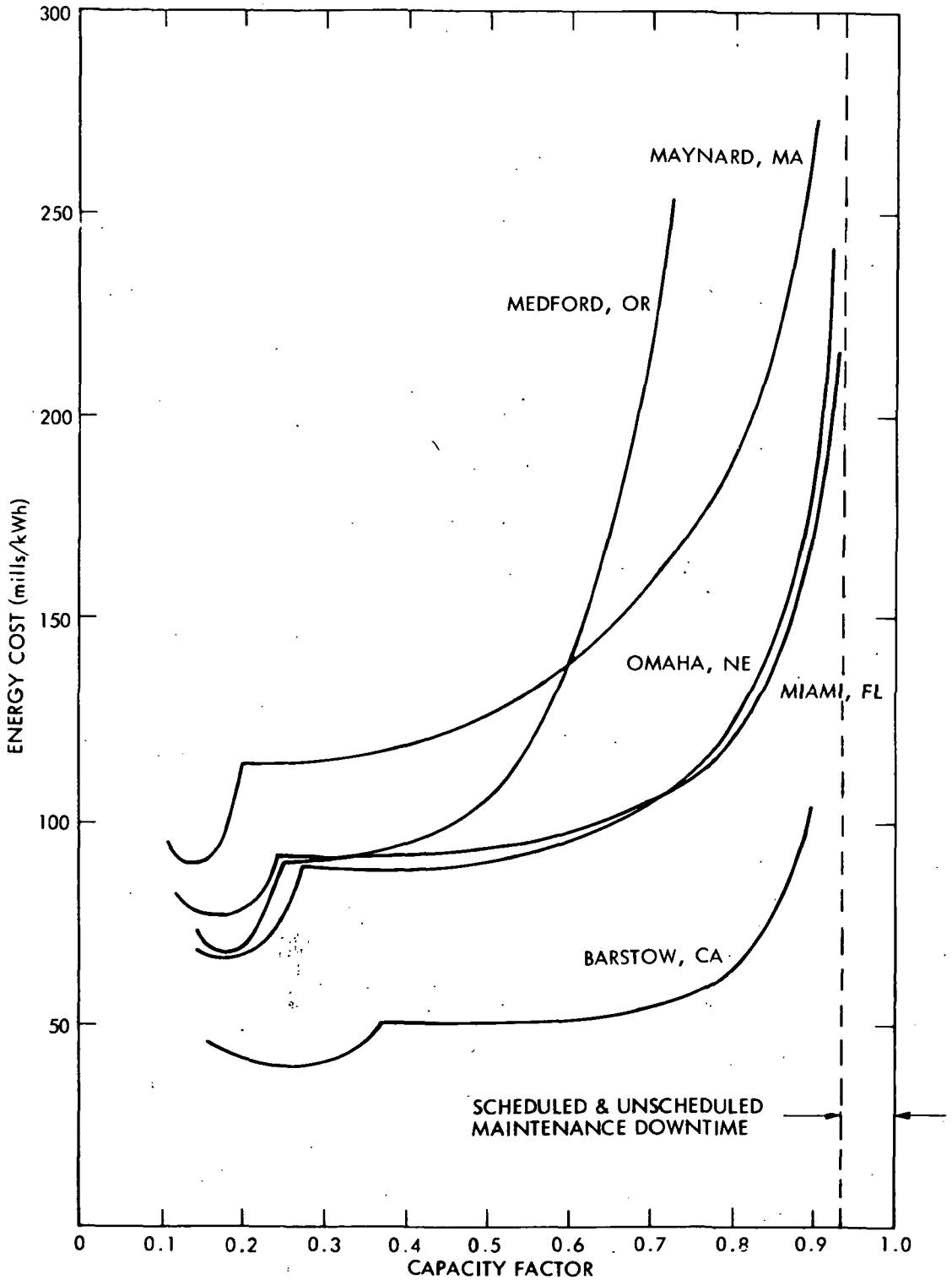

Figure B-6. Minimum Energy Cost Envelopes for the Parabolic Trough System

Additionally, Albuquerque, N.M., is shown on Figure B-4 to illustrate that significant site-specific differences exist within any region. Both Albuquerque and Barstow are in the Southwest, but Barstow has a higher level of annual direct insolation and consequently achieves lower energy costs.

The envelope curves are generally characterized by a sharp dip in energy costs at a low capacity factor and a rapid rise at high capacity factors. The dip at low capacity factors occurs when storage is no longer beneficial. The cost of a storage system is composed of a term proportional to plant power rating (or the rate at which energy is stored and extracted) and a term proportional to storage capacity (see Ref B-25). As long as even a small amount of energy is to be stored, the power-dependent cost term remains virtually unchanged for a fixed power from storage. Thus, at a low capacity factor when the storage system is no longer needed, the power-dependent capital cost is deleted and a corresponding decrease in energy costs results.

As the average annual insolation decreases, the no-storage dip occurs at lower capacity factors, e.g., the dip occurs at a lower capacity factor at Maynard, MA, than at Barstow, CA. The annual total direct insolation at Maynard is 1253 kWh/m^2 yr as compared to 2848 kWh/m^2 yr in Barstow. Regions of low insolation require a larger collector field area at a given capacity factor (or annual level of energy delivery). In these regions, there are some days where insolation intensity is comparable to that in high insolation regions. For these sunny days, the large field area results in excess energy that needs to be stored. Hence, storage is generally employed at lower capacity factors for low-insolation regions.

The dip in energy cost is more pronounced when it occurs at low capacity factors. This results because the energy cost savings is proportional to the capital cost change (which is essentially constant) divided by the capacity factor (which is a measure of energy delivered). Therefore, when capacity factor is low, larger energy cost changes occur.

As the collector area and capacity factor decrease beyond the dip, energy costs increase. This occurs because of the selected operational groundrules. The power systems were not allowed to operate at below ten percent of rated power. For plants of smaller collector area, this cut-off becomes increasingly significant.

The minimum point in the dip corresponds approximately to the no-storage case where the plant is able to produce rated power only on those days having high solar intensities. For capacity factors lower than this minimum, the plant cannot produce rated power. This region is not of interest and is presented only in the context of identifying the minimum-energy-cost, no-storage plant.

The rapid increase in the minimum energy cost envelope at high capacity factors is governed by characteristics of the insolation patterns. The maximum capacity factor that can be achieved is determined by the scheduled and unscheduled maintenance downtime. (A 7 percent downtime is used for all plants in this study.) As this maximum level is approached, the plant must operate on a nearly

continuous basis. To operate on a continuous basis, large storage times are needed since, in all regions, there are periods of inclement weather where days of storage are required for the plant to produce power. To provide days of storage requires large collector field areas. The combination of large field areas and large storage results in high capital costs for a small increase in capacity factor and results in the rapid increase in energy costs at high capacity factors shown in Figures B-4, B-5, and B-6.

At Medford, OR, the rapid increase in energy cost with increasing capacity factor occurs at a relatively low capacity factor. This effect is due to a large seasonal shift in insolation characteristics as shown in Appendix A. The area and storage combination that is best for one season performs poorly during the other seasons. This mismatch results in the need for large areas and storage capacities at unusually low capacity factors.

All the minimum energy cost envelopes for the three systems exhibit the same basic trends. The lowest energy costs are achieved in the solar-intensive Southwest. At the lower insolation levels corresponding to other sites, the curves shift to higher energy costs. The two-axis tracking central receiver and paraboloidal dish achieve energy costs of about 50 mills/kWeh in the Southwest sunbelt, whereas the one-axis tracking parabolic trough has a value between 50 and 100 mills/kWe hr. The non-tracking CPC exhibits similar trends but at a higher energy costs.

C. COLLECTOR FIELD AREAS AND STORAGE TIMES

Each point along the minimum envelope curves in each of Figures B-4, B-5, and B-6, coprresponds to a different variant of the power plant type presented by the figure. Each variant plant has a different combination of field area and storage time. If the capacity factor and regional location (insolation characteristics) are specified, the collector field area and storage time corresponding to a plant yielding minimum energy costs can be determined. Figures B-7 through B-9 address collector field areas whereas Figures B-10 through B-12 pertain to storage.

Collector areas for minimum energy cost plants are presented in Figures B-7, B-8, and B-9 for capacity factors of 0.55, 0.40, and no storage (capacity factor variable), respectively. The following overall trends are shown by these charts: (1) Higher capacity factors require larger areas. (2) Regions of lower insolation need larger collector areas for any given capacity factor. (3) Two-axis tracking systems (PDS and CR) generally require smaller collector areas than one-axis tracking systems as represented by the parabolic trough (PT). The non-tracking CPC (now shown) required a larger collector area than the PT.

At a capacity factor of 0.55 (Figure B-7), the areas required at Medford, OR are considerably higher than is indicated by the general trend. As previously described, this is due to the strong seasonal variation in insolation at Medford. At a capacity factor of 0.40 (Figure B-8), the Medford data are consistent with general trends.

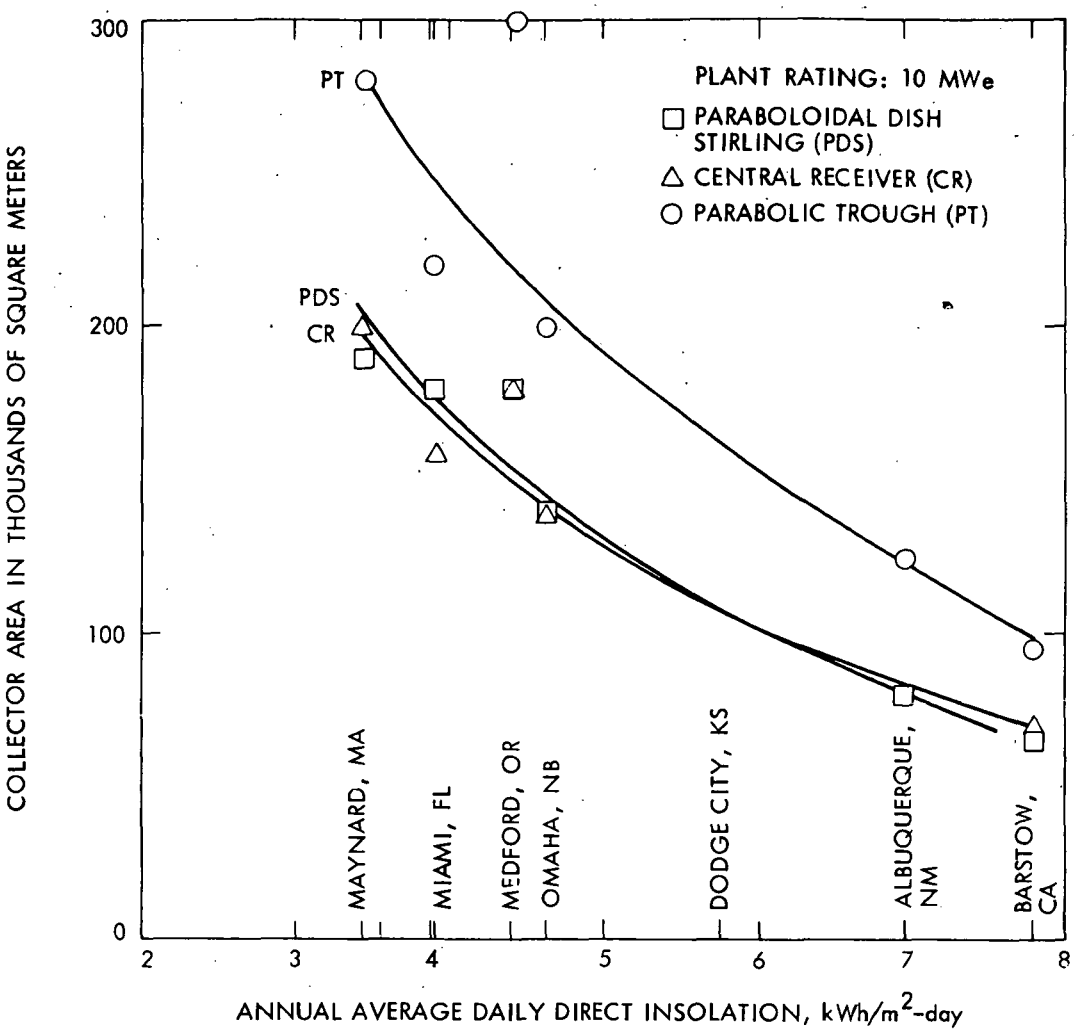

Figure B-7. Effect of Regional Insolation Differences on Collector Field Area for Capacity Factor = 0.55

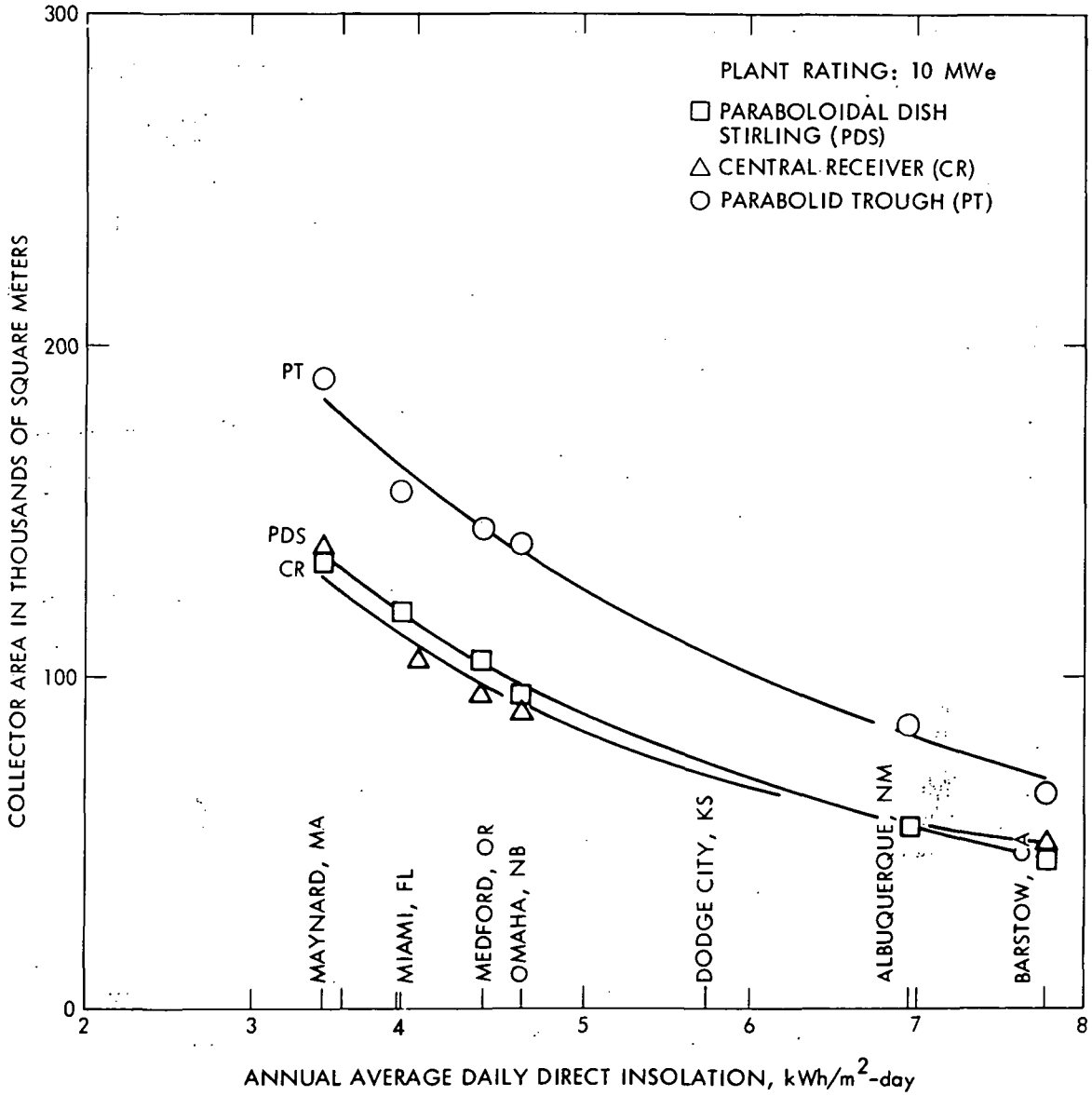

Figure B-8. Effect of Regional Insolation Differences on Collector Field Area for Capacity Factor = 0.40

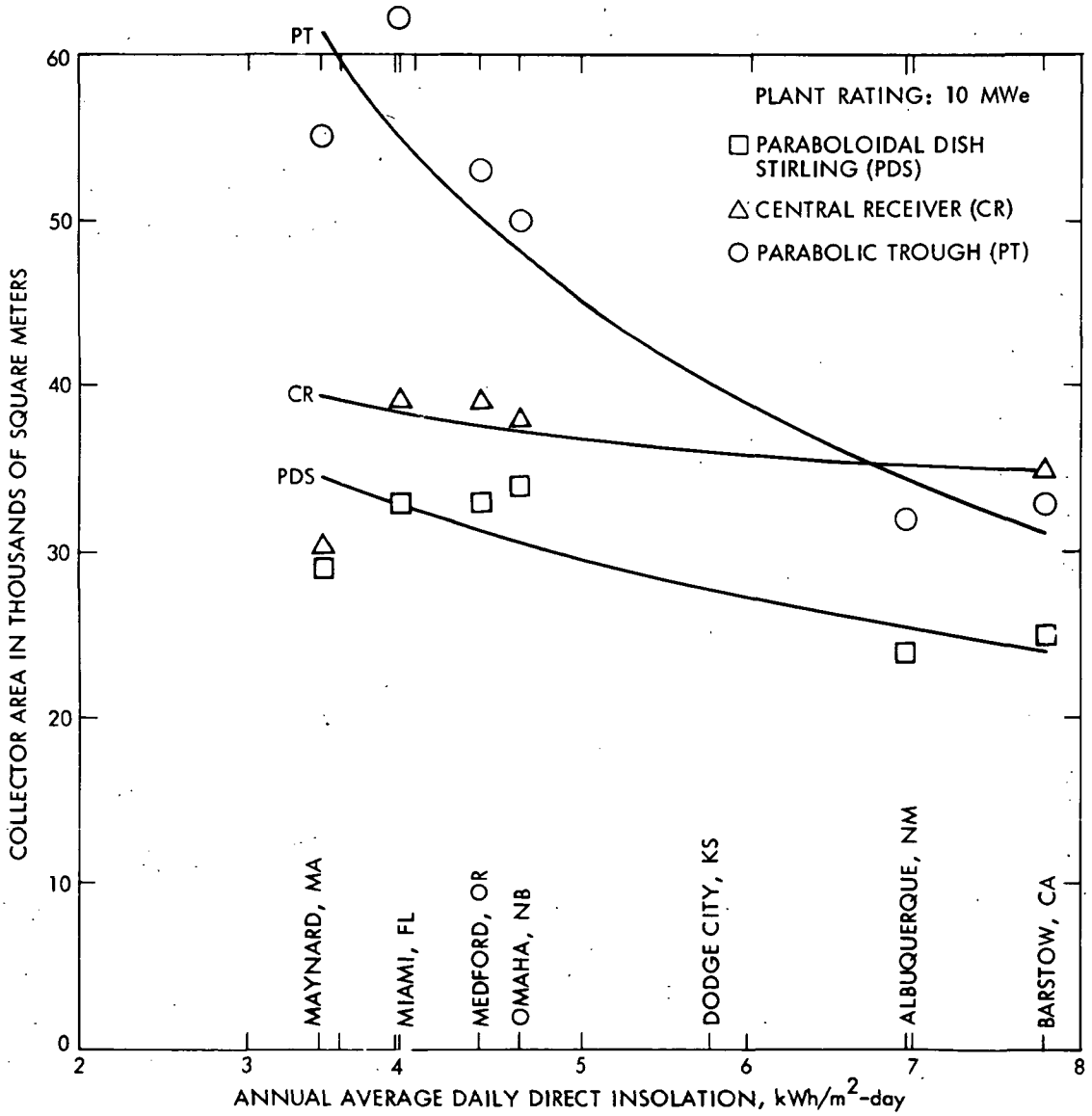

Figure B-9. Effect of Regional Insolation Differences on Collector Field Area for No Storage

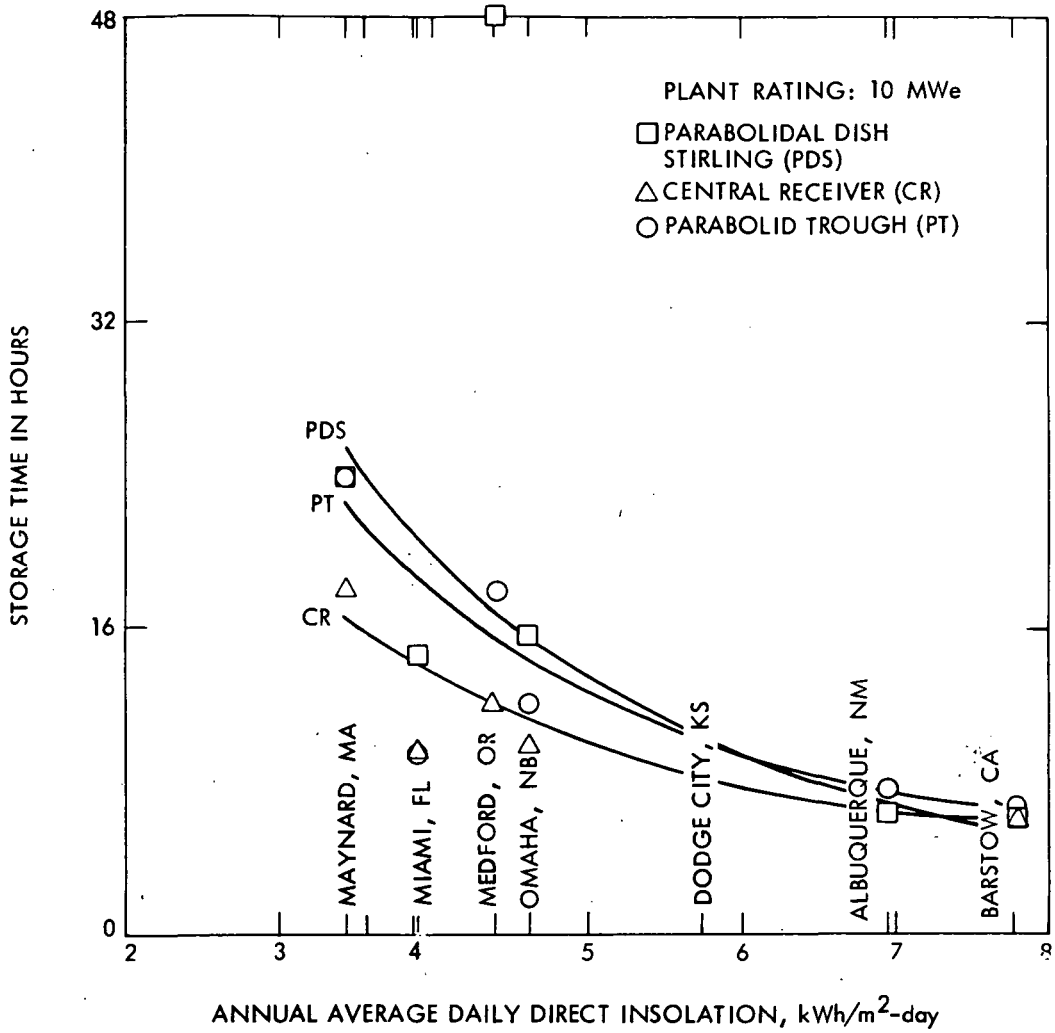

Figure B-10. Effect of Regional Insolation Differences on Storage Time for Capacity Factor = 0.55

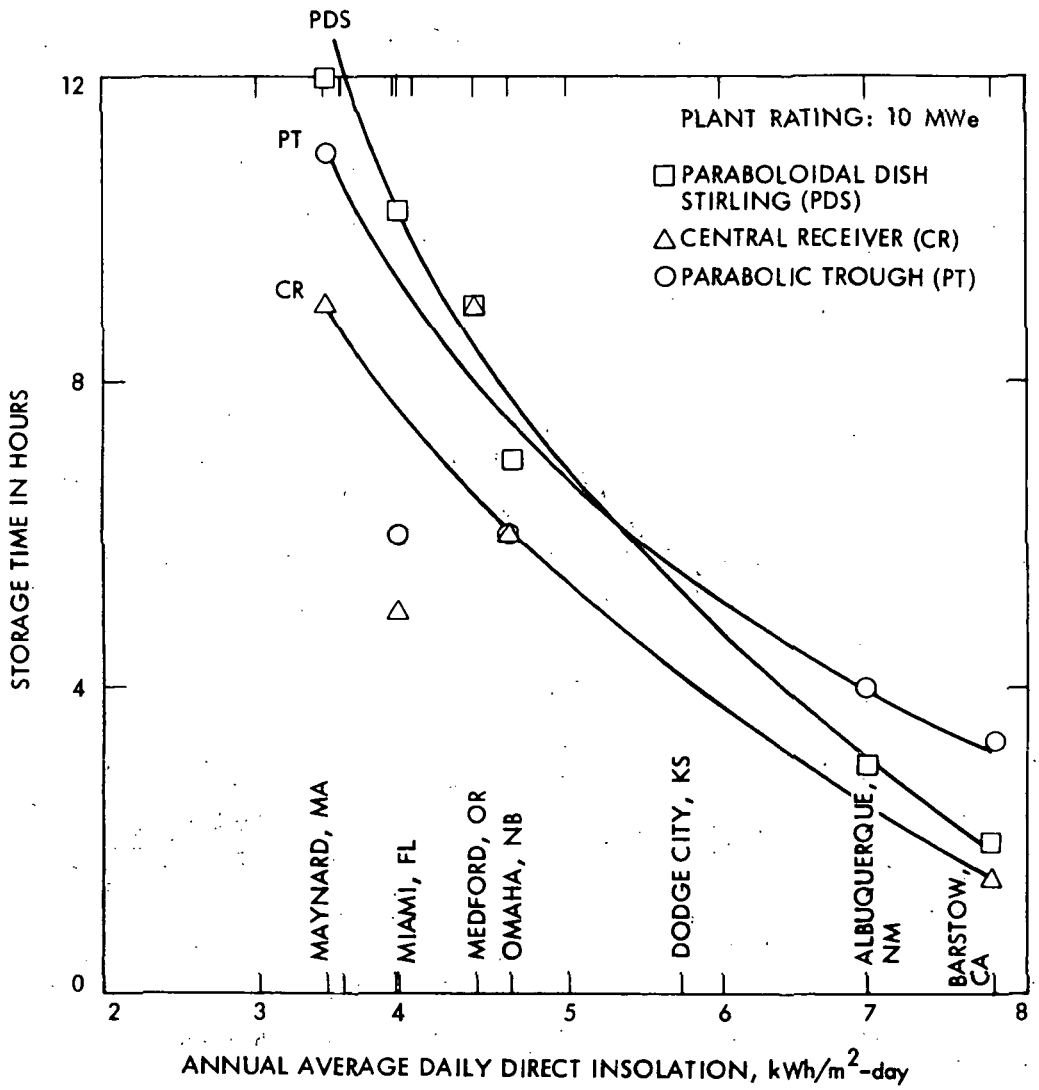

Figure B-11. Effect of Regional Insolation Differences on Storage Time for Capacity Factor = 0.4

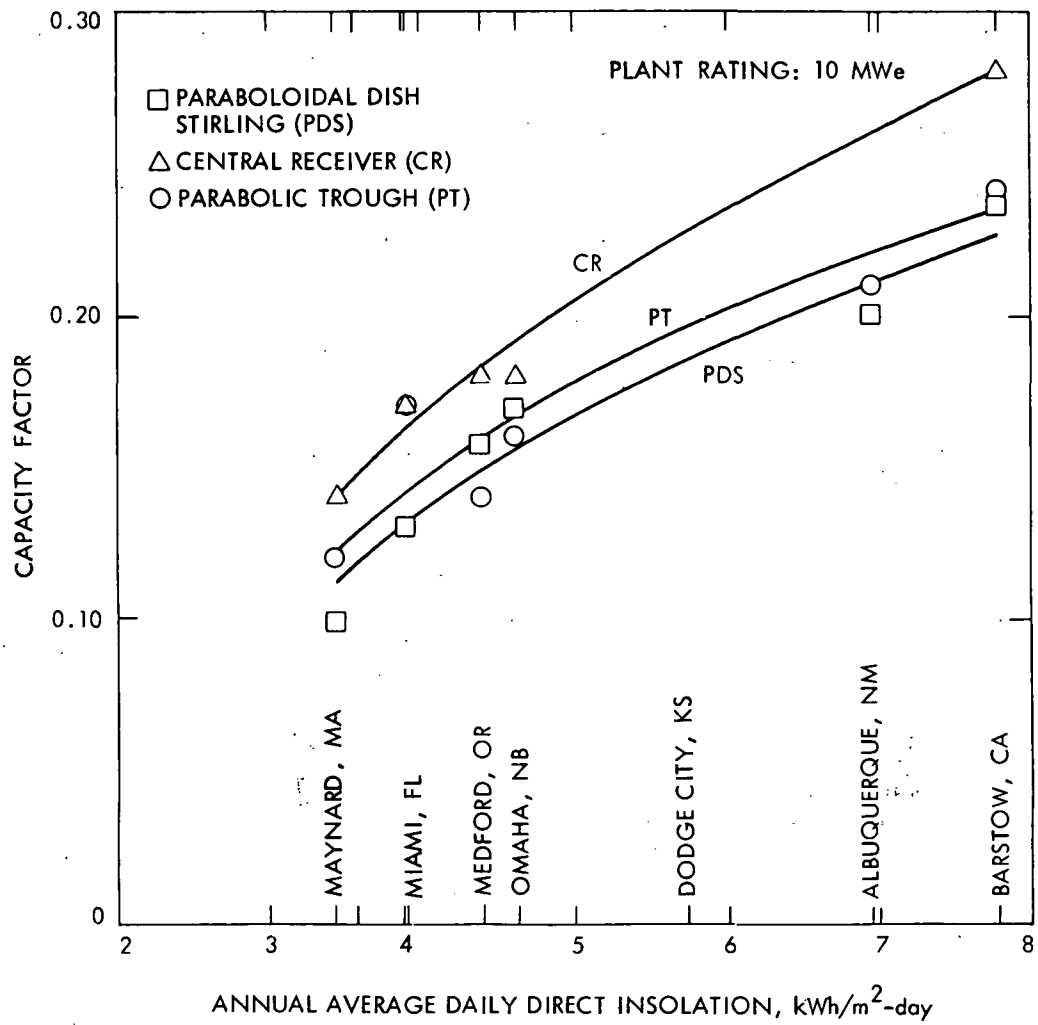

Figure B-12. Effect of Regional Insolation Differences on Capacity Factor for No Storage

C-2

The no-storage case (Figure B-9) is presented primarily to show that relatively small areas are sufficient for all regions. These areas were estimated by interpolation in the dip region of the minimum energy cost enevelope curves, and this accounts for the scatter in some of these data. Detailed computer calculations to improve the accuracy of these estimates were not undertaken in this study since such improvement would not alter the study conclusions.

The storage times corresponding to optimum plants at capacity factors of 0.55 and 0.40 (Figures B-7 and B-8) are presented in Figures B-10 and B-11, respectively. General trends are that storage time increases with capacity factor and decreases with increasing insolation, i.e., the lowest storage requirements are in the sunbelt region. For the no-storage case, capacity factor is presented as a function of insolation level in Figure B-12. As discussed earlier, the capacity factor corresponding to the no-storage case decreases as the insolation level decreases. The points shown on Figure B-10 through B-12 were determined by approximate interpolation procedures using the minimum-energy-cost envelopes. Although the procedure results in some data scatter, the general trends are well delineated. Interpolation accuracy can be improved by using a fine mesh of collector areas and storage times to determine the envelope curves. However, this would have required additional costly computer runs, and improved accuracy was not considered to be warranted by the purposes of the present study.

D. CAPITAL COST BREAKDOWN FOR SELECTED SYSTEMS

Capital costs for the four selected systems are presented in Figure B-13 for three locations (Barstow, Omaha, and Maynard). The capacity factor is 0.55 for all the plants shown in this figure. The capital costs for the two-axis tracking systems (PDS and CR) are lower than the one-axis tracking PT and the non-tracking CPC at all locations. Lowest costs occur in the sunbelt region as represented by Barstow.

As the insolation level decreases, progressively higher capital costs are required. This follows from the increased requirements for both collector field area and storage time as shown in Figures B-7 through B-12. Capital costs at Maynard are roughly double those at Barstow.

For each of the plants, capital costs are broken down into major cost categories. Collectors are the largest single cost item of the major categories shown. Electrical transport costs for PDS and thermal transport within the tower of CR are relatively small. For the CR, the transport costs, as well as the tower cost, are included in the collector cost. The pipeline network thermal transport systems used for both the PT and the CPC comprise a significant fraction of their total capital costs.

Storage cost increases for locations such as Maynard relative to Barstow are directly related to the need for greater storage times, cf. Figure B-10. Also, less efficient systems, such as the CPC,

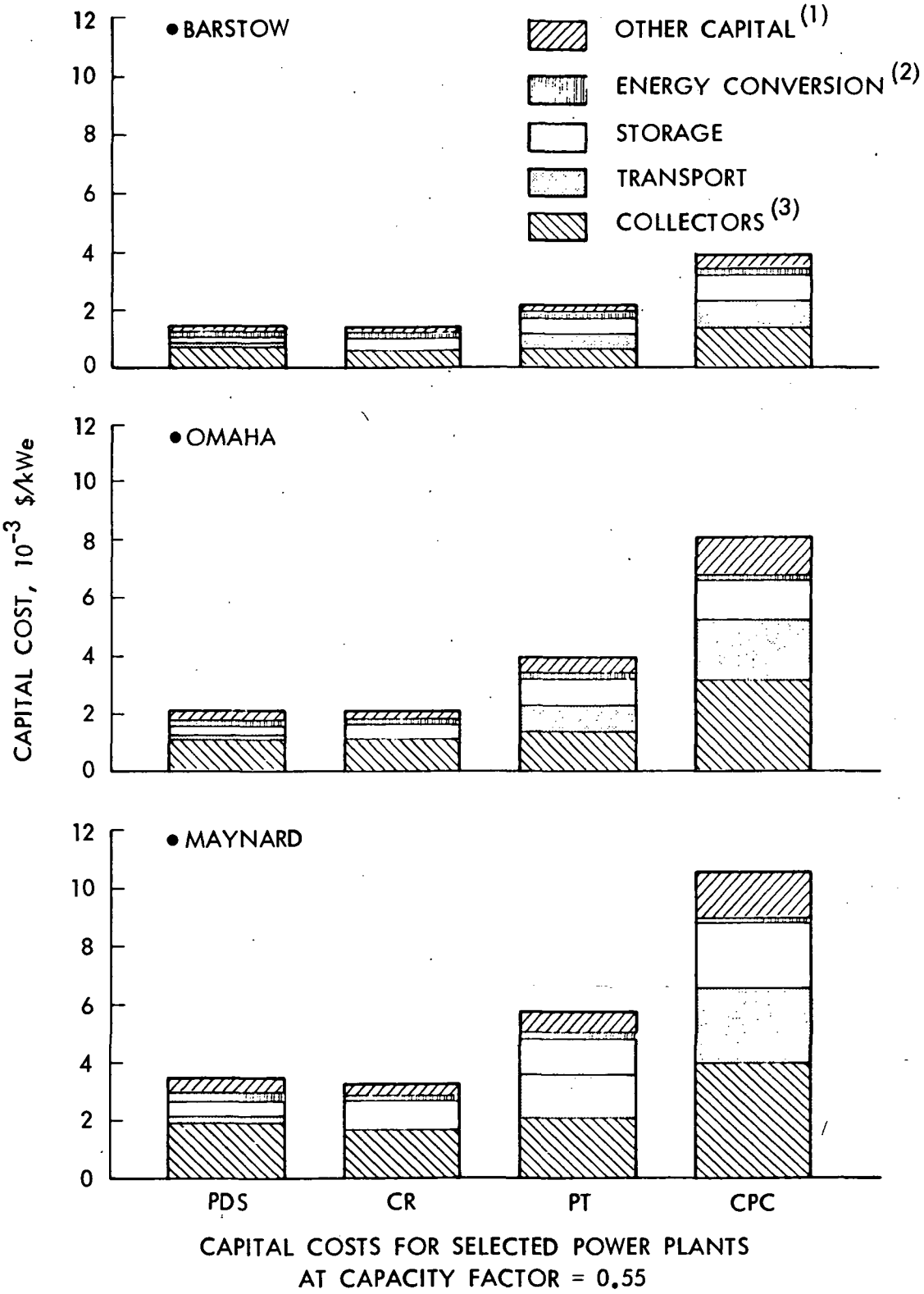

Figure B-13. Capital Costs for Selected Power Plants at Capacity Factor = 0.55

require larger size thermal storage units since a relatively smaller fraction of the stored energy is converted to electricity.

The energy conversion costs (including balance of plant) are the same for all the three systems which employ a central 10 MWe power generation unit (CR, PT, and CPC) since the same unit cost was assumed for all engine types. For the PDS system, conversion costs are linked to collector field area. The basic power generation module is a dish with a small heat engine/generator assembly at the focal point of each collector and, hence, as the collector field area is increased by adding more modules, the number of engines increases proportionately.

Other capital includes indirect costs such as architect and engineering (A&E) and construction management fees. Spares and contingencies are also included in other capital. A value of fifteen percent of total direct costs is used for all systems.

IV. REFERENCES

B-1. "Thermal Power Systems Multi-Year Program Plan," Draft, Department of Energy, April 7, 1978.

B-2. "Advanced Thermal Energy Storage Technology Development For Solar Thermal Power," Draft of FY 1980-85 Program Plan, Department of Energy, September 13, 1978.

B-3. Pettit, R. B., "Characterization of the Reflected Beam Profile of Solar Mirror Materials," Sandia Laboratories, Albuquerque, Solar Energy, Vol. 19, pp. 733-741, Pergamon Press, Great Britain, 1977.

B-4. Butler, B. L., and Pettit, R. B., "Optical Evaluation Techniques for Reflecting Solar Concentrators," Sandia Laboratories, Albuquerque, SPIE Vol. 114, Society of Photo-Optical Instrumentation Engineers, Bellingham, Washington, 1977.

B-5. Pettit, R. B., and Butler, B. L., "Laser Ray Trace and Bi-Directional Reflectometry Measurements of Various Solar Concentrators," Sandia Laboratories, Albuquerque, SAND-77-1466, Presented at the ERDA Concentration Solar Collector Conference, Georgia Inst. of Tech., Atlanta, GA., Sept 26-28, 1977.

B-6. Pettit, R. B., and Butler, B. L., "Mirror Materials and Selective Coatings," Sandia Laboratories Report SAND 77-0111, February 1977.

B-7. Fujita, T.; Manvi, R.; Roschke, E. J.; El Gabalawi, N.; Herrera, G.; Kuo, T. J.; and Chen, K. H. "Techno-Economic Projects for Advanced Small Solar-Thermal Electric Power Plants to Years 1990-2000," DOE/JPL-1060-78/4, Jet Propulsion Laboratory, Pasadena, CA, November 1978.

B-8. Holl, R. J., "Small Central Receiver Cost Definition Final Review," McDonnell-Douglas, Oct. 21, 1977.

B-9 "Definition of Two Small Central Receiver Systems," SAND-78-7001, Sandia Laboratories, Albuquerque, N.M., January 1978.

B-10. Woodard, Joan, Private Communication, 1979.

B-11. Schimmel, Walt, Private Communication, 1979.

B-12. Winston, R., "Solar Concentrators of a Novel Design," Solar Energy 16, 89, 1974.

B-13. Teagan, W. P. and Cunningham, D. R., "Conceptual Design and Analysis of a Compound Parabolic Concentrator Collector Array," ANL-K77-3855-1, prepared by Arthur D. Little, Inc., for Argonne National Laboratory, Argonne, IL, August 1977.

B-14. Duvall, G. D., "Operational Evaluation of a Closed Brayton Cycle Laboratory Engine," David Taylor Naval Ship Research and Development Center, Paper No. 76029, presented at the 11th IECEC, Stateline, Nevada, Sept. 12-17, 1976.

B-15. "Central Receiver Solar Thermal Power System, Phase 1, Pilot and Commercial Plant Cost and Performance," Preliminary Draft No. MDC G6776, Vol. VII, McDonnell-Douglas Astronautics Company, Huntington Beach, CA, May 1977.

B-16. Powell, J. C., "Solar Pilot Plant Phase I, Preliminary Design Report, Pilot Plant Cost and Commercial Plant Cost and Performance," Report No. F3419-DR-302-III, Vol. VII, Honeywell Energy Resources Center, Minneapolis, MN, June 7, 1977.

B-17. Turner, R. H., "Economic Optimization of the Eergy Transport Component of a Large Distributed Collector Solar Power Plant," presented at the 11th IECEC, State Line, Nevada, Sept. 12-17, 1976.

B-18. DOE, "Proceedings of Second Annual Thermal Energy Storage Contractor's Information Exchange Meeting," September 1977, Gatlinburg, TN, DOE Publication No. CONF-770955, September 1977.

B-19. Public Service Electric and Gas Co., "An Assessment of Energy Storage Systems Suitable for Use by Electric Utilities," ERDA Report No. E(11-1)-2501, July 1976.

B-20. Gintz, J. R., "Advanced Thermal Energy Storage Concept Definition Study for Solar Brayton Power Plants," Boeing Engineering and Construction Co., Report No. SAN/1300-1,2,3,4, Seattle, WA, November 1977.

B-21. Bramlete, T., et al., "Survey of High Temperature Thermal Energy Storage," Sandia Laboratories, March 1976.

B-22. Boruck, A., "Survey and Selection of Inorganic Salts for Application to Thermal Energy Storage," ERDA, June 1976.

B-23. "Technical Assessment Guide," EPRI PS-866-SR, Electric Power Research Institute, Palo Alto, CA, June 1978.

B-24. Doane, J. W., et al., "The Cost of Energy from Utility-Owned Solar Electric Systems, A Required Revenue Methodology for ERDA/EPRI Evaluations," Internal Report 5040-29, ERDA/JPL-1012/7613, Jet Propulsion Laboratory, Pasadena, CA, June, 1976.

B-25. El Gabalawi, N, Hill, G., Bowyer, J.M., and Slonski, M. L., "A Modularized Computer Simulation Program for Solar Thermal Power Plants," JPL Internal Report 5102-80, Jet Propulsion Laboratory, Pasadena, CA, July, 1978.

APPENDIX C

PARAMETRIC TRADEOFF AND SENSITIVITY ANALYSES OF ADVANCED SOLAR THERMAL POWER PLANTS

CONTENTS

Figures

I. INTRODUCTION

The nominal performance and cost values used in this study anticipate the successful development of advanced technologies and a level of market penetration for solar systems that will result in high-volume mass production of critical cost components such as concentrators. These projections were made in the context of the 1990-2000 timeframe, and, accordingly, computer simulations (Appendix B) were based on plant startup in the year 2000.

Variations in the extent to which advanced technologies are developed and the level of market penetration will result in variations about the selected nominal values. To delineate the effect of variation about the nominal projected values, selected parametric tradeoff and sensitivity analyses have been performed, and the corresponding results are presented in this appendix.

II. BASIC TRADEOFFS

For the different types of solar thermal power plants, the key factors governing comparative techno-economics are system efficiency and collector costs. This basic tradeoff and its ramifications are first described for four types of plants consisting of the (1) paraboloidal dish Stirling (PDS), (2) central receiver (CR), (3) parabolic trough (PT), and (4) Compound Parabolic Concentrator (CPC). Then, fundamental design tradeoffs are discussed in the context of the effect of site-specific or regional insolation differences.

A. EFFICIENCY VS COST

The effect of system design efficiency on busbar energy costs of the four selected advanced systems is presented in Figure C-1. System design efficiency is the ratio of delivered electrical energy to the design value chosen for the product of direct insolation and collector field area. For a fixed plant rating and specified annual energy delivery as denoted by capacity factor, power plant types having higher system design efficiencies require smaller collector field areas.

Generally, more efficient plant types (CR and PDS) employ two-axis tracking collector configurations that are more costly per unit area than simpler one-axis tracking (PT) and non-tracking arrangements (CPC). Although lower collector costs were projected for the simpler collector systems (PT and CPC), the higher system efficiencies of the two-axis tracking systems (CR and PDS) exert a dominant influence which results in lower busbar costs for the systems. As illustrated by the charts for Barstow, CA., Omaha, NE., and Maynard, MA., this basic trend holds for all the regions examined in the study.

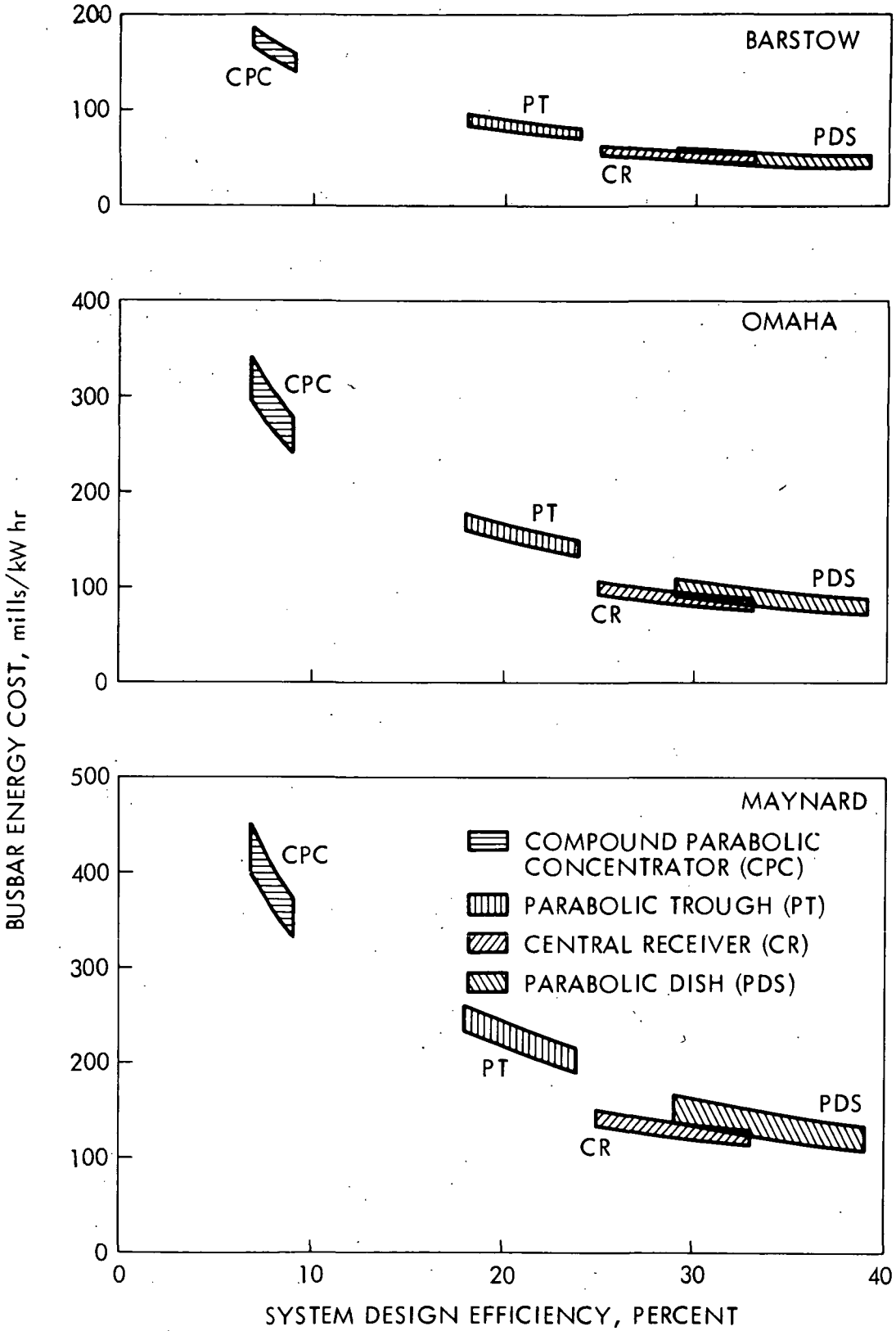

Figure C-1. System Design Efficiency and Collector Cost Tradeoffs

The effects of variations in concentrator costs and system design efficiency are delineated on Figure C-1. For the PDS system, the concentrator cost target range is 70-100 $/m^2$. A nominal value of 85$/m^2$ was used in this study. The target range of concentrator cost represents a ±18% vertical variation about the nominal value. This variation was applied to all the plant types to determine the energy cost range shown on Figure C-1. The cost values are given below:

Type of Plant	Concentrator Costs, $/m^2 Low	Nominal	High
PDS	70	85	100
CR	53	65	77
PT(1)	57	70	83
CPC(1)	41	50	59

(1)Includes receiver costs.

The nominal system efficiency was based on achieving 70% of Carnot. Present engines achieve about 60% of Carnot whereas very advanced engine concepts are projected to attain values approaching 80% of Carnot (Ref. C-1). A range of system design efficiencies corresponding to energy conversion efficiencies ranging from 60%, to 80% of Carnot has been applied in Figure C-1 and results in the horizontal variation about the nominal value.

B. SITE-SPECIFIC INSOLATION EFFECTS ON POWER PLANT DESIGN

For each of the power plant types considered, design tradeoffs can be performed to optimize plant design for a given set of site-specific factors. Insolation differences from site-to-site require detailed design perturbations in order to achieve optimum performance at each of the sites. Application of these extensive design optimization procedures was not within the scope of the present study. However, it is important to identify key tradeoffs and note, as a caveat, that some tradeoffs remain to be identified before further design improvements/refinements can be made to the power plants analyzed in this study.

1. Concentration Ratio and Operating Temperature

The concentration ratio and operating temperature of the receiver can be tailored to match prevailing insolation characteristics with the objective of maximizing receiver efficiency. For a given operating temperature, receiver heat losses (reradiation, convection, and conduction) are essentially constant. Since receiver efficiency is the heat input rate minus the loss rate divided by the heat input rate, it follows that receiver efficiency improves as the heat input rate increases (for constant temperature). Thus, for a fixed collector geometry and given operating temperature, highest receiver efficiencies are attained in the sunbelt regions having the highest insolation and, hence, the highest receiver heat input rate.

For sites where insolation is low, the reduction in receiver efficiency can be at least partially offset by allowing the receiver to operate at a lower temperature. However, reducing the temperature decreases the power conversion efficiency. For an optimum system, the product of these two efficiencies must be maximized. The systems treated in the present study were designed for optimal performance in the Southwest sunbelt. Thus, in other regions (particularly those having low insolation levels), a reduction in operating temperature might result in improved performance.

Another variable that affects receiver performance is concentration ratio. Since receiver performance at a given temperature improves as the heat input rate increases, higher concentration ratios (which increase the heat input rate) are generally desirable. This is particularly true at high operating temperatures. Increases in concentration ratio require more accurate concentrator surfaces. Since the advanced projections are already based on the achievement of highly accurate reflective surfaces, a further improvement in accuracy to increase concentration ratio was not considered to be a feasible way of compensating for lower insolation levels.

The CPC concept involves a further tradeoff. A part of the diffuse insolation is used to heat the receiver. As the concentration ratio is reduced, a greater portion of the diffuse insolation can reach the receiver because side-wall reflective surfaces are smaller and impose less limitations on the collector's field of view . However, the direct beam insolation will be less concentrated. This results in a reduced heat rate to the receiver from beam insolation. Thus, concentration ratios for the CPC are chosen to achieve a balance between these effects so as to provide the highest overall performance.

Argonne National Laboratory, developers of the CPC concept, recommend concentration ratios of 3 to 5 for all regions. For most regions the diffuse component is very small, and, even for locations such as Miami, FL, which is known to have a high level of diffuse insolation, the diffuse component reaches a value of only about 30 percent of the total horizontal insolation. Thus, insolation is available primarily in the direct or beam form, and large departures from the concentration ratios deemed appropriate for sunbelt regions are expected to degrade the performance of solar thermal collectors.

2. Engine Selection and Sizing

Regional insolation levels can affect both engine selection and sizing. If the receiver operating temperature is decreased for regions of low insolation, the choice of engine type could be affected. For example, steam Rankine engines appear to be preferable to Brayton engines at 1000°F. Brayton engines provide a relatively higher performance at temperature above 1500°F where present steam Rankine engines and their advanced derivatives are unable to operate.

For systems employing thermal storage (CR, PT, and CPC), engine sizing is not affected by insolation patterns. The engines are sized in accord with the desired plant rating. (A rating of 10 MWe was selected for this study). For the PDS system, which uses battery storage, the selection of engine size for the study was based on choosing engine rated power so as to accept peak levels of insolation available in the Southwest sunbelt regions. As seen from the histograms presented in Appendix A, most sites achieve peak insolation values approaching those of the sunbelt but, in many cases, for only a very small fraction of the total time during which insolation is received. Under these conditions (which occur primarily in regions of low insolation), the Stirling engine operates at part-load ratings (Appendix B) where efficiency is appreciably degraded.

In these regions of low insolation, if a smaller engine of lesser power rating were employed, it would operate closer to its design efficiency during those periods when the bulk of the power was being generated. A higher system efficiency would result from this small-engine design, even though a small amount of power at peak intensities would be wasted (via, e.g., collector defocusing). Further, the smaller engine would require a smaller capital investment. Thus, the possibility exists for improving the techno-economics of the PDS system in low-insolation regions.

SECTION III. SENSITIVITY TO UNCERTAINTIES IN PROJECTIONS

The sensitivities of solar thermal plant energy costs to variations in the cost and efficiency of all major subsystems were determined in Ref. C-2. Although updated cost and efficiency values are used in the present study, the trends shown in Ref. C-2 generally still hold. Selected sensitivity results are presented herein only to make specific points.

A. CONCENTRATOR UNIT COSTS

Concentrator unit costs are the most critical cost driver. The low-cost values used in this study are based on high-volume mass production (Refs. C-3 and C-4). Sensitivity of busbar energy cost to concentrator unit cost is shown on Figure C-2. Curves for the four selected systems are presented at Barstow, Omaha, and Maynard.

It is seen that the variation in energy cost with concentrator unit cost becomes more pronounced in regions of low insolation such as Maynard. For a given capacity factor (0.4 is used on Figure C-2), collector field areas are larger in regions of low insolation. Hence, energy costs are relatively more sensitive to concentrator unit costs in regions of low insolation.

Further, the more efficient systems (CR and PDS) require smaller collectors areas and are therefore less sensitive than the PT and CPC systems to collector unit costs.

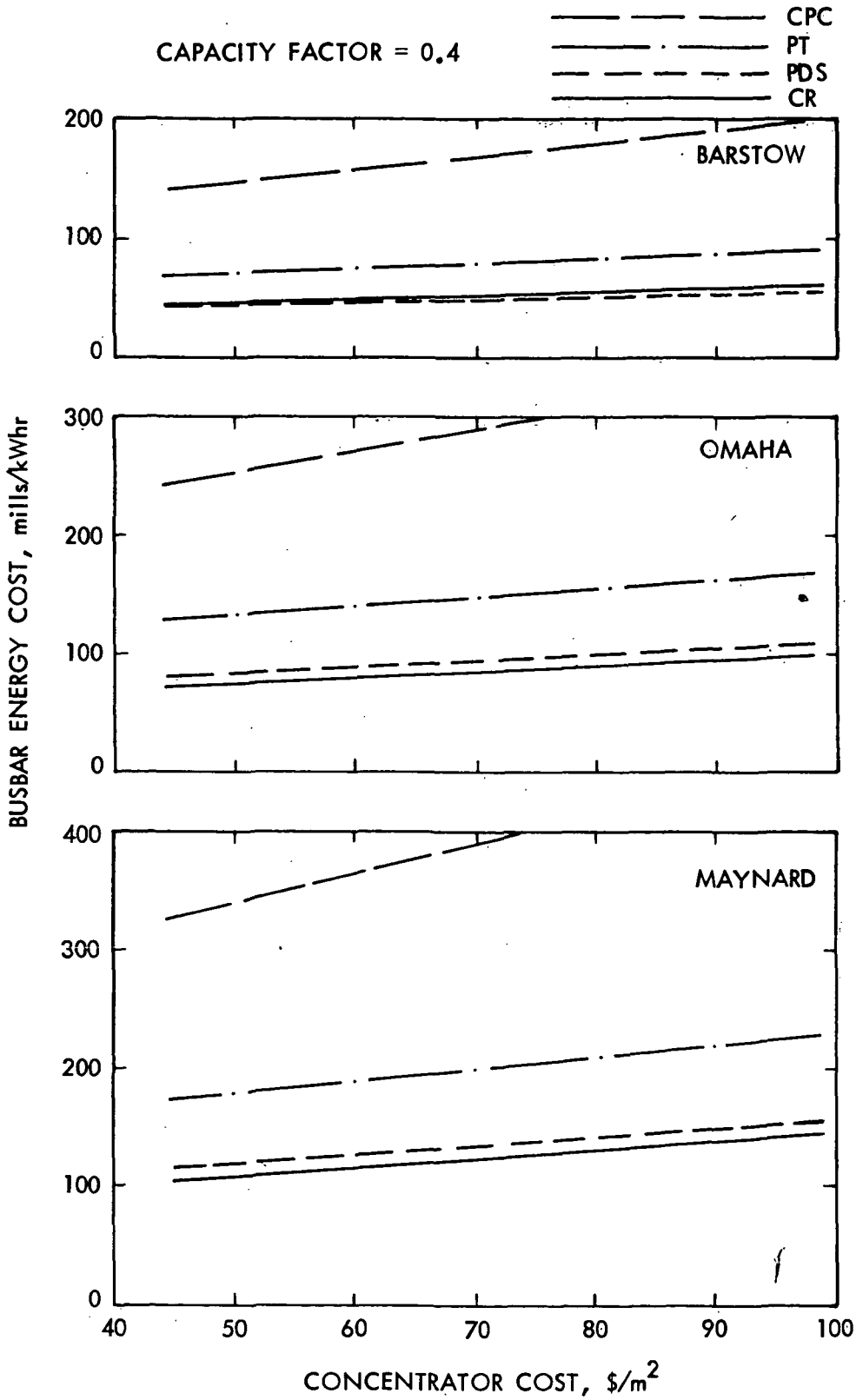

(1) Includes Receiver Cost.

Figure C-2. Sensitivity of Energy Costs to Concentrator Costs

B. ENERGY CONVERSION COSTS

For large 10 MW central energy conversion systems, a cost of 60 $/kWe was used as a lower-bound, mass production target. At present, engines in this size category are not mass produced and cost about $300/kWe. Since this low-bound value is considered to be a particularly difficult target for 10 MWe engines, sensitivity curves of incremental energy cost as a function of energy conversion cost are presented in Figure C-3. This curve pertains to all three systems (CR, PT, and CPC) which employ 10 MWe central engines.

Incremental energy costs read from the curves are to be added to the energy cost values determined for an engine cost of 60 $/kWe, e.g., for an engine cost of 140 $/kWe at a capacity factor of 0.4, an incremental energy cost of 3-4 mills/kWe hr is to be added.

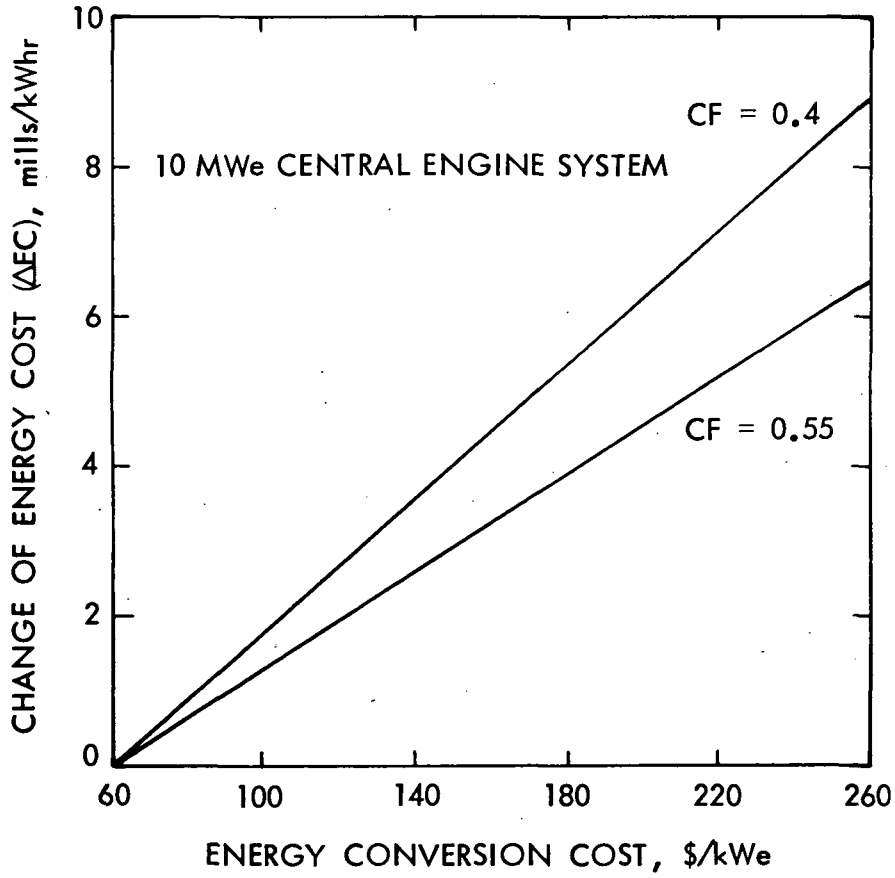

Figure C-3. Sensitivity to Energy Conversion Cost

C. OPERATIONS AND MAINTENANCE COSTS

The costs for operation and maintenance (O&M) of advanced solar thermal plants are subject to a high degree of uncertainty. A nominal value of 1% of total capital costs is employed in this study per EPRI (Ref. C-5). Sensitivity of busbar energy costs to O&M costs are presented in Figure C-4 for the four selected power systems when located at Barstow, California and operating at a capacity factor of 0.55.

Since the two-axis tracking systems (CR and PDS) have lower capital costs, they also have lower O&M costs. If the O&M for these systems increased from 1% to 3% of capital, energy costs increase by approximately 15 mills/kWe hr. For the same variation in O&M, energy cost increases are even greater for the PT and CPC systems.

D. STORAGE SYSTEM COSTS

Storage system costs comprise a significant part of total plant capital costs at capacity factors in the neighborhood of $\approx$0.5 (see Figure B-13 of Appendix B). Since there are large uncertainties regarding the costs of advanced storage systems, sensitivities to these costs are presented in Figures C-5 and C-6 for thermal and battery storage systems, respectively.

In Figure C-5, the energy cost associated with the capital cost of thermal storage is presented as a function of the combined storage throughput and energy conversion system efficiency for a range of unit thermal storage cost values. For illustrative purposes, a capacity factor of 0.55 and storage time of 6 hours are assumed. Here, unit thermal storage cost is defined as the capital cost of the total storage subsystem divided by its maximum storage capacity in kWt hrs.

In determining the size of a thermal storage system that is to be used in a solar thermal power plant, it is noted that, for a specified production of electrical energy from stored thermal energy, the size of the thermal storage system depends on the product of storage throughput and energy conversion system efficiency (Ref. C-6). As this product or combined efficiency increases, a greater portion of stored thermal energy is converted to electricity and, hence, storage size decreases. Also, it will generally not be possible to withdraw all of the stored energy, and this inability will require additional oversizing. For this study, a required oversizing of about 5% was assumed.

The reduction in thermal storage size with increasing efficiency results in lower capital costs and associated energy costs as shown by the curves of Figure C-5. More efficient systems such as the CR thus gain an advantage over less efficient systems, particularly for high unit storage costs. This advantage is partially offset since low-efficiency systems generally employ lower temperature thermal storage having lower unit costs (see Table 3 of the body of this report).

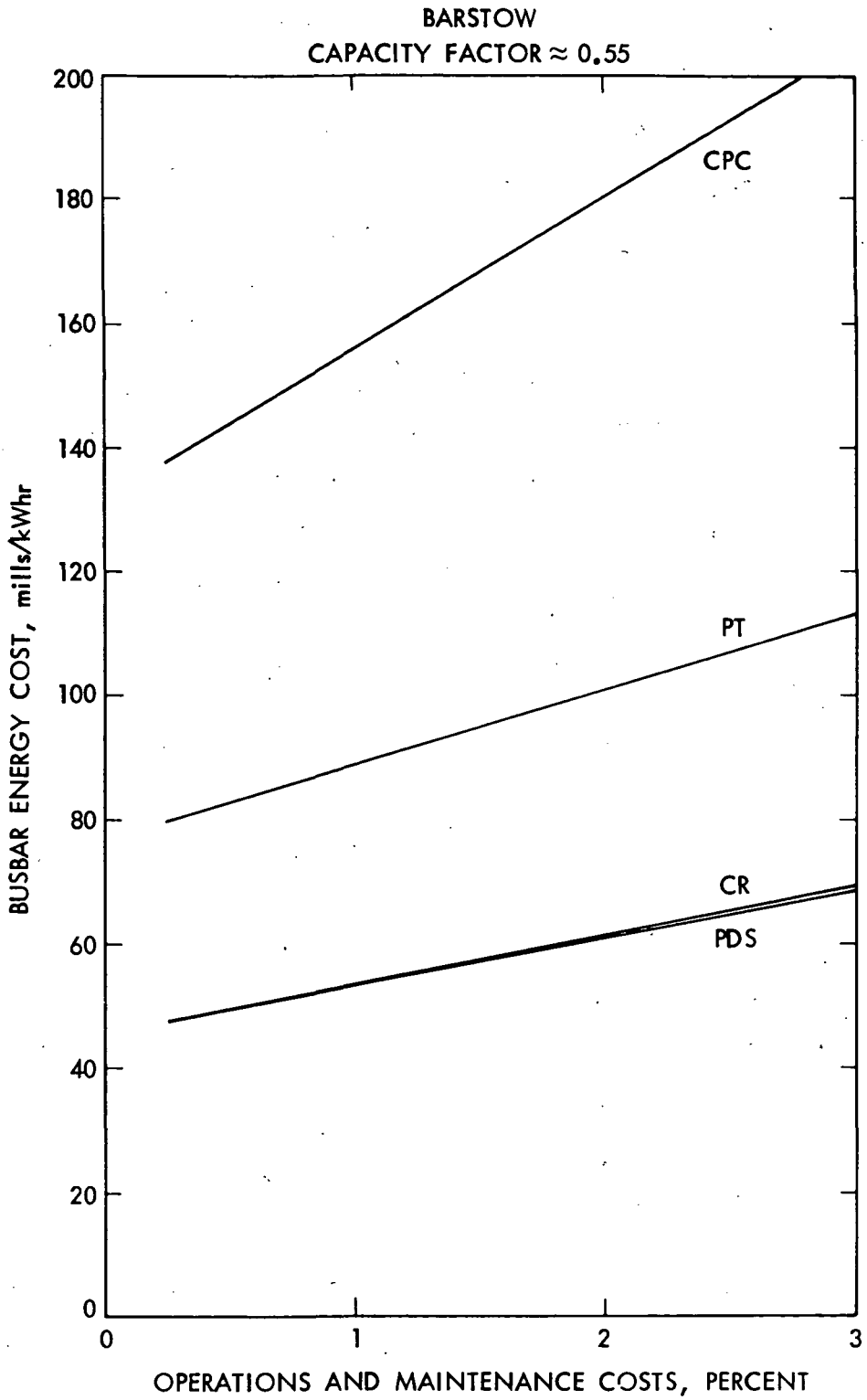

Figure C-4. Sensitivity of Energy Costs to Operations and Maintenance

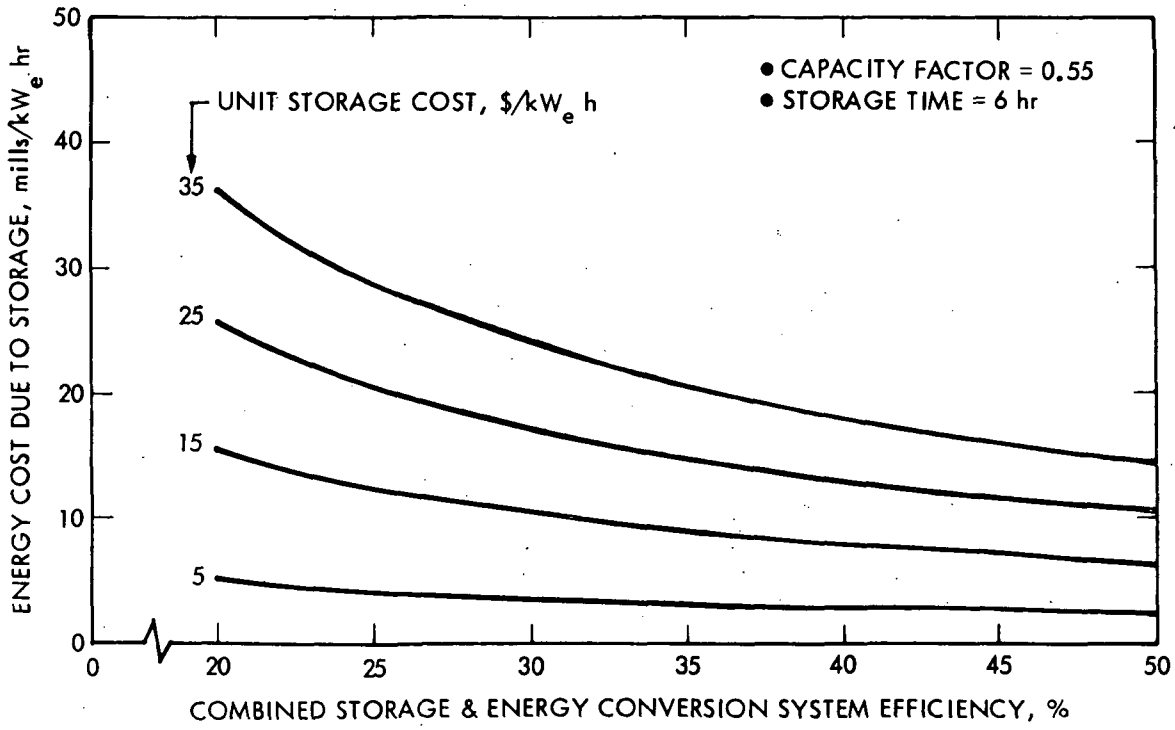

Figure C-5. Sensitivity to Thermal Storage Costs

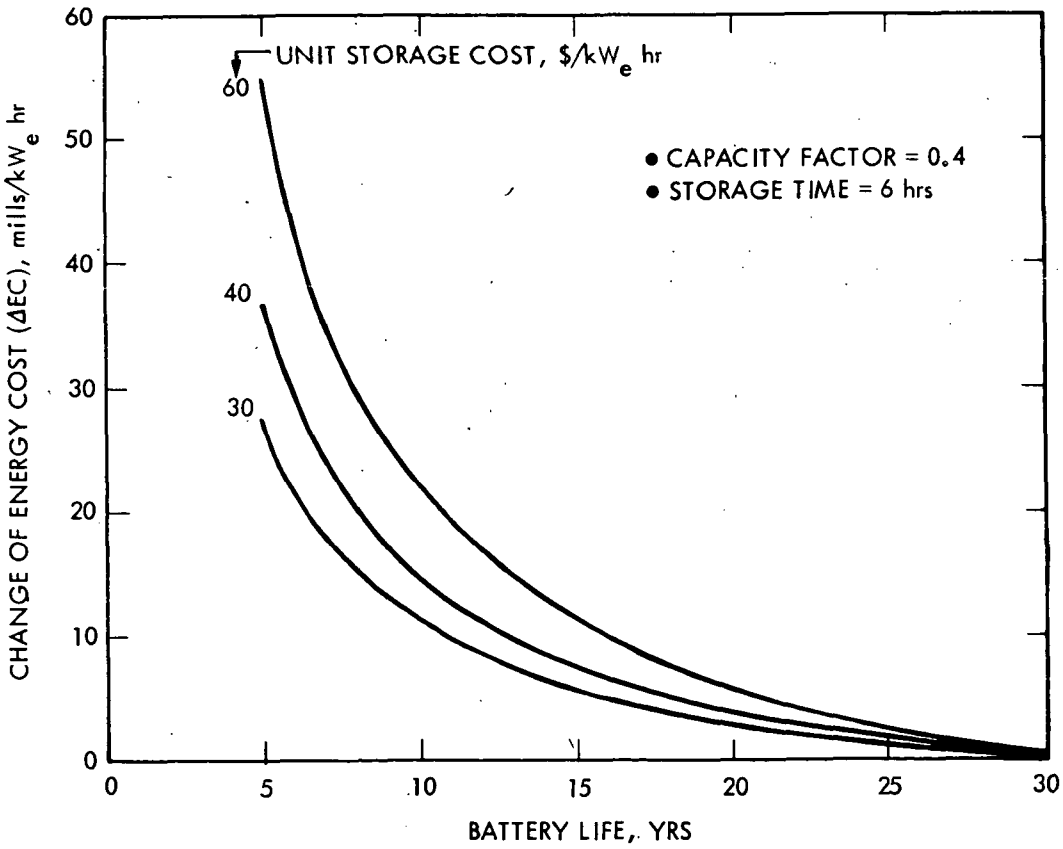

Figure C-6. Sensitivity to Cost and Life of Battery Storage

The unit thermal storage cost range used in this study ranged from 21 to 26 $/kWt-hr, where unit costs were assumed to increase with temperature. There is considerable uncertainty in storage costs since advanced systems being projected in this study are in an early stage of development. Recent activities at NASA/LeRC have established targets or goals for some advanced systems in the range of approximately 5 to 15 $/kWt-hr. If these targets are achieved, energy costs of the order of 10 mills/kWe-hr lower than the nominal values presented in the present study will result.

In addition to cost uncertainties, advanced batteries also face uncertainties regarding life. If battery life is less than the 30 year plant life, energy costs increase as shown in Figure C-6. These energy cost increases for battery replacements are determined via the present value economic methodology of Ref. C-7.

A unit battery storage cost range of 30 to 60 $/kWe-hr is used in Figure C-6 to illustrate how unit costs affect the impact of battery replacements. For the selected unit cost range, energy costs increase from 5 to 10 mills/kW_e-hr if battery life decreases from 30 to 15 years (corresponding to one replacement). At short battery lifetimes of the order of 5 years (representative of present lead-acid batteries) substantial cost increases occur.

Thus, there is considerable incentive for developing an advanced battery, such as the Redox, which has potential for both low cost and long life. Other storage systems, such as underground pumped hydro and compressed air, can be used to store electro-mechanical energy, but, if cost and performance targets are achieved, battery systems are desirable because of implementation flexibility.

IV. REFERENCES

C-1. Fujita, T.; Manvi, R.; Roschke, E. J.; El Gabalawi, N.; Herrera; G.; Kua, T. J.; and Chen, K. H., "Techno-Economic Projections for Advanced Small Solar-Thermal Electric Power Plants to Years 1990-2000," DOE/JPL-1060-78/4, Jet Propulsion Laboratory, Pasadena, CA, November 1978.

C-2. Fujita, T.; El Gabalawai, N.; Herrera, G.; and Turner, G., "Projection of Distributed-Collector Solar-Thermal Electric Power Plant Economics to Years 1900-2000," DOE/JPL-1060-77/1, Jet Propulsion Laboratory, Pasadena, CA, December, 1977.

C-3. "Central Receiver Solar Thermal Power System, Phase 1, Pilot and Commercial Plant Cost and Performance," Preliminary Draft No. MDC G6776, Vol. VII, McDonnell-Douglas Astronautics Company, Huntington Beach, CA, May 1977.

C-4. Powell, J. C., "Solar Pilot Plant Phase I, Preliminary Design Report, Pilot Plant Cost and Commercial Plant Cost and Performance," Report No. F3419-DR-302-III, Vol. VII, Honeywell Energy Resources Center, Minneapolis, MN, June 7, 1977.

C-5. "Technical Assessment Guide," EPRI PS-866-SR, Electric Power Research Institute, Palo Alto, CA, June 1978.

C-6 El Gabalawi, N.; Hill, G.; Bowyer, J.M.; and Slonski, M.L., "A Modularized Computer Simulation Program for Solar Thermal Power Plants," JPL Internal Report 5102-80, Jet Propulsion Laboratory, Pasadena, Ca., July 1978.

C-7 Doane, J.W.; et al., "The Cost of Energy from Utility-Owned Solar Electric Systems, a Required Revenue Methodology for ERDA/EPRI Evaluations," JPL Internal Report 5040-29, ERDA/JPL-1012-7613, Jet Propulsion Laboratory, Pasadena, Ca., June 1976.